JULY

11-14

2017

6th International Workshop on Model Reduction in Reactive Flow

Topics

Theoretical Foundations
Theoretical foundations of model reduction techniques, definitions of slow, fast, invariant manifolds and related subjects.

Mechanism Simplification
Chemical kinetic mechanisms simplification.

Model Reduction in ODE's, DAE's and PDE's

Computational Tools
Computational tools to compute and analyze reacting flows.

Applied Engineering

WWW.MODELREDUCTION.NET

PRINCETON UNIVERSITY

Acknowledgment

The workshop organization committee would like to acknowledge:

- The financial support from the U.S. Army Research Office by Dr. Ralph A. Anthenienm (Proposal No. 70808-EG-CF)
- The organization support by Mrs. Tara Zarillo, Deputy Director Conference and Event Services at Princeton University
- The Andlinger Center for Energy and Environment for hosting the workshop
- Mrs. Kari Gim, webmaster of the IWMRRF website

Information

Contact:

Dr. Temistocle Grenga (co-host) Email: tgrenga@princeton.edu Tel: 574-299-3428

Prof. Yiguang Ju (co-host) Email: yju@princeton.edu

Emergencies:

For emergencies, the University Department of Public Safety can be reached by dialing 911 from a campus phone or 609-258-3333 from a cell phone. In non-emergencies, the Department of Public Safety can be reached at 609-258-1000.

Princeton University maintains a website for any Emergency Alerts (https://www.princeton.edu/main/news/emergency).

Day 1 – Tuesday 11/7	
05:00 pm – 08:00 pm	Registration
06:00 pm – 08:00 pm	Welcome Reception: Maeder Hall, Andlinger Center for Energy and the Environment, Olden Street, Princeton, NJ

Day 2 – Wednesday 12/7		
08:00 am – 08:30 am	Breakfast	
08:30 am – 08:45 am	Welcome – Y. Ju, T. Grenga, H.N. Najm	
08:45 am – 09:30 am	Invited Talk Chair: Y. Ju	No equation, no variable, no parameters: data, gauge invariance and the modeling of complex system - Prof. Y.G. Kevrekidis
09:30 am – 09:55 am	Reaction Diffusion System 1 Chair: U. Maas	Evolution in the State Space and Model Reduction of a Reactive Flow System – U. Maas, V. Bykov
09:55 am – 10:20 am		Physically-Derived Reduced-Order Manifolds for Multi-Modal Turbulent Combustion – M.E. Mueller, B.A. Perry, A.C. Nunno
10:20 am – 10:50 am	Coffee Break	
10:50 am – 11:15 am	Attractive Manifold 1 Chair: J.M. Powers	Reduced Manifolds and Trajectory Curvature – J.M. Powers
11:15 am – 11:40 am		An Online Slow Manifold Approach for Efficient Optimal of Multiple Time-Scale Kinetics – M. Heitel, D. Lebiedz
11:40 am – 12:05 am		Revealing Approximative Low Dimensional Manifold for Accelerating Atomistic Simulations – E. Chiavazzo, J.M. Bello-Rivas, C.W. Gear, I.G. Kevrekidis
12:05 am – 01:35 pm	Lunch Break	
01:35 pm – 02:00 pm	Mechanism Simplification 1 Chair: D.A. Goussis	Asymptotic Analysis of a Pharmacokinetics Model – L.Y. Michalaki, D.A.Goussis
02:00 pm – 02:25 pm		ASVDADD Algorithm for Automatic Selection of RCCE Constraints – G.P. Beretta, M. Janbozorgi
02:25 pm – 02:50 pm		Computational Identification of Quasi-Steady State and Partial Equilibrium in Chemical Kinetics – P. Zhao, T. Lu, C.K. Law, S.H. Lam
02:50 pm – 03:20 pm	Coffee Break	
03:20 pm – 03:45 pm	Mechanism Analysis 1 Chair: H.N. Najm	Computational Singular Pertirbation Analysis of Stotastic Chemical System with Stiffness – X. Han, L. Wang, Y. Cao, H.N. Najm
03:45 pm – 04:10 pm		Ignition Delay Control through Additives in DME/Air and EtOH/Air Mixtures – E.A. Tingas, D.C. Kyritsis, D.A. Goussis
04:10 pm – 04:35 pm		Extinction and Re-ignition Predictions of a Time-Evolving Turbulent Non-Premixed Flame: Sensitivity to Chemical Kinetics Models – S. Yang, R. Ranjan, V. Yang, W. Sun, S. Menon
04:35 pm – 05:00 pm		Machine Learning to Predict Combustion Chemistry Phenomenon – V. van Oudenhoven, S. Mani Sarathy
06:30 pm – 08:30 pm	Banquet: Prospect House, Chancellor Way, Princeton, NJ	

Day 3 – Thrusday 13/7		
08:00 am – 08:30 am	Breakfast	
08:30 am – 09:15 am	Invited Talk Chair: C.K. Law, Y. Ju	"Model Reducrion" by Singular Perturbation – Prof. S.H.Lam
09:15 am – 09:40 am	Attractive Manifold 2 Chair: D. Lebiedz	Covariant Geometric Characterization of Slow Invariant Manifolds: New Concepts and Viewpoints – D. Lebiedz
09:40 am – 10:05 am		Slow Manifolds Localization from Canonical Formats of the Evolution Law– D. Frezzato
10:05 am – 10:35 am	Coffee Break	
10:35 am – 11:00 am	Reaction Diffusion System 2 Chair: T. Lu	Reduced Models for Mixture-Averaged Diffusion – Y. Gao, J.-W. Park, T. Lu
11:00 am – 11:25 am		Identification of Low-Order Dynamics in Turbulent Premixed Flames with Dynamic Mode Decomposition – T. Grenga, J.F. MacArt, M.E. Mueller
11:25 am – 11:50 am		Multi-scale Adaptive Reduced Chemistry Solver (MARCS) for High-Dimensional Combustion Modeling with Detailed Chemical Kinetics – W. Sun, L. Wang, T. Grenga, Y. Ju
11:50 am – 12:15 am		Computation of supersonic reacting mixing layerswith detailed and reduced kinetic mechanisms – C Qian, Z. Huiqiang, Z. Weijiang, B. Peng, Y. Yunjun
12:15 am – 01:45 pm	Lunch Break	
01:45 pm – 02:10 pm	Mechanism Simplification 2 Chair: M. Valorani	A Novel Strategy for Analysis and Reduction of Uncertain Chemical Kinetic Models – R. Malpica Galassi, M. Valorani, H.N. Najm, C. Safta
02:10 pm – 02:35 pm		LES for Turbulent Non-Premixed Jet Flame with CODAC Reduction – Z. Liu, W. Han, W. Kong, Y. Ju
02:35 pm – 03:00 pm		Automated Construction, Reduction, and Optimization of Chemistry for Reactive Flow Modelling – X. Gou, Z. Chen, W. Sun, Y. Ju
03:00 pm – 03:25 pm		Propagation of Kinetic Uncertainty thregh Surrogate Subspace in Combustion Simulations – W. Ji, J. Wang, B. Yang, Z. Ren, C.K. Law
03:25 pm – 03:35 pm	Group Photo	
04:00 pm – 06:00 pm	Social: *Princeton Museum of Art*, McCosh Walk, Princeton, NJ *Lake Walk*, Faculty Road, Princeton, NJ	
06:00 pm – 09:00 pm	Social Dinner: Prof. Ju's Residence, 77 Christopher Dr., Princeton, NJ	

Day 4 – Friday 12/7		
08:00 am – 08:30 am	Breakfast	
08:30 am – 08:55 am	Mechanism Analysis 2 Chair: H.G. Im	Dynamics of n-Heptane/Air Low Temperature Autoignition – E.A. Tingas, Z. Wang, S. Mani Sarathy, H.G. Im, D.A. Goussis
08:55 am – 09:20 am		Enhancements of the G-Scheme Framework – M. Valorani, P.P. Ciottoli, R. Malpica Galassi, S. Paolucci, T. Grenga, E. Martelli
09:20 am – 09:45 am		Using Global Pathway to Understand Chemical Kinetics – X. Gao, S. Yang, W. Sun
09:45 am – 10:15 am	Coffee Break	
10:15 am – 10:40 am	Mechanism Simplification 3 Chair: F. Mauss	Horizontal Species Lumping Using Structural Information from a Mechanism Generator – M. Hilbig, L. Seidel, F. Mauss
10:40 am – 11:05 am		Reduced High-Temperature Combustion Chemistry Models of Jet Fuels – Y. Gao, R. Xu, H. Wang, T. Lu
11:05 am – 11:45 am	Open Discussion Chair: Y. Ju	Challenges on Model Reduction Research
11:45 am – 12:00 am	Adjourn – Y. Ju, T. Grenga	

Session: Reaction Diffusion System 1

Chair: U. Maas

Title: Evolution in the State Space and Model Reduction of a Reactive Flow System
Authors: U. Maas, V. Bykov

Title: Physically-Derived Reduced-Order Manifolds for Multi-Modal Turbulent Combustion
Authors: M. E. Mueller, B. A. Perry, A. C. Nunno

Evolution in the state space and model reduction of a reacting flow system

Ulrich Maas*, Viatcheslav Bykov*

* Karlsruher Institute für Technologie (KIT) / Institute für Technische Thermodynamik, Karlsruhe, Germany

***Abstract*—Nowadays, low-dimensional manifolds defined in the composition / state space of a reacting flow system are widely used as a basic framework for model reduction. These can also be used for development of efficient and robust implementation strategies. However, the problem of existence of manifolds appropriate for a reduced description and their spatial dependence is not yet completely understood and investigated. Typically, the existence of manifolds of certain dimension is postulated and its spatial dependence is neglected. In the current study, problems of existence, identification of manifolds and their properties suitable for model reduction will be investigated and discussed.**

I. Introduction

Reacting flows can be described mathematically based on the conservation equations for mass, momentum, energy, and species masses [1]. There are two main problems in analysis and integration of this system: first, the high dimensionality of the models / mechanisms of chemical kinetics (number of species involved in elementary reactions) and, second, the wide range of characteristic time scales of chemical kinetic processes covering time scales from nanoseconds to seconds. These scaling problems lead to the problem with the length scales as well. Due to these problems, the system of partial differential equations is very large in dimension and very stiff.

In general, model reduction aims at finding efficient methods to simplify the description of the chemical kinetics to solve the above mentioned problems [2]. The problem of model reduction can be formulized rigorously by using the framework of low-dimensional manifolds (see e.g. [3-6]). The problem of model reduction then is cut down to the problem of definition of suitable manifolds, which describe the evolution of the detailed system in the physical space by/through the parameters of the manifold only.

Therefore, the existence of the manifold represents a very important and not yet sufficiently investigated topic of model reduction. Typically, the manifold of low-dimension is postulated and the system dynamics is restricted to evolve within this manifold [2,3,6]. By using a very simple and transparent problem the question of existence is treated in this study. The evolution of the detailed systems solution profile is in the focus of the study. The mapping of the solutions' scalar fields into the system state space is considered.

By studying this mapping several observations concerning the dimension (minimal dimension) of manifolds and dependence of the low-dimensional manifold on the spatial variable can be drawn. First of all, the minimal dimension can be investigated, then this can be used to verify the main crucial assumptions of the manifold's spatial independence.

II. Problem statement

It is evident any scalar field of a reacting flow in d-dimensional physical space with spatial coordinates r and time t: $\psi = \psi(r,t)$ leads to a temporarily varying manifold in composition space, which has a dimension of at most d. These manifolds evolve in time, and though the dimension is limited, but they might become arbitrarily complicated both in physical space and in the system state space. Nevertheless, if manifolds of a given dimension can be found, which represent the evolving manifolds with a good accuracy, then these manifolds can be used to approximate the system's dynamics. Based on this observation a strategy to study the properties of the low-dimensional manifolds used for model reduction is to investigate how the dynamics of the detailed systems' manifold evolves in time. In this way the properties of the manifold (of the reduced model) can be studied, because the evolution of the solution manifolds should themselves be embedded in the reduced manifold. In a previous study (see [7]) the physical boundary of the solution manifold (parametrized by spatial coordinates and time and represented in the state space) and the boundary of the low-dimensional manifold were discussed. In the current study, however, the evolution of the system solution profiles is suggested to be used to verify both the existence of the manifold of certain dimension as well as the spatial dependence of the manifold.

III. Toy example

The proposed strategy can be visualized and illustrated by a simple 3D toy system ($n=3$) in an artificial one-dimensional ($d=1$) physical space. This system models a free reaction wave propagation problem in the so-called Lagrangian coordinates, i.e. the advection term can be excluded. 3D Michaelis-Menten model [4] was extended to include the diffusion. The reaction-diffusion system has the following chemical source term:

$$F = \begin{pmatrix} -\psi_1\psi_3 + L_1\left(1-\psi_3-\mu(1-\psi_2)\right) \\ -L_3\psi_2\psi_3 + L_2/L_4(1-\psi_2) \\ 1/L_2\left(-\psi_1\psi_3+1-\psi_3-\mu(1-\psi_2)\right)+\mu\left(-L_3\psi_2\psi_3+L_2/L_4(1-\psi_2)\right) \end{pmatrix}$$

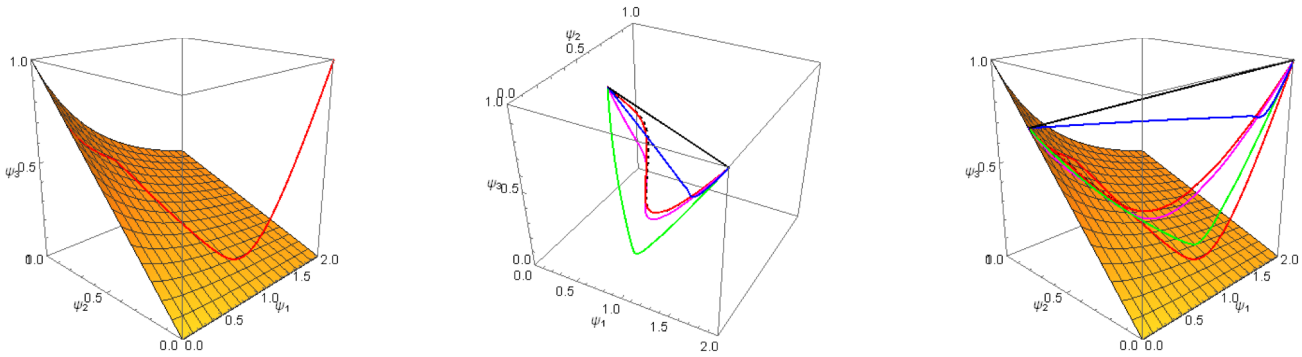

Fig. 1 Left: Plot of the homogenous system solution in state space (red line), surface shows the 2D slow manifold for homogenous system only; Middle: Transient solution profiles (1D in space) starting from the black initial profile, dashed line shows the stationary solution profile. Right: Two plots together are show here.

The diffusion is modelled by the standard Laplace operator $d(\Delta\psi_1, \Delta\psi_2, \Delta\psi_3)$, where d=0.001 is taken for dimensionless diffusion coefficient and $L_1 = 0.99, L_2 = 1, L_3 = 0.05, L_4 = 0.1, \mu = 1$ are dimensionless kinetic parameters. This simple example can be used to show clearly how the solution manifold (1D in this case) evolves in time, and how the physical dimension can be related to the manifolds dimension.

IV. Results and Discussion

Figure 1 (left) shows the homogeneous system solution trajectory (by the red line) and the 2D slow manifold generated for the homogenous (ODEs) system only. As typical for chemical kinetic systems the solution trajectory evolves towards the 2D slow manifold and then stays in its neighborhood and evolves to the equilibrium. In the Figure 1 (middle) the PDE system solution profiles are shown starting from the straight line (black curve) that joins the initial *(2,0,1)* and the equilibrium *(0,0.73,0.73)* states, which has been taken as the initial state. Then, several snapshots of the solution profiles in the state space are shown by blue, cyan, magenta and red lines, which finally converges to the 1D stationary solution profile shown by the black dashed line. The figure on the right shows the transient profiles with respect to the 2D slow manifold for homogenous system from another point of view.

It is clear that systems close to the stationary state can be well described by the 1D stationary manifold (this in fact the basis of flamelet models). However, the evolution of the 1D initial manifold towards this stationary solution generates itself a 2-dimensional manifold. Such a two-dimensional manifold is in the focus of the study and might describe the systems dynamics better especially for the states away from the stationary states.

Based on these observations several properties of approximating manifolds (like reaction-diffusion manifolds) can be investigated, such as:

- The attractive properties of low-dimensional manifolds
- The ability of low-dimensional manifolds to describe transient processes
- The necessary dimension of a low-dimensional manifold such that it embeds the solution manifolds.

In this study we show how the information about the evolution of detailed systems solution in the compositions space can be used to find the necessary dimension of the manifold. Furthermore, the question of a gradient estimate, which depends only on the location in the state space and not on the location in physical space needed for REDIM implementation. This question can also be addressed based on an investigation of the detailed system's evolution profiles.

V. Conclusion

In spite of the progress made in the development of the manifolds based reduction approaches, there are several very difficult and complicated issues concerning the spatial dependence of these manifold. The simplest and most obvious way to solve this problem is to postulate "complete" independence of the manifold on the spatial phenomena. In this study, however, we show how these problems can be handled in a more sophisticated way by looking at the evolution of detailed system solution profiles.

Acknowledgment

Funding by the Deutsche Forschungsgemeinschaft (DFG) is gratefully acknowledged.

References

[1] J. Warnatz, U. Maas and R.W. Dibble, *Combustion*, 4th ed. Springer-Verlag, New York, 2006.

[2] V. Bykov and U. Maas, "The extension of the ILDM concept to reaction-diffusion manifolds", *Combustion Theory and Modelling*, 11(6), pp. 839, 2007.

[3] U. Maas, S. B. Pope, "Simplifying chemical kinetics: Intrinsic low-dimensional manifolds in composition space", *Comb. Flame,* 88, pp. 239, 1992.

[4] Marc R. Roussel and Simon J. Fraser, "Global analysis of enzyme inhibition kinetics". *J. Phys. Chem.,* 97(31), pp. 8316, 1993.

[5] S.H. Lam, D.M. Goussis, The CSP Method for Simplifying Kinetics, *Int. J. of Chemical Kinetics*, 26, pp. 461, 1994.

[6] A.N. Gorban, I.V. Karlin, A.Yu. Zinovyev, Constructive Methods of Invariant Manifolds for Kinetic Problems, *Physics Reports*, V. 396, 4-6, pp. 197, 2004.

[7] A. Neagos, V. Bykov, U. Maas, Adaptive hierarchical construction of Reaction–Diffusion Manifolds for simplified chemical kinetics, *Proc. Comb. Inst.*, 36(1), pp. 663, 2017.

Physically-Derived Reduced-Order Manifolds for Multi-Modal Turbulent Combustion

Michael E. Mueller*, Bruce A. Perry*, A. Cody Nunno*
*Department of Mechanical and Aerospace Engineering, Princeton University, Princeton, NJ, USA

***Abstract*— A new turbulent combustion model for LES has been developed that breaks the inherent trade-off between generality and computational cost in existing turbulent combustion models. The new model relies on a more general low-dimensional manifold to describe combusiton processes that does not *a priori* limit combustion to a single, local asymptotic mode. The model is constructed by first assuming that all (adiabatic, isobaric, two-stream) combustion processes can be described on a two-dimensional manifold defined by a mixture fraction and a generalized progress variable. A transformation of the governing equations is performed into these coordinates to describe the evolution of the thermochemical state on the manifold, which also leads to an explicit definition for the generalized progress variable. This two-dimensional space is shown to recover the three asymptotic modes of combustion under appropriate limits. Implementation challenges with LES are highlighted.**

I. Introduction

Turbulent combustion models for Large Eddy Simulation (LES) can divided into two distinct classes of models. In the first class of models, no *a priori* assumption is made about the underlying combustion processes such as Transported Probability Density Function (TPDF) [1] and the Linear Eddy Model (LEM) [2]. These models have the potential to be very general, but the computational cost is high and scales with the number of species considered. In the second class of models, *a priori* assumptions are made about the underlying combustion processes, restricting the combustion processes to some low-dimensional or reduced-order manifold that can be described by a number of variables much less than the total number of chemical species, resulting in a significant reduction in computational cost. These reduced-order manifolds are often derived directly from physical arguments, including "flamelet"-like models [3], [4] and Conditional Moment Closure [5], but usually restrict combustion processes to a single, local asymptotic mode.

Various attempts have been made to generalize physically-derived reduced-order manifolds to accommodate more complex multi-modal combustion processes. Knudsen and Pitsch [6] derived a set of governing equations for a two-dimensional manifold over mixture fraction Z, constant for premixed combustion, and a flame index Λ, constant for nonpremixed combustion. The goal of that work was not to model multi-modal combustion processes directly but, instead, use the balance of terms in the multi-dimensional manifold equation to develop a "regime index" to distinguish between locally premixed and locally nonpremixed combustion. Nguyen *et al.* [7] proposed a similar set of two-dimensional manifold equations over the mixture fraction Z and an undefined progress variable Y_C that is limited to some linear combination of species mass fractions. The shortcoming of this formulation is that the progress variable Y_C is not necessarily constant for nonpremixed combustion, so the equations do not simplify to the classical nonpremixed equations in mixture fraction space in that limit. While the authors did solve the two-dimensional manifold equations, the model has not been applied as a turbulent combustion model in LES.

The goals of this work are three-fold. First, a new, consistent, physically-derived reduced-order manifold approach is developed for multi-modal turbulent combustion. The manifold will be defined over a mixture fraction Z and an explicitly defined generalized progress variable Λ. Second, the model will be shown to recover the asymptotic limits of nonpremixed combustion, premixed combustion, and homogeneous combustion in the appropriate limits. Finally, strategies for implementation within LES are discussed.

II. Model Details

To describe multi-modal combustion (for a [effectively] two-stream problem), two manifold coordinates are required. The first coordinate is the mixture fraction Z, defined by its transport equation to be a conserved scalar with unity Lewis number [8]. The mixture fraction is defined to be zero in the oxidizer stream and unity in the fuel stream. The second coordinate is a generalized progress variable Λ whose explicit definition will be left open at this point, but it will be defined to be *independent* of the mixture fraction and to to be zero for an unburned gas mixture and unity at equilibrium. Note that this generalized progress variable *cannot* be defined to be any [linear combination of] species mass fraction, for this would introduce a dependence on the mixture fraction into the definition of the generalized progress variable. The working hypothesis of the two-dimensional manifold then is that all (isobaric, adiabatic, two-stream) combustion processes can be described on the unit square, varying between oxidizer and fuel and between unburned and equilibrium.

To obtain the manifold evolution equations, a coordinate transformation is performed from physical space and time

to the manifold coordinates, that is, $(t, x_j) \rightarrow (Z, \Lambda)$. For brevity, the details of the coordinate transformation are not included here, but the resulting manifold equation for the species mass fraction, assuming unity Lewis numbers, is given by

$$\frac{\partial Y_k}{\partial \Lambda}\left[\frac{\partial \Lambda}{\partial t} + u_j \frac{\partial \Lambda}{\partial x_j} - \frac{1}{\rho}\frac{\partial}{\partial x_j}\left(\rho D \frac{\partial \Lambda}{\partial x_j}\right)\right] = \frac{\chi_{ZZ}}{2}\frac{\partial^2 Y_k}{\partial Z^2} + \chi_{Z\Lambda}\frac{\partial^2 Y_k}{\partial Z \partial \Lambda} + \frac{\chi_{\Lambda\Lambda}}{2}\frac{\partial^2 Y_k}{\partial \Lambda^2} + \dot{w}_k \,, \tag{1}$$

where $\chi_{\phi\psi} = 2D\frac{\partial \phi}{\partial x_j}\frac{\partial \psi}{\partial x_j}$.

The problem with the above equation is that the evolution of Λ in space and time remains, so the equation is unclosed. Therefore, an explicit definition for the generalized progress variable Λ is required and is obtained by choosing a reference species that will define Λ. The reference species should be "progress variable like" and evolve monotonically between unburned and equilibrium. Rearranging Eq. 1 for the reference species results in an explicit definition for the generalized progress variable Λ:

$$\frac{\partial \Lambda}{\partial t} + u_j \frac{\partial \Lambda}{\partial x_j} - \frac{1}{\rho}\frac{\partial}{\partial x_j}\left(\rho D \frac{\partial \Lambda}{\partial x_j}\right) = \dot{w}_\Lambda \equiv \left[\frac{1}{\partial Y_k / \partial \Lambda}\left(\frac{\chi_{ZZ}}{2}\frac{\partial^2 Y_k}{\partial Z^2} + \chi_{Z\Lambda}\frac{\partial^2 Y_k}{\partial Z \partial \Lambda} + \frac{\chi_{\Lambda\Lambda}}{2}\frac{\partial^2 Y_k}{\partial \Lambda^2} + \dot{w}_k\right)\right]_R , \tag{2}$$

where the subscript $_R$ refers to the terms evaluated for the reference species and has been used to define a source term for the generalized progress variable Λ.

With this definition for Λ, the species evolution on the manifold is then given by

$$\frac{\partial Y_k}{\partial \Lambda}\dot{w}_\Lambda = \frac{\chi_{ZZ}}{2}\frac{\partial^2 Y_k}{\partial Z^2} + \chi_{Z\Lambda}\frac{\partial^2 Y_k}{\partial Z \partial \Lambda} + \frac{\chi_{\Lambda\Lambda}}{2}\frac{\partial^2 Y_k}{\partial \Lambda^2} + \dot{w}_k . \tag{3}$$

Analogous equations can be derived for the temperature or without the assumption of unity Lewis numbers.

III. Recovery of Asymptotic Limits

Premixed Combustion: In the premixed limit, gradients of mixture fraction vanish $\nabla Z \rightarrow 0$. For the species evolution on the manifold, Eq. 3 simplifies to

$$\frac{\partial Y_k}{\partial \Lambda}\dot{w}_\Lambda = \frac{\chi_{\Lambda\Lambda}}{2}\frac{\partial^2 Y_k}{\partial \Lambda^2} + \dot{w}_k \,. \tag{4}$$

The same equation would be obtained by considering a single-variable manifold coordinate transformation in Λ.

Nonpremixed Combustion: In the nonpremixed limit, gradients of the generalized progress variable vanish $\nabla \Lambda \rightarrow 0$. For the species evolution on the manifold, Eq. 3 simplifies to

$$\frac{\partial Y_k}{\partial \Lambda}\dot{w}_\Lambda = \frac{\chi_{ZZ}}{2}\frac{\partial^2 Y_k}{\partial Z^2} + \dot{w}_k \,. \tag{5}$$

The term on the left-hand-side is a time-like term that describes the evolution of the nonpremixed combustion process between its steady "flamelet" limits: toward the stable burning (upper) and non-burning (lower) branches and away from the unstable (middle) branch of the S-shaped curve (i.e., extinction and reignition processes).

Homogeneous Combustion: In the homogeneous limit, gradients of both the mixture fraction and the generalized progress variable vanish. For the species evolution on the manifold, Eq. 3 simplifies to

$$\frac{\partial Y_k}{\partial \Lambda}\dot{w}_\Lambda = \dot{w}_k \,. \tag{6}$$

The role of the left-hand-side as a time-like term in nonpremixed and homogenous combusiton is even more apparent. In the homogeneous limit during autoignition, $\Lambda = 0$ corresponds to $t = 0$, and $\Lambda = 1$ corresponds to $t \rightarrow \infty$.

IV. Implementation with LES

A new shared-memory parallel solver, ***P***hysically-***D***erived ***R***educed-Order Manifold***s*** (PDRs), has been developed to solve the two-dimensional manifold equations. The equilibrium boundary condition is computed using CEQ [9]. The discretized non-linear equations are solved using the SUNDIALS package [10]. Example solutions are not included in this abstract for brevity but will be shown to describe a wide range of combustion pheneomena.

The major impediment to the use of this two-dimensional manifold as a turbulent combustion model in LES is the sheer number of database dimensions that is required for *a priori* calculation of the manifold: the mixture fraction Z, the generalized progress variables Λ, and three scalar dissipation rates. Pre-computation of the manifold would require a five-dimensional database, which is just possible with node memory limitations. As an alternative, rather than pre-computing the manifold, new capability is being developed to solve the manifold equations 'on-the-fly' during a LES calculation and tabulating the manifold solutions using In-Situ Adaptive Tabulation (ISAT) [11], which would also allow for the consideration of additional physics including heat losses, pressure/energy variation, multi-component oxidizers/fuels, inhomogeneous oxidizers/fuels, all of which require additional database dimensions.

References

[1] S.B. Pope, Prog. Energy Combust. Sci. 11 (1985) 1189-192
[2] P.A. McMurthy, S. Menon, A.R. Kerstein, Proc. Combust. Inst. 24 (1992) 271-278
[3] N. Peters, Prog. Energy Combust. Sci. 10 (1984) 319-339
[4] J.A. van Oijen, A. Donini, R.J.M. Bastiaans, J.H.M. ten Thije Boonkkamp, L.P.H. de Goey, Prog. Energy Combust. Sci. 57 (2016) 30-74
[5] A.Y. Klimenko, R.W. Bilger, Prog. Energy Combust. Sci. 25 (1999) 595-687
[6] E. Knudsen, H. Pitsch, Combust. Flame 156 (2009) 678-696
[7] P.-D. Nguyen, L. Vervisch, V. Subramanian, P. Domingo, Combust. Flame 157 (2010) 43-61
[8] H. Pitsch, N. Peters, Combust. Flame 114 (1998) 26-40
[9] S.B. Pope, Combust. Flame 139 (2004) 222-226
[10] A.C. Hindmarsh *et al.*, ACM Trans. Math. Software 31 (2005) 363-396
[11] S.B. Pope, Combust. Theory Model. 1 (1997) 41-63

Session: Attractive Manifold 1

Chair: J. M. Powers

Title: Reduced Manifolds and Trajectory Curvature
Author: J. M. Powers

Title: An Online Slow Manifold Approach for Efficient Optimal of Multiple Time-Scale Kinetics
Authors: M. Heitel, D. Lebiedz

Title: Revealing Approximate Low Dimensional Manifold for Accelerating Atomistic Simulations
Authors: E. Chiavazzo, J. M. Bello-Rivas, C. W. Gear, I. G. Kevrekidis

Reduced Manifolds and Trajectory Curvature

Joseph M. Powers*,
*University of Notre Dame, Department of Aerospace and Mechanical Engineering, Notre Dame, Indiana, USA

***Abstract*— It is shown by counter-example that slow invariant manifolds are not associated with points of vanishing solution trajectory curvature. However, vanishing trajectory curvature may be associated with an intrinsic low-dimensional manifold, which approaches a slow invariant manifold as stiffness increases.**

I. Introduction

The identification of slow invariant manifolds associated with nonlinear dynamical systems that describe spatially homogeneous chemical kinetics is a key problem of model reduction for reactive systems. See [1], [2] and references therein for background. In short, the phase space in which non-reduced reactive systems evolves is typically of high dimension, and manifold methods identify manifolds of lower dimension to which the system is attracted at long time. Projection of high-dimensional trajectories onto lower dimensional manifolds can potentially reduce the stiffness of the system while maintaining high fidelity to the underlying high-dimensional system. This can enable more computationally efficient calculation of reaction dynamics.

Ginoux and co-workers [3], [4] have stated that one can identify slow invariant manifolds (SIMs) of two-dimensional dynamical systems by identifying zero-curvature manifolds (ZCMs): those points within the phase space where the curvature of solution trajectories vanishes. Additional development is in [5]. It will be shown here that this criterion fails for the well known Davis-Skodje (DS) [6] system. Instead, the ZCM is found to identify the so-called intrinsic low-dimensional manifold (ILDM) [7].

II. General analysis

We summarize some concepts discussed in detail in [1]-[7]. Spatially homogeneous chemical kinetics can be cast as dynamical system of the form

$$\frac{d\mathbf{x}}{dt} = \mathbf{v}(\mathbf{x}). \tag{1}$$

Here, we consider $\mathbf{x}$ to be related to the species concentration and think of it as a position in phase space. We consider $\mathbf{v}$ to be the constitutive equation for chemical kinetics, and think of it as a velocity in phase space. Local dynamics may often be analyzed with the aid of the Jacobian matrix $\mathbf{J}$ which is the Fréchet derivative of $\mathbf{v}$ with respect to $\mathbf{x}$:

$$\mathbf{J} = \frac{\partial \mathbf{v}}{\partial \mathbf{x}}. \tag{2}$$

It is the reciprocals of the real parts of the eigenvalues of $\mathbf{J}$ that give the local time scales of reaction. The acceleration $\mathbf{a}$ in phase space is given by

$$\mathbf{a}(\mathbf{x}) = \frac{\partial \mathbf{v}}{\partial \mathbf{x}} \frac{d\mathbf{x}}{dt} = \mathbf{J} \cdot \mathbf{v}. \tag{3}$$

The curvature κ of any trajectory is given by

$$\kappa = \frac{||\mathbf{a} \times \mathbf{v}||}{||\mathbf{v}||^3}. \tag{4}$$

The curvature κ vanishes at points $\mathbf{x}$ for which the velocity $\mathbf{v}$ is aligned with the acceleration $\mathbf{a}$.

III. Analysis of the DS System

A. Exact Solution

Consider the DS system, taking $x > 0$, $\gamma > 1$:

$$\frac{dx}{dt} = -x, \qquad x(0) = x_0, \tag{5}$$

$$\frac{dy}{dt} = -\gamma y + \frac{(\gamma-1)x + \gamma x^2}{(1+x)^2}, \qquad y(0) = y_0. \tag{6}$$

The exact solution is

$$x(t) = x_0 e^{-t}, \tag{7}$$

$$y(t) = \frac{x_0 e^{-t}}{1 + x_0 e^{-t}} + \left(y_0 - \frac{x_0}{1+x_0} \right) e^{-\gamma t}. \tag{8}$$

Eliminating t, the exact solution in the phase plane is

$$y(x) = \frac{x}{1+x} + \left(y_0 - \frac{x_0}{1+x_0} \right) \left(\frac{x}{x_0} \right)^{\gamma}. \tag{9}$$

As $\gamma > 1$, the curve approached from arbitrary initial conditions is

$$y_{SIM} = \frac{x}{1+x}. \tag{10}$$

Thus, y_{SIM} captures the slow dynamics of the system. Moreover, if the initial conditions are such that they lie on $y_{SIM}(x)$: $y_0 = x_0/(1+x_0)$, then y_{SIM} is itself a solution trajectory, and thus an invariant manifold.

The exact expressions for $\mathbf{J}$ and $\mathbf{a}$ are

$$\mathbf{J} = \begin{pmatrix} -1 & 0 \\ \frac{\gamma - 1 + (\gamma+1)x}{(1+x)^3} & -\gamma \end{pmatrix}, \tag{11}$$

$$\mathbf{a} = \begin{pmatrix} x \\ \gamma^2 y - \frac{x\left(\gamma^2 (x+1)^2 + x - 1\right)}{(x+1)^3} \end{pmatrix}. \tag{12}$$

The eigenvalues of $\mathbf{J}$ are $\lambda_1 = -1$, $\lambda_2 = -\gamma$. The stiffness ratio is $|\lambda_2/\lambda_1| = \gamma$. Stiffness increases as γ increases. The unique finite fixed point $(0, 0)$ is guaranteed stable because both eigenvalues are everywhere negative, including in the neighborhood of the fixed point.

B. ILDM

As derived in [7] and shown in [2], [6], the ILDM is found by projecting Eqs. (5,6) onto a basis formed from fast and slow eigenmodes of $\mathbf{J}$ and equilibrating the differential equation associated with the fastest time scale. This yields an algebraic equation for the ILDM; solving this for y and simplifying, the ILDM for the DS system is given by

$$y_{ILDM} = \underbrace{\frac{x}{x+1}}_{y_{SIM}} + \frac{2x^2}{\gamma(\gamma-1)(1+x)^3}. \tag{13}$$

Obviously the ILDM and SIM are different, but approach each other as stiffness γ increases.

C. ZCM

The ZCM is seen from Eq. (4) to exist when the velocity and acceleration vectors are parallel:

$$\mathbf{a} \times \mathbf{v} = \mathbf{0}. \tag{14}$$

Use Eqs. (5,6) to form $\mathbf{v}$ and Eq. (12) for $\mathbf{a}$, substitute into Eq. (14), and solve to find the ZCM:

$$y_{ZCM} = \underbrace{\frac{x}{x+1}}_{y_{SIM}} + \frac{2x^2}{\gamma(\gamma-1)(1+x)^3}. \tag{15}$$

The ZCM is exactly the ILDM and is not the SIM. The ZCM is not a solution trajectory, so it is not an invariant manifold. Note that the ZCM itself has curvature. Solution trajectories possess no curvature when they intersect the ZCM. The ZCM approaches the SIM as stiffness γ increases.

Figure 1 shows a phase plane for the DS system with moderate stiffness, $\gamma = 3$. Included are the trajectory $y(x)$ corresponding to $x(0) = 1$, $y(0) = 3/5$, $y_{ZCM} = y_{ILDM}$, and y_{SIM}. Also shown are the vector fields of $\mathbf{v}$ and $\mathbf{a}$. The trajectory crosses through y_{ZCM} at a point where the trajectory itself has no curvature, with $\mathbf{v}$ parallel to $\mathbf{a}$. The trajectory then approaches y_{SIM}.

D. Quantification at a point

Still taking $\gamma = 3$, consider the point $x = 1$. At that point the reduction that is Eq. (10) recommends for us to project to the SIM, yielding $y_{SIM} = 1/2$. At this point, the original Eqs. (5,6) tell us $dx/dt = -1$ and $dy/dt = -1/4$. Dividing, we see at that this point Eqs. (5,6) tell us $dy/dx = 1/4$. We can differentiate directly Eq. (10) for the SIM and get

$$\frac{dy_{SIM}}{dx} = \frac{1}{(1+x)^2}, \qquad \left.\frac{dy_{SIM}}{dx}\right|_{x=1} = \frac{1}{4}. \tag{16}$$

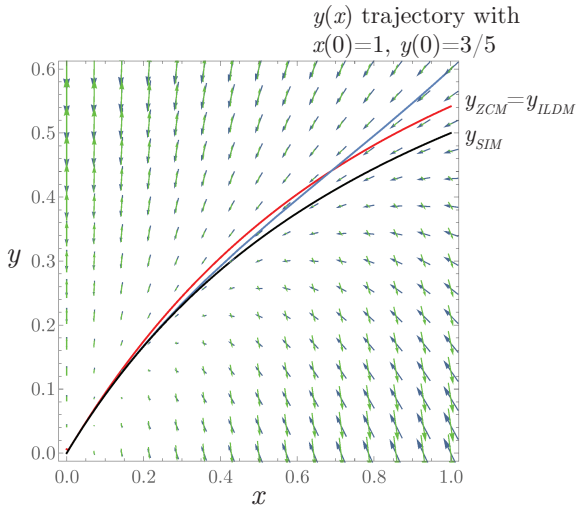

Fig. 1. Trajectory, ZCM, ILDM, SIM, $\mathbf{v}$, and $\mathbf{a}$ for DS system with $\gamma = 3$.

Thus the slope of the SIM is identical to that predicted by Eqs. (5,6). This is consistent with the SIM also being a trajectory, necessary for it to be an invariant manifold.

At the same point $x = 1$, the ZCM, Eq. (15) recommends we project to $y_{ZCM} = 13/24$. At this point, the original Eqs. (5,6) tell us $dx/dt = -1$ and $dy/dt = -3/8$. Dividing, we see at that this point Eqs. (5,6) tell us $dy/dx = 3/8$. We can differentiate directly Eq. (15) for the ZCM and get

$$\frac{dy_{ZCM}}{dx} = \frac{1}{(1+x)^2} + \frac{(x-2)x}{3(1+x)^4}, \qquad \left.\frac{dy_{ZCM}}{dx}\right|_{x=1} = \frac{13}{48}. \tag{17}$$

The slope of the ZCM is not predicted by Eqs. (5,6).

IV. Conclusion

The ZCM is an ILDM but not a SIM. The ZCM and ILDM better approximate the SIM as stiffness increases.

References

[1] J. M. Powers, S. Paolucci, J. D. Mengers, and A. N. Al-Khateeb, "Slow attractive canonical invariant manifolds for reactive systems *J. Math. Chem.*, vol. 53, 2015, pp. 737-766.

[2] S. Singh, J. M. Powers, and S. Paolucci, "On slow manifolds of chemically reactive systems," *J. Chem. Phys.*, vol. 117, 2002, pp. 1482-1496.

[3] J. M. Ginoux and B. Rossetto, "Differential geometry and mechanics: applications to chaotic dynamical systems," *Int. J. Bifurcation Chaos*, vol. 16, 2006, pp. 887-910.

[4] J. M. Ginoux, B. Rossetto, and L. O. Chua, "Slow invariant manifolds as curvature of the flow of dynamical systems," *Int. J. Bifurcation Chaos*, vol. 18, 2008, pp. 3409-3430.

[5] J. M. Ginoux, "The slow invariant manifold of the Lorenz-Krishnamurthy Model," *Quant. Theory Dyn. Syst.*, vol. 13, 2014, pp. 19-37.

[6] M. J. Davis and R. T. Skodje, "Geometric investigation of low-dimensional manifolds in systems approaching equilibrium," *J. Chem. Phys.*, vol. 111, 1999, pp. 859-874.

[7] U. Maas and S. B. Pope, "Simplifying chemical kinetics: intrinsic low-dimensional manifolds in composition space," *Combust. Flame*, vol. 88, 1992, pp. 239-264.

An online slow manifold approach for efficient optimal control of multiple time-scale kinetics

Marcus Heitel*, Dirk Lebiedz*
*Institute for Numerical Mathematics, Ulm University, Germany

***Abstract*— Chemical reactions modeled by ordinary differential equations are finite-dimensional dissipative dynamical systems with multiple time-scales. They are numerically hard to tackle – especially when they enter an optimal control problem as "infinite-dimensional" constraints. Since discretization of such problems usually results in high-dimensional nonlinear problems, model (order) reduction via slow manifold computation seems to be an attractive approach. We discuss the use of slow manifold computation methods in order to solve optimal control problems more efficiently having real-time applications in view.**

I. Introduction

Chemical kinetics with multiple time scales and their control involve highly stiff and often high-dimensional ordinary differential equations (ODE). This poses hard challenges to the numerical solution and is the reason why model reduction methods are considered. The dynamics can be simplified by focusing on the long time behavior of such systems (leaving fast transients unresolved) and calculating fast modes as functions of the slow ones. Ideally this leads to low dimensional manifolds in high-dimensional state space. In the special case of singularly perturbed system, they are understood quite well and called slow invariant manifolds.

An open problem is how the slow manifolds can be used to simplify the solution of optimal control problems (OCP) that involve multiple time scale ODE constraints.

II. Slow Manifold Computation

In dissipative dynamical systems geometrically the bundling of trajectories (on a fast time scale) to low-dimensional manifolds is observed. Once trajectories reach the neighborhood of the slow manifold, they will evolve slowly and will never leave this manifold neighborhood. Thus, this manifold is called *slow invariant attracting manifold* (SIAM).

The aim of slow manifold computation techniques is to approximately compute the SIAM as the graph of a function of only a few selected species (so called *reaction progress variables*). Thus, manifold-based model reduction generate a function $h : \mathbb{R}^{n_s} \to \mathbb{R}^{n_f}$ (n_s is the number of slow variables resp. reaction progress variables and n_f is the number of fast variables), such that $\big(z_s, h(z_s)\big)$ approximates points of the SIAM.

In order to investigate optimal control benchmark problems, we consider singularly perturbed systems, i.e. systems where the ODE can be transformed into the following form:

$$\dot{z_s}(t) = f_s(z_s(t), z_f(t)) \tag{1a}$$
$$\varepsilon\dot{z_f}(t) = f_f(z_s(t), z_f(t)). \tag{1b}$$

Two methods relevant in our context for the approximative calculation of the SIAM are briefly reviewed in the following subsections.

A. Zero Derivative Principle

The main idea of the Zero Derivative Principle (ZDP) [1],[6] for model reduction of singularly perturbed systems is to identify for given values of the slow variables z_s^* a point z_f^* such that the higher-order time derivatives of fast components vanish, i.e

$$\frac{\mathrm{d}^m f_f(z_s^*, z_f^*)}{\mathrm{d}t^m} = 0 \qquad \text{for a given } m \in \mathbb{N}. \tag{2}$$

B. Method of Lebiedz and Unger

Another approach proposed by Lebiedz and Unger [4] is motivated geometrically: Among arbitrary trajectories of (1) for which the slow components end within the time $t_1 - t_0$ in the state z_s^* the corresponding part of the trajectory on the SIAM is characterized by the smallest curvature (see also [2],[3]). This motivates optimization problem (3) which is a variational boundary value problem (BVP).

$$\min_{z(\cdot)=\left(z_s(\cdot),z_f(\cdot)\right)} \quad \left\|\ddot{z}(t_0)\right\|_2^2 \tag{3a}$$
$$\text{s.t.} \quad \dot{z}_s = f_s\big(z_s, z_f\big), \quad t \in [t_0, t_1] \tag{3b}$$
$$\varepsilon\dot{z}_f = f_f\big(z_s, z_f\big), \quad t \in [t_0, t_1] \tag{3c}$$
$$z_s(t_1) = z_s^*. \tag{3d}$$

In our application context we also use the local reformulation of problem (3), where $t_0 = t_1$.

III. Optimal Control

One of our research interests is to solve optimal control problems involving multiple time scales as it appears frequently e.g. in the field of chemical engineering. Thus, we

consider the following (typically high-dimensional) OCP:

$$\min_{z_s,z_f,u} \quad \int_0^T L(z_s,z_f,u)\,\mathrm{d}t \tag{4a}$$
$$\text{subject to} \quad \dot{z_s} = f_s(z_s,z_f,u) \tag{4b}$$
$$\varepsilon \dot{z_f} = f_f(z_s,z_f,u) \tag{4c}$$
$$z_s(0) = z_s^{(0)},\ z_f(0) = z_f^{(0)} \tag{4d}$$

Applying the model reduction methods presented in the last section and assuming the control u to be a slow variable, yields the lower dimensional problem (cf. [5])

$$\min_{z_s,u} \quad \int_0^T L(z_s,h(z_s,u),u)\,\mathrm{d}t \tag{5a}$$
$$\text{subject to} \quad \dot{z_s} = f_s(z_s,h(z_s,u),u) \tag{5b}$$
$$z_s(0) = z_s^{(0)}. \tag{5c}$$

This systems has the advantage, that it has significantly less optimization variables and the ODE (5) is less stiff, which makes it solvable by fast explicit numerical integrators compared to implicit methods required for stiff ODE. However, numerical solution methods for OCPs like the multiple shooting method need repeated evaluation of the function h as well as its partial derivatives h_{z_s} and h_u.

Therefore, it would be beneficial to combine the calculation of the SIM and the optimal control problem. This is obviously possible, if the approximation $h(z_s)$ of the SIM can be formulated as a (nonlinear) root finding problem $r(z_s,z_f,u) = 0$, e.g. with the ZDP method. Thus, we propose to solve the following OCP instead of (5):

$$\min_{z_s,z_f,u} \quad \int_0^T L(z_s,z_f,u)\,\mathrm{d}t \tag{6a}$$
$$\text{subject to} \quad \dot{z_s} = f_s(z_s,z_f,u) \tag{6b}$$
$$0 = r(z_s,z_f,u) \tag{6c}$$
$$z_s(0) = z_s^{(0)}. \tag{6d}$$

IV. Application to Chemical Reactions

We apply the ideas presented in the last sections to a benchmark OCP motivated by the Michaelis-Menten-Henri mechanism

$$S + E \leftrightharpoons SE \to P + E, \tag{7}$$

modeling the reaction of substrate S to a product P via a substrate-enzyme-complex SE with the help of enzyme E. Simplifying the ODE given by (7) and introducing an artificial objective function yields OCP (8).

$$\min_{z_s,z_f,u} \quad \int_0^5 -50 z_f + u^2\,\mathrm{d}t \tag{8a}$$
$$\text{s.t.} \quad \begin{aligned} \dot{z_s} &= -z_s + (z_s+0.5)\,z_f + u, \\ \varepsilon \dot{z_f} &= z_s - (z_s+1)\,z_f, \\ z_s(0) &= 1, \end{aligned} \tag{8b}$$

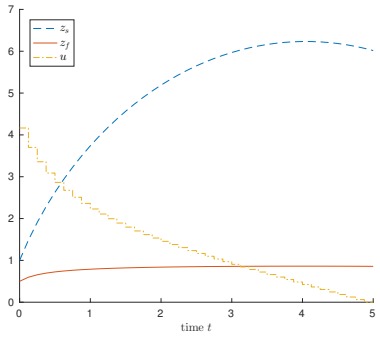

Fig. 1. Numerical Solution of (8).

where the control $u(t) \in [0,10]$ represents the possibility to add some substrate (corresponds to variable z_s) to the system and ε describes the time-scale separation (between the time evolution of z_s and z_f).

Figure 1 shows the results of the numerical solution of (8) using the multiple-shooting scheme with an implicit Radau-2A integrator. If we refer to the solution of the proposed OCP (6) as $(z_s^{\text{app}}, z_f^{\text{app}}, u^{\text{app}})$ and to the solution of (8) as $(z_s^{\text{orig}}, z_f^{\text{orig}}, u^{\text{orig}})$, then it holds

$$\begin{aligned} &\max\left\{||z_s^{\text{orig}} - z_s^{\text{app}}||_\infty, ||z_f^{\text{orig}} - z_f^{\text{app}}||_\infty, ||u^{\text{orig}} - u^{\text{app}}||_\infty\right\} \\ &= ||z_s^{\text{orig}} - z_s^{\text{app}}||_\infty \approx 0.05, \end{aligned} \tag{9}$$

which gives a relative error of $\approx 0.2\%$ for both objective functional value and $||z_s^{\text{orig}} - z_s^{\text{app}}||_\infty / ||z_s^{\text{orig}}||_\infty$. Although, the proposed method uses exactly as many variables than the original OCP, we observe a speed up of factor 4 for solving OCP (8) due to the use of an explicit integration scheme.

References

[1] C. W. Gear and T. J. Kaper and I. G. Kevrekidis and A. Zagaris, *Projecting to a Slow Manifold: Singularly Perturbed Systems and Legacy Codes*, SIAM Journal on Applied Dynamical Systems, 4 (2005), pp. 711–732.

[2] D. Lebiedz, *Computing minimal entropy production trajectories: An approach to model reduction in chemical kinetics*, Journal of Chemical Physics, 120 (2004), pp. 6890–6897.

[3] D. Lebiedz, J. Siehr and J. Unger, *A variational principle for computing slow invariant manifolds in dissipative dynamical systems*, SIAM Journal on Scientific Computing, 33 (2011), pp. 703–720.

[4] D. Lebiedz and J. Unger, *On unifying concepts for trajectory-based slow invariant attracting manifold computation in kinetic multi-scale models*, Mathematical and Computer Modelling of Dynamical Systems, 22 (2016), pp. 87–112.

[5] M. Rehberg , *A Numerical Approach to Model Reduction for Optimal Control of Multiscale ODE*, PhD thesis, 2013.

[6] A. Zagaris, C. W. Gear, T. J. Kaper and Y. G. Kevrekidis, *Analysis of the accuracy and convergence of equation-free projection to a slow manifold*, Mathematical Modelling and Numerical Analysis, 43 (2009), pp. 757–784.

Revealing approximate low dimensional manifolds for accelerating atomistic simulations

Eliodoro Chiavazzo*, Juan M. Bello-Rivas†, C. William Gear†, Ioannis G. Kevrekidis †
*Politecnico di Torino/Energy Department, Turin, Italy
†Princeton University/Department of Chemical and Biological Engineering, Princeton, NJ-USA

***Abstract*— When studying big molecules, a notorious issue in using molecular dynamics simulators is often the time scale separation. While most of the phenomena of interest occurs on pretty large timescales (e.g. from millisecond to minutes), typical current computational capabilities only allow us to explore much shorter dynamics, with the system configuration trapped within small irrelevant regions of the configuration space. In this work, we report the latest developments on iMapD, a method that has been recently proposed to help alleviate the above computational issue. To this end, we show an effective approach to gradually construct low-dimensional effective free energy surfaces in the configuration space and, concurrently, exploit their smoothness (and slowness) to rapidly access new unexplored system configurations.**

I. Introduction

When using atomistic models, a typical behavior of complex systems can be trapping into small regions of the configuration space for very long time before the transitioning to a different (and interesting) system conformation happens.

We have recently proposed the iMapD method [1], [2] with the purpose of enhancing the sampling of stochastic solvers among which, interestingly, those that are used for molecular dynamics. The very basic idea of our approach consists in letting the solver explore a neighborhood of the current metastable state in order to collect enough samples to learn the local geometry of the low-dimensional effective free energy surface - FES. To this end, the FES geometry can be revealed automatically using machine learning algorithms, such as Diffusion Maps - DMAP [3], [4] as done in our work. First of all, the above step enables us to establish a low-dimensional description of the problem in terms of only a few meaningful diffusion coordinates. Moreover, with the help of appropriate algorithms [5], the edge of the so far explored FES portion can be identifies (conveniently in the low-dimensional space). In the attempt of finding new conformations of the system (i.e. new metastable states), in the spirit of the "equation-free approach [6], [7], samples at the boundary are projected outwards with respect to the already known phase-space region. Here, relying upon the smoothness of the FES surface, we are able to force the simulator to restart in regions that are likely sufficiently far from the already explored ones. Clearly, the above procedure can be iterated several times and, according to our experience and numerical results, it can potentially lead to a saving of several orders of magnitudes in computational time (as compared to the original simulation).

The most interesting features of iMapD are: i) it does not require prior knowledge on the investigated system (e.g. in terms of the suitable collective variables); ii) it does not perturb significantly the system as no external forces are applied and most of the simulation runs unbiased. In this work, we will present the implementation details of iMapD and, with the help of a few examples, we will critically discuss both challenges and opportunities of the method.

Acknowledgment

Gerhard Hummer, Roberto Covino and Ralph Coifman are gratefully acknowledged for fruitful discussions. E.C. acknowledges partial financial support by the Politecnico di Torino through the Starting Grant 56_RIL16CHE01. I.G.K. acknowledges partial support by the US National Science Foundation, the US AFOSR (Dr. Darema) and DARPA.

References

[1] Chiavazzo E., Coifman R.R., Covino R., William Gear C., Georgiou A.S., Hummer G. and Kevrekidis I.G., *iMapD: intrinsic Map Dynamics exploration for uncharted effective free energy landscapes*, arXiv:1701.01513, 2016.

[2] Georgiou A.S. , Bello-Rivas J.M., Gear C.W., Wu Hau-Tieng, Chiavazzo E., Kevrekidis I.G. *An exploration algorithm for stochastic simulators driven by energy gradients*, Entropy (in press), 2017.

[3] Coifman R.R. et al. *Geometric diffusions as a tool for harmonic analysis and structure definition of data: Diffusion maps*, Proceedings of the National Academy of Sciences 102:74267431, 2005.

[4] Chiavazzo E., Gear C., Dsilva C., Rabin N., Kevrekidis I. G. *Reduced models in chemical kinetics via nonlinear data-mining*, Processes 2:112140, 2014.

[5] Gear C., Chiavazzo E., Kevrekidis I.G. *Manifolds defined by points: Parameterizing and boundary detection (extended abstract)*, AIP Conference Proceedings 1738(020005):14, 2016.

[6] Kevrekidis I. G., Gear C., Hummer G. *Equation free: The computed-aided analysis of complex multiscale systems*, AIChe Journal 50:13461355, 2004.

[7] Kevrekidis I.G. et al. *Equation free: The computed-aided analysis of complex multiscale systems*, Comm. Math. Sci 1:715762, 2003.

Session: Mechanism Simplification 1

Chair: D. A. Goussis

Title: Asymptotic Analysis of a Pharmacokinetics Model
Authors: L. Y. Michalaki, D. A. Goussis

Title: ASVDADD Algorithm for Automatic Selection of RCCE Constraints
Authors: G. P. Beretta, M. Janbozorgi

Title: Computational Identification of Quasi-Steady State and Partial Equilibrium in Chemical Kinetics
Authors: P. Zhao, T. Lu, C. K. Law, S. H. Lam

Asymptotic analysis of a pharmacokinetics model

Lida Y. Michalaki*, Dimitris A. Goussis †‡
*School of Chemical Engineering, NTUA, Athens, Greece
†School of Applied Mathematical and Physical Sciences, NTUA, Athens, Greece
‡Department of Mechanical Engineering, Khalifa University of Science, Technology and Research, Abu Dhabi, UAE

***Abstract*— The dynamics of a multiscale pharmacokinetics model are investigated. In particular, the influence of the reaction rate constant k_{tp} of a reaction involving two forms of the drug, $C_T \rightarrow C$, is explored. The solution of this model is immediately directed on a manifold, on which increasing values of k_{tp} generate the expected behavior; i.e., larger concentrations of C. However, when further in time the dimensions of the manifold change, this behavior is reversed. By employing the CSP methodology, it is shown that this unexpected feature is the result of conflicting fast and slow dynamics.**

I. Introduction

One major challenge in the design of drugs is that a certain compound might not be the appropriate for all patient. Genetic or epigenetic factors, life style, diet, sex, age, weight and other such factors might cause variations in the response to drug treatment [1]. The degree to which such factors affect the action of a given drug is a subject of current research.

These issues are currently studied on the basis of pharmacology-based mathematical models, among them the target-mediated drug disposition models. These models simulate the phenomenon in which a drug binds with high affinity to its pharmacological target site (such as a receptor), to such an extent that this affects its pharmacokinetic characteristics. TMDD models are often over-parameterized and their parameters are difficult to estimate based on available data [2], [3]. Model reduction methodologies are thus employed in order to identify the most influential components of the model.

Here, the results of the analysis of a popular TMDD model will be reported. The discussion will focus on an unexpected behavior, which highlights the significance of the fast/slow dynamics.

II. The Pharmacokinetics Model

The TMDD model considered here describes the interaction of a drug with its target, the formation of their biding and its degradation. This model, shown in the left panel of Fig. 1 is a three-compartment pharmacokinetic model, the central compartment of which represents the blood plasma and involves N=5 variables [4]. Drug in the central compartment (C) binds (reaction 5) to free receptors (R), in order to form a drug receptor complex (RC). The complex may dissociate at the first-order rate (reaction 6) or be internalized and degraded by the first-order rate process of endocytosis (reaction 10). Free drug can also be directly eliminated at a first-order rate (reaction 3) or be distributed to a nonspecific tissue-binding site (C_T) by first- order processes (reactions 7 and 4). Free receptor can be synthesized at a zero-order rate (reaction 8) and degraded at a first-order rate (reaction 9). Regarding the way the free drug is administrated to the central compartment, there are three distinct cases. First, the free drug can be transferred from another compartment, the depot compartment. There, the concentration of the drug is referred by the variable C_d and through reaction 1 it can be transferred in the central compartment. Alternatively, drug can be administered by intravenous bolus (a relatively large dose of medication

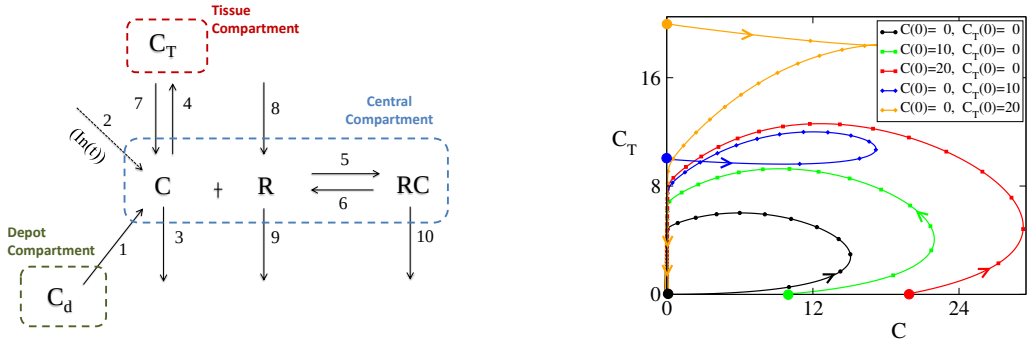

Fig. 1. Left: A schematic representation of the pharmacokinetic mechanism. Right: The multiscale character of the TMDD model dots on the trajectories denote equidistant intervals of time.

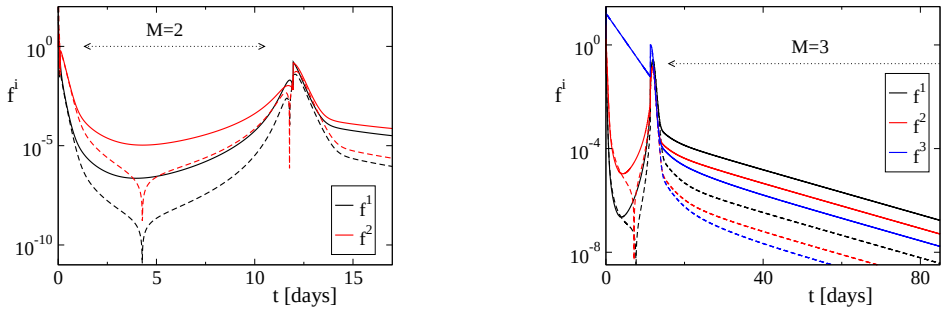

Fig. 2. The evolution of the fast amplitudes after one (solid) and two (dashed) $\mathbf{b^r}$-refinements, for M=2 (left) and M=3 (right).

administered into a vein) in a short period a time-depending function, which is represented by the function In(t). Finally, drug can be administered by a subcutaneous dose, represented by a non-zero initial value of the free drug in the central compartment.

This model is characterised by multiple time scales, as suggested by the right panel of Fig. 1, where the projection of the trajectory on the $C - C_T$ plane is displayed. A more detailed picture of the multiscale character of model emerges from the evolution of the fast amplitudes for the M=2 and M=3 cases, shown in Fig. 2. These are the first M amplitudes, after casting the governing system in the CSP form $d\mathbf{y}/dt = \mathbf{a}_1 f^1 + \cdots + \mathbf{a}_5 f^5$ [5]. The amplitudes, shown in Fig. 2 are computed after one and two $\mathbf{b}^r$-refinements.

Figure 2 shows that the solution initially evolves on a 3-dim. manifold (N-M) and then on a 2-dim. one. Figure 3 shows the temporal evolution of C and C_T for two values of the rate constant k_{tp} of the 7th reaction, which involves two forms of the drug, $\mathbf{C}_T \rightarrow \mathbf{C}$. It is shown that when the solution evolves on the M=2 manifold, increasing values of k_{tp} generates the expected results; i.e. larger values of C. However, when the solution evolves on the M=3 manifold this is reversed; i.e., smaller values of C are obtained.

III. Results

As it is suggested by the pharmacokinetics mechanism displayed in the left panel of Fig. 1, the dependence of the drug concentration in the central compartment, C, to the rate of the 7th reaction, r_7, can be schematically depicted as $dC/dt = g(+r_7)$; i.e., the 7th reaction tends to generate C. The same functional form applies when the trajectory evolves on the M=2 manifold. However, when the solution evolves on the M=3 manifold this form changes to $dC/dt = g(-r_7)$; i.e., the 7th reaction tends to deplete C. It will be shown that this reversal is due to the additional constraint that accompanies the transition from M=2 to M=3.

References

[1] V. Kantae, E. H. Krekels, M. J. Van Esdonk, P. Lindenburg, A. C. Harms, C. A. Knibbe, P. H. Van der Graaf, T. Hankemeier, Integration of pharmacometabolomics with pharmacokinetics and pharmacodynamics: towards personalized drug therapy, Metabolomics 13 (1) (2017) 9.

[2] L. Gibiansky, E. Gibiansky, T. Kakkar, P. Ma, Approximations of the target-mediated drug disposition model and identifiability of model parameters, Journal of pharmacokinetics and pharmacodynamics 35 (5) (2008) 573–591.

[3] W. E. De Witte, M. Danhof, P. H. Van Der Graaf, E. C. de Lange, In vivo target residence time and kinetic selectivity: the association rate constant as determinant, Trends in Pharmacological Sciences 37 (10) (2016) 831–842.

[4] D. E. Mager, W. Krzyzanski, Quasi-equilibrium pharmacokinetic model for drugs exhibiting target-mediated drug disposition, Pharmaceutical research 22 (10) (2005) 1589–1596.

[5] S. H. Lam, D. A. Goussis, Understanding complex chemical kinetics with Computational Singular Perturbation, Proc. Combust. Institute 22 (1989) 931–941.

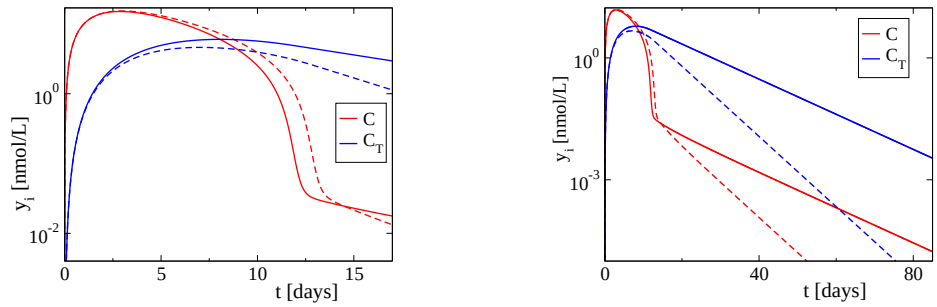

Fig. 3. The evolution of the concentration of C and C_T for $k_{pt} = 0.1$ (solid) and $k_{pt} = 0.2$,(dashed).

ASVDADD algorithm for automatic selection of RCCE constraints

Gian Paolo Beretta* and Mohammad Janbozorgi†
*Department of Mechanical and Industrial Engineering (DIMI), Brescia State University, Brescia, Italy
†Department of Mechanical and Aerospace Engineering (MAE), University of California, Los Angeles, CA

***Abstract*— The Rate-Controlled Constrained-Equilibrium (RCCE) model reduction scheme for chemical kinetics provides acceptable accuracies with a number of differential equations much lower than the number of species in the underlying Detailed Kinetic Model (DKM). It was originally proposed by James C. Keck (see [1-3] and references therein). To yield good approximations the method requires accurate identification of the rate controlling constraints. Until recently, a drawback of the RCCE scheme has been the absence of a fully automatable and systematic procedure to identify the most effective constraints for a given range of thermodynamic conditions and a required level of approximation. In a recent paper [4], we have proposed a new methodology for such identification based on a simple algebraic analysis of the results of a preliminary simulation of the full underlying DKM, focusing on the behavior of the degrees of disequilibrium (DoD) of the individual chemical reactions. The new methodology is based on computing an Approximate Singular Value Decomposition of the Actual Degrees of Disequilibrium (ASVDADD) obtained as functions of time in the probe DKM simulation. The procedure identifies a low dimensional subspace in DoD space, from which the actual DoD traces do not depart beyond a fixed distance related to the first neglected singular value of the matrix of DoD traces. The effectiveness and robustness of the method has been demonstrated [4-6] for various cases of a very rapid supersonic nozzle expansion of the products of hydrogen and methane oxycombustion and for the case of methane/oxygen ignition.**

The RCCE method models the local non-equilibrium states as partially equilibrated states with the local composition $\boldsymbol{X}^{\rm CE} = N_j/\sum_{k=1}^{n_{\rm sp}} N_k$ that minimizes the Gibbs free energy subject to: (1) the local values of temperature T, pressure p, molar amounts of elements $N_i^{\rm EL} = \sum_{j=1}^{n_{\rm sp}} a_{ij}^{\rm EL} N_j$ (where $a_{ij}^{\rm EL}$ represents the number of atoms of element i in a molecule of species j) and (2) the local values of a set of n_c slowly varying and, hence, rate-controlling (RC) constraints given by linear combinations of the molar amounts, $c_i(\boldsymbol{N}) = \sum_{j=1}^{n_{\rm sp}} a_{ij}^{\rm RC} N_j$, where the matrix $a_{ij}^{\rm RC}$ is the heart of the model in that it is assumed to fully characterize the rate-controlling bottlenecks of the kinetic mechanism. For ideal gas behavior, $\mu_j(T,p,\boldsymbol{X}) = g_{j,\rm pure}(T,p) + RT\ln X_j$, the constrained maximization yields the composition $\ln X_j^{\rm CE} = -g_{j,\rm pure}(T,p)/RT - \sum_{i=1}^{n_{\rm el}} \gamma_i^{\rm EL} a_{ij}^{\rm EL} - \sum_{i=1}^{n_c} \gamma_i^{\rm RC} a_{ij}^{\rm RC}$. The Lagrange multipliers $\gamma_i^{\rm EL}$ and $\gamma_i^{\rm RC}$ are called elemental and constraint potentials, respectively. For the ℓ-th chemical reaction $\sum_{j=1}^{n_{\rm sp}} \nu_{j\ell} A_j = 0$, the stoichiometric balance requires that $b_{i\ell}^{\rm EL} = \sum_{j=1}^{n_{\rm sp}} a_{ij}^{\rm EL} \nu_{j\ell} = 0$. An advantage of the RCCE approximation is that the composition depends only on the $n_{\rm el} + n_{\rm c}$ parameters $\gamma_i^{\rm EL}$ and $\gamma_i^{\rm RC}$, instead of the $n_{\rm sp}$ molar amounts of species which can be many more. In the CFD modeling context, this means that in addition to the continuity, Navier-Stokes, and energy balance equations, the $n_{\rm sp}$ species balance equations can be effectively substituted by the $n_{\rm el} + n_{\rm c}$ balance equations for the elemental and constraint potentials, thus achieving a substantial model reduction that has a built-in strong thermodynamic consistency and does not require to cut the number of species nor the number of reactions to be taken into account.

The recently proposed ASVDADD algorithm [4] allows the identification of optimal sets of constraints with no need for deep knowledge and understanding of chemical kinetics fundamentals such as chain branching, radical formation, etc., thus making the RCCE method accessible to a broad range of scientists and engineers. The algorithm is based on the following basic observation. The degree of disequilibrium (DoD) of reaction ℓ, defined by $\phi_\ell = \ln r_\ell^+/r_\ell^-$ where $r_\ell^\pm$ are the forward and reverse rates of reaction ℓ, is given in general by $\phi_\ell = \ln(r_\ell^+/r_\ell^-) = \sum_{j=1}^{n_{\rm sp}} \Lambda_j\, \nu_{j\ell}$ where $\Lambda_j = -\mu_j/RT$ are the dimensionless entropic chemical potentials that can be viewed as the components of the $n_{\rm sp}$-vector $\boldsymbol{\Lambda}$. Also the $n_{\rm el}$ rows of the elemental composition matrix $a_{ij}^{\rm EL}$ can be viewed as the components of the $n_{\rm sp}$-vectors $\boldsymbol{a}_i^{\rm EL}$. Due to relation $\sum_{j=1}^{n_{\rm sp}} a_{ij}^{\rm EL}\nu_{j\ell} = 0$, the $n_{\rm el}$-dimensional linear span of vectors $\boldsymbol{a}_i^{\rm EL}$ is the left null space of the matrix $\nu_{j\ell}$ of stoichiometric coefficients, often called the inert subspace.

The projection of vector $\boldsymbol{\Lambda}$ onto the inert subspace can be written as $\boldsymbol{\Lambda}_{{\rm span}(\{\boldsymbol{a}_i^{\rm EL}\})} = \sum_{i=1}^{n_{\rm el}} \gamma_i^{\rm EL} \boldsymbol{a}_i^{\rm EL}$ where the coefficients $\gamma_i^{\rm EL}$ can be readily computed (see, e.g., the appendix of Ref. [7]). Since $\boldsymbol{\Lambda}_{{\rm span}(\{\boldsymbol{a}_i^{\rm EL}\})}$ does not contribute to the DoD of any reaction (in fact, $\sum_{j=1}^{n_{\rm sp}} \sum_{i=1}^{n_{\rm el}} \gamma_i^{\rm EL}\, a_{ij}^{\rm EL}\, \nu_{j\ell} = \sum_{i=1}^{n_{\rm el}} \gamma_i^{\rm EL}\, b_{i\ell}^{\rm EL} = 0$), we call the vector $\boldsymbol{\Lambda}_{\rm DoD} = \boldsymbol{\Lambda} - \boldsymbol{\Lambda}_{{\rm span}(\{\boldsymbol{a}_i^{\rm EL}\})} = \boldsymbol{\Lambda} - \sum_{i=1}^{n_{\rm el}} \gamma_i^{\rm EL} \boldsymbol{a}_i^{\rm EL}$ or, equivalently, $\Lambda_{{\rm DoD},j} = \Lambda_j - \sum_{i=1}^{n_{\rm el}} \gamma_i^{\rm EL}\, a_{ij}^{\rm EL}$ the "overall DoD vector." In fact, it contains the information about the DoD's ϕ_ℓ of all the reactions, $\phi_\ell = \sum_{j=1}^{n_{\rm sp}} \Lambda_{{\rm DoD},j}\, \nu_{j\ell}$, and it is the null vector if and only if all reactions are equilibrated, in the sense that their DoD's are all zero. Notice that within

the RCCE model $\boldsymbol{\Lambda}_{\rm DoD}^{\rm RCCE} = \sum_{i=1}^{n_{\rm c}} \gamma_i^{\rm RC} \boldsymbol{a}_i^{\rm RC}$ or, equivalently, $\Lambda_{{\rm DoD},j}^{\rm RCCE} = \sum_{i=1}^{n_{\rm c}} \gamma_i^{\rm RC}\, a_{ij}^{\rm RC}$.

Now let us consider a CFD numerical simulation in which the index $z = 1, \ldots, Z$ labels the space-time discretization (i.e., z labels both the finite volumes or elements of the mesh as well as the time grid). If we adopt the full DKM and solve the full set of balance equations including those for all the species, the resulting overall DoD vectors form an $n_{\rm sp} \times Z$ matrix $\Lambda_{{\rm DoD},jz}^{\rm DKM} = \Lambda_{{\rm DoD},j}(z)$ that has rank $r = n_{\rm sp} - n_{\rm el}$. If instead the local states are described according to the RCCE assumption defined above, the $n_{\rm sp} \times Z$ matrix $\Lambda_{{\rm DoD},jz}^{\rm RCCE} = \Lambda_{{\rm DoD},j}^{\rm RCCE}(z) = \sum_{i=1}^{n_{\rm c}} \gamma_i^{\rm RC}(z) a_{ij}^{\rm RC}$ has rank equal to the (typically much smaller) number $n_{\rm c}$ of constraints.

In order to identify the constraint matrix $a_{ij}^{\rm RC}$ that allows such approximation, the idea behind the ASVDADD algorithm is to probe the DKM by running a preliminary full DKM computation, possibly on a submesh of the full problem and for a shorter time so as to span a limited range of temperatures, pressures and compositions. The goal of such computation is to obtain the $r \times Z$ matrix $\boldsymbol{D}$ with elements $\Lambda_{{\rm DoD},jz}^{\rm DKM}$. Then we compute its singular value decomposition (SVD). As is well known the result can be written formally in reduced form as $\boldsymbol{D} = \boldsymbol{U}\, {\rm diag}(\boldsymbol{\sigma})\, \boldsymbol{V}$ where $\boldsymbol{U}$ is an $n_{\rm sp} \times r$ unitary matrix whose r columns represent an orthonormal basis for the column space of $\boldsymbol{D}$, $\boldsymbol{V}$ is an $r \times Z$ unitary matrix whose r rows represent an orthonormal basis for the row space of $\boldsymbol{D}$, and $\boldsymbol{\sigma}$ is the r-vector of singular values of $\boldsymbol{D}$ in decreasing order. Explicitly, the (reduced form) SVD decomposition of the overall DoD matrix can be written as $\Lambda_{{\rm DoD},jz}^{\rm DKM} = \sum_{k=1}^{r} U_{jk}\, \sigma_k\, V_{kz} = \sum_{k=1}^{r} U_{jk}\, \gamma_{kz}^{\rm DKM}$, where $\sigma_1 \geq \sigma_2 \geq \cdots \geq \sigma_r > 0$ and we defined $\gamma_{kz}^{\rm DKM} = \sigma_k\, V_{kz}$.

Next, we use the well-known Eckart-Young theorem of linear algebra, whereby if in the SVD of matrix $\boldsymbol{D}$ we set to zero the singular values for $k > n_{\rm c}$ (i.e., we set $\sigma_{n_{\rm c}+1} = \sigma_{n_{\rm c}+2} = \cdots = \sigma_r = 0$) then we obtain the "closest" rank$\leq n_{\rm c}$ approximation $\boldsymbol{D}_{\rm approx}$ of the original matrix $\boldsymbol{D}$ in the sense that the Frobenius norm distance $\|\boldsymbol{D}_{\rm approx} - \boldsymbol{D}\|_{\rm Fro}$ between the two matrices is minimal. Such norm distance is equal to $\sum_{k=n_{\rm c}+1}^{r} \sigma_k^2)^{1/2}$ and can be taken as a measure of the error introduced by the approximation. Therefore, if we accept such level of approximation, we can setup an optimal RCCE model with $n_{\rm c}$ constraints by selecting as our constraint matrix the first $n_{\rm c}$ columns of the matrix $\boldsymbol{U}$. In fact, by setting (ASVDADD choice of RCCE constraints): $a_{ij}^{\rm RC} = U_{ji}$ for $i = 1, \ldots, n_{\rm c}$ we obtain $\Lambda_{{\rm DoD},jz}^{\rm RCCE} = \sum_{k=1}^{n_{\rm c}} U_{jk}\, \gamma_{kz}^{\rm RC} = \sum_{i=1}^{n_{\rm c}} \gamma_{iz}^{\rm RC}\, a_{ij}^{\rm RC}$ Interestingly, the r columns of the matrix $\boldsymbol{U}$ provide at once the entire set of optimal RCCE constraints, already ordered in decreasing order of importance. Essentially, in conclusion, the ASVDADD algorithm identifies all the constraints that characterize the kinetic bottlenecks of the underlying DKM in effect in the range of conditions of the chosen probe simulation, and it ranks them in decreasing order of their relative contribution to the overall degree of disequilibrium. These features make the algorithm suitable for adaptive or tabulation strategies and therefore opens up the advantages of the RCCE method to CFD simulation.

The effectiveness and robustness of the methodology has already been demonstrated in [4-5] for several test cases of increasing complexity in the framework of oxy-combustion of hydrogen (8 species, 24 reactions) and methane (29 species, 133 reactions) as well as in [6] where a demonstration is given for the even more complex full GRI-Mech 3.0 kinetic scheme (53 species, 325 reactions) for methane/air combustion including nitrogen oxidation.

The excellent performance of the ASVDADD constraints confirms the conclusion that the new algorithm essentially resolves the difficulties that have prevented the RCCE method from a more widespread use in model order reduction of detailed combustion kinetic models of hydrocarbon fuels, making it accessible to the non-experts in chemical kinetics.

The RCCE model can be integrated most efficiently by rewriting the balance equations as rate equations for the elemental and constraint potentials (see Eqs. 136-139 of Ref. 3) to obtain $n_{\rm el} + n_{\rm nc} + 2$ implicit differential equations which together with the $n_{\rm sp}$ RCCE expressions for the mole fractions can be solved for the $n_{\rm sp} + 2$ state variables $T(t)$, $p(t)$, and $N_j(t)$, and the $n_{\rm el} + n_{\rm c}$ constraint potentials $\gamma_i^{\rm EL}(t)$ and $\gamma_i^{\rm RC}(t)$.

REFERENCES

[1] J.C. Keck, "Rate-controlled constrained equilibrium method for treating reactions in complex systems," in: R.D. Levine, M. Tribus (Eds.), *The Maximum Entropy Formalism*, MIT Press, Cambridge, MA, 1979, pp. 219-245.[1]

[2] G.P. Beretta and J.C. Keck, "The constrained-equilibrium approach to nonequilibrium dynamics," in: R.A. Gaggioli (Ed.), *Second Law Analysis and Modeling*, ASME Book H0341C-AES, vol.3, ASME, New York, 1986, pp. 135-139.[1,2]

[3] G.P. Beretta, J.C. Keck, M. Janbozorgi, and H. Metghalchi, "The rate-controlled constrained-equilibrium approach to far-from-local-equilibrium thermodynamics," *Entropy*, vol. 14, 92-130 (2012).

[4] G.P. Beretta, M. Janbozorgi, and H. Metghalchi, "Degree of Disequilibrium Analysis for Automatic Selection of Kinetic Constraints in the Rate-Controlled Constrained-Equilibrium Method," *Combustion and Flame*, vol. 168, 342-364 (2016).

[5] G.P. Beretta, M. Janbozorgi, and H. Metghalchi, "Use of Degree of Disequilibrium Analysis to Select Kinetic Constraints for the Rate-Controlled Constrained-Equilibrium (RCCE) Method," *Proceedings of ECOS 2015* – the 28th International Conference On Efficiency, Cost, Optimization, Simulation and Environmental Impact of Energy Systems, Pau, France, June 30-July 3, 2015.[2]

[6] L. Rivadossi and G.P. Beretta, "Validation of the ASVDADD constraint selection algorithm for effective RCCE modeling of natural gas ignition in air," *Proceedings of IMECE2016* – the ASME 2016 International Mechanical Engineering Congress and Exposition, November 11-17, 2016, Phoenix, Arizona, USA – paper IMECE2016-65323.[2]

[7] G.P. Beretta, "Nonlinear Quantum Evolution Equations to Model Irreversible Adiabatic Relaxation With Maximal Entropy Production and Other Nonunitary Processes," *Reports on Mathematical Physics*, vol. 64, 139-168 (2009).

[1] Available online: http://www.jameskeckcollectedworks.org/

[2] Available online: http://www.gianpaoloberetta.info/

Computational Identification of Quasi-Steady State and Partial Equilibrium in Chemical Kinetics

Peng Zhao*, Tianfeng Lu†, Chung K. Law‡ and Sau H. Lam‡
* Department of Mechanical Engineering, Oakland University, Rochester, MI 48309, USA
† Department of Mechanical Engineering, University of Connecticut, Storrs, CT 06269, USA
‡Department of Mechanical and Aerospace Engineering, Princeton University, Princeton, NJ 08544, USA

***Abstract*— Assumptions of quasi steady-state (QSS) species and partial equilibrium (PE) reactions have long been applied in the computation and analysis of reacting flows to reduce stiffness and cost. In this study, based on a recent CSP theory, numerical evidence is presented for an explicit analytical expression of fast radicals exhibiting QSS behavior. Meanwhile, a strategy of identifying non-independent equations induced by partial equilibrium reactions is proposed by analyzing the partial Jacobian of fast species. A two-stage ignition case of n-heptane/air using a detailed mechanism is taken as an example to demonstrate both aspects.**

I. Introduction

Stiffness removal in chemical kinetics has attracted extensive research interests in recent years [1]. An analytical formulation for the efficient implementation of computational singular perturbation (CSP) has been theoretically constructed by Lam in CSP 2016 [2], in which insights have been made on the fastest species based on its time scale ($\tau_i = -\frac{1}{\mathbf{J}_{ii}}$), and the corresponding QSS value could be accurately predicted across the thin transition layer at each time step. As a result, tedious explicit integration to resolve the apparent exponential transition layer is avoided and the integration time step could be largely extended. Furthermore, the process does not involved expensive eigen-decomposition.

In Sec. 2 of [2], a toy problem is proposed to address the potential coupling between the fast species by a fast reversible reaction. It is shown that a linear combination of a pair of fast species could be a slow variable, and can be considered approximately constant within the thin transition layer. However, in real kinetic systems, those fast species coupled by a fast reversible reaction frequently do not appear in pairs; instead, there are many different ways of coupling among them.

In this study, the enabling assumption of Eqns. 4 and 5 in [2] is computationally demonstrated for a toy problem together with different real systems to show the usefulness and application of the theory, especially for simpler ones where the number of radicals is limited and large gaps in the species lifetime exist. To further computationally demonstrate PE in real problems, a general formulation is then proposed, based on the idea of adaptive hybrid integration (AHI) [3], and the number of independent reactions could be identified in the integration process or by post-processing.

II. Method of Identifying non-independent equations

The underlying thought is that at any given instant, those species with time scale faster than the wanted integration time step Δt, i.e., $\tau_i < \Delta t^* \beta$ where β is a safety factor larger than 1, are considered to be fast, and implicit integration is used for its evolution. As such, we have $\frac{d\boldsymbol{y}}{dt} = \boldsymbol{\omega}(\boldsymbol{y})$, where $\boldsymbol{y}$ is a vector including concentration and temperature,

$$\frac{\boldsymbol{y}^{n+1} - \boldsymbol{y}^n}{\Delta t} = \boldsymbol{\omega}(\boldsymbol{y}^{n+1}) \approx \boldsymbol{\omega}(\boldsymbol{y}^n) + \mathbf{J}(\boldsymbol{y}^{n+1} - \boldsymbol{y}^n)$$

$$\left(\mathbf{J} - \frac{\mathbf{I}}{\Delta t}\right)(\boldsymbol{y}^{n+1} - \boldsymbol{y}^n) \approx -\boldsymbol{\omega}(\boldsymbol{y}^n)$$

$$\text{Let } \mathbf{A} \equiv \left(\mathbf{J} - \frac{\mathbf{I}}{\Delta t}\right) = \mathbf{F} + \mathbf{S}$$

where $\mathbf{F}$ is a sparse matrix only with large entries and $\mathbf{S}$ has no large entries, and let $\mathbf{F} = \frac{\tilde{\mathbf{F}}}{\varepsilon}, \tilde{\mathbf{F}} = \boldsymbol{O}(1)$

$$\tilde{\mathbf{F}}(\boldsymbol{y}^{n+1} - \boldsymbol{y}^n) \approx -\varepsilon\left(\mathbf{S}(\boldsymbol{y}^{n+1} - \boldsymbol{y}^n) + \boldsymbol{\omega}(\boldsymbol{y}^n)\right) = O(\varepsilon)$$

After eliminating the equations with all zero coefficients and applying sparse QR decomposition $\tilde{\mathbf{F}} = \mathbf{QR}$, we have:

$$\mathbf{R}(\boldsymbol{y}^{n+1} - \boldsymbol{y}^n) \approx -\varepsilon\mathbf{Q}^{-1}\left(\mathbf{S}(\boldsymbol{y}^{n+1} - \boldsymbol{y}^n) + \boldsymbol{\omega}(\boldsymbol{y}^n)\right)$$

The set of independent algebraic equations can be obtained by retaining only those equations corresponding to the non-zero diagonal entries in $\mathbf{R}$, while the rest are "conserved" modes by the coupling of fast reversible reactions - PE.

III. Results and Discussion

A. QSS demonstration

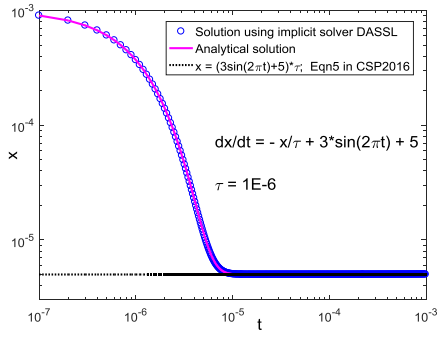

Fig. 1. A toy problem to show the usefulness of Eqns. 4 & 5 in [2].

Fig. 1 shows an example of the usefulness of Eqns. 4 and 5 in a simple initial value problem in the form of

$$\frac{dx}{dt} = -\frac{x}{\tau} + f(t)$$

When τ is very small, as long as *f(t)* changes relatively slow, x will approach $\tau f(t)$ in a thin transition layer of $O(\tau)$ as shown in Fig. 1. However simple this is, it exactly shows the behavior of fast radicals in general chemical kinetics if its reaction source term is linearized by using Eqn. 4. Based on this fact, the thin transition layer corresponding to the fastest species at each time step could be skipped such that the explicit integration time step can be significantly extended as shown in the H_2/air autoignition case in Fig. 2.

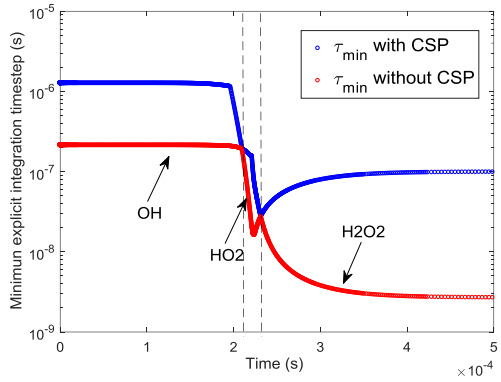

Fig. 2. Capability of integration time step elongation using CSP 2016: an example of autoignition of H_2/air using mechanism by Li *et al*. [4].

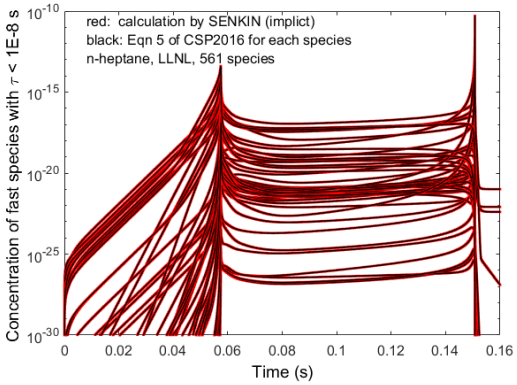

Fig. 3. Demonstration of the usefulness of Eqn 5 from CSP 2016 in n-heptane/air two-stage ignition.

Even in the case of simulating the two-stage ignition of n-heptane/air using the LLNL detailed kinetics with 561 species [5], by analyzing the data calculated by SENKIN, it is seen that Eqn. 5 works perfectly for each fast species throughout the entire ignition process. The results indicate that the linearized reaction source term by Eqns. 4 and 5 can be utilized in general for all fast species.

B. PE demonstration

The constant volume two-stage ignition of stoichiometric n-heptane/air under 10 atm and 800K using detailed LLNL mechanism is simulated using the hybrid integration method (AHI) and implicit integration by SENKIN, with Δt being 10^{-7}s and β 15. Figure 4 is the phase plot of key species concentration versus temperature and shows good agreement.

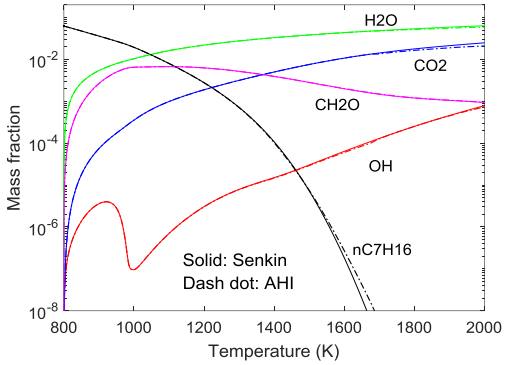

Fig. 4. Comparison of two-stage ignition of n-heptane/air using LLNL detailed chemistry using hybrid integration and SENKIN.

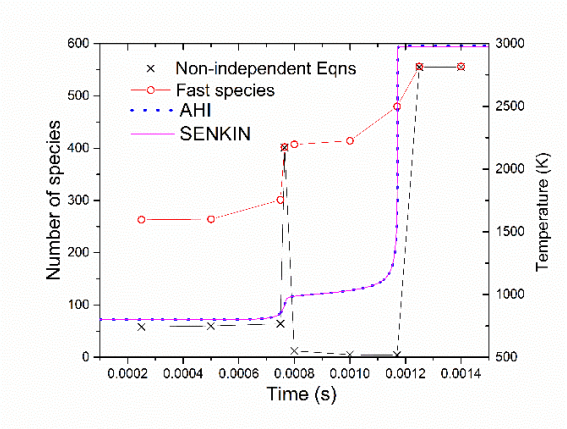

Fig. 5. Evolution of number of fast species and non-independent equations during n-heptane/air two-stage ignition.

By analyzing the sparse Jacobian of the fast species, with fixed $\Delta t = 10^{-7}$s, the number of fast species steadily increases due to the elevated temperature and pressure and consequently reduced species lifetime; however, the number of non-independent equations approaches the total number of fast species at the first-stage ignition, implying that the first-stage ignition is controlled by the equilibrium shift of fast reversible reactions; while the number of non-independent equations is significantly less than the total number of fast species during the entire second-stage ignition, showing radical accumulation and the explosive nature of the second-stage ignition.

REFERENCES

[1] T. Lu, C.K. Law, C.S. Yoo, J.H. Chen. "Dynamic stiffness removal for direct numerical simulations," Combust. Flame, 156(2009) 542-1551

[2] S.H. Lam. "An efficient implementation of CSP." Presented at the Spring Technical Meeting of the Eastern States Section of the Combustion Institute, Princeton, NJ, 2016. PDF file available at www.princeton.edu/~lam/, unpublished.

[3] Y. Gao, Y. Liu, Z. Ren, T. Lu. "A dynamic adaptive method for hybrid integration of stiff chemistry," Combust. Flame, 62(2015) 287-295.

[4] J. Li, Z. Zhao, A. Kazakov, F. Dryer. "An updated comprehensive kinetic model of hydrogen combustion," Int. J. Chem. Kinetics, 36(2004) 566-575.

[5] H.J. Curran, P. Gaffuri, W.J. Pitz, C.K. Westbrook, Combust. Flame 114 (1998) 149-177.

Session: Mechanism Analysis 1

Chair: H. N. Najm

Title: Computational Singular Pertirbation Analysis of Stotastic Chemical System with Stiffness
Authors: X. Han, L. Wang, Y. Cao, H. N. Najm

Title: Ignition Delay Control through Additives in DME/Air and EtOH/Air Mixtures
Authors: E. A. Tingas, D. C. Kyritsis, D.A. Goussis

Title: Extinction and Re-ignition Predictions of a Time-Evolving Turbulent Non-Premixed Flame: Sensitivity to Chemical Kinetics Models
Authors: S. Yang, R. Ranjan, V. Yang, W. Sun, S. Menon

Title: Machine Learning to Predict Combustion Chemistry Phenomenon
Authors: V. van Oudenhoven, S. Mani Sarathy

Computational Singular Perturbation Analysis of Stochastic Chemical Systems with Stiffness

Xiaoying Han[†], Lijing Wang[*], Yanzhao Cao[‡], Habib Najm[§]
[†‡] 221 Parker Hall, Department of Mathematics and Statistics, Auburn University, Auburn, AL 36849, USA
[*]School of Mathematical Sciences, University of Chinese Academy of Sciences,
19 YuQuan Road, Shijingshan District, Beijing 100049, China
[§]Sandia National Laboratories, P. O. Box 969, MS 9051,Livermore, CA 94551, USA

***Abstract*— Computational singular perturbation (CSP) is a useful framework for analysis, reduction, and time integration of stiff ordinary differential equation systems. It has found dominant utility in chemical reaction systems with a large range of time scales at a continuum deterministic level. On the other hand, CSP is not directly applicable to chemical reaction systems at micro or meso-scale, where stochasticity plays a significant role and thus has to be taken into account. In this work we develop a novel stochastic computational singular perturbation (SCSP) analysis and time integration framework, and associated algorithm, that can be used to not only construct accurately and efficiently the numerical solutions to stiff stochastic chemical reaction systems, but also analyze the dynamics of the reduced stochastic systems.**

I. Introduction

Consider a stochastic reaction system of N unknowns denoted by the column stochastic process vector

$$\boldsymbol{z}(t) = (z_1(t), z_2(t), \ldots, z_N(t))^T,$$

with the governing stiff stochastic differential equations (or chemical Langevin equations):

$$\mathrm{d}\boldsymbol{z} = \boldsymbol{f}(\boldsymbol{z})\mathrm{d}t + \boldsymbol{g}(\boldsymbol{z}) \circ \mathrm{d}W(t), \tag{1}$$

where $\boldsymbol{f}$ and $\boldsymbol{g}$ are $N \times 1$ column vectors, $W(t) \in \mathbb{R}$ is a standard Brownian motion, and $\circ$ denotes the Stratonovich product. Our goal is to design an algorithm to split the amplitudes of both $\boldsymbol{f}$ and $\boldsymbol{g}$ in (1) into two classes, fast/rapid and slow, as

$$\boldsymbol{f} = \begin{pmatrix} \boldsymbol{f}^r \\ \boldsymbol{f}^s \end{pmatrix}, \quad \boldsymbol{g} = \begin{pmatrix} \boldsymbol{g}^r \\ \boldsymbol{g}^s \end{pmatrix}, \tag{2}$$

where $\boldsymbol{f}^r = (f_1, \ldots, f_m)^T$ and $\boldsymbol{g}^r = (g_1, \ldots, g_m)^T$ are m vectors representing the deterministic and stochastic fast amplitudes respectively, and $\boldsymbol{f}^s = (f_{m+1}, \ldots, f_N)^T$ and $\boldsymbol{g}^s = (g_{m+1}, \ldots, g_N)^T$ are $N-m$ vectors representing the deterministic and stochastic slow amplitudes respectively.

II. Algorithm

The idea is to find two sets of basis vectors, $\boldsymbol{a}_i$ and $\boldsymbol{\alpha}_i$ for $i = 1, \ldots, N$, iteratively, such that the deterministic and stochastic vector field of (1) can be decomposed to

$$\boldsymbol{f}(\boldsymbol{z}) = A^r \boldsymbol{f}^r + A^s \boldsymbol{f}^s, \quad \boldsymbol{g}(\boldsymbol{z}) = \mathcal{A}^r \boldsymbol{g}^r + \mathcal{A}^s \boldsymbol{g}^s. \tag{3}$$

To this end, the evolution of deterministic and stochastic fast and slow modes are derived to follow a stochastic ODE

$$\mathrm{d}\begin{pmatrix} \boldsymbol{f}^r \\ \boldsymbol{f}^s \\ \boldsymbol{g}^r \\ \boldsymbol{g}^s \end{pmatrix} = P\ \mathrm{d}\omega(t) \begin{pmatrix} \boldsymbol{f}^r \\ \boldsymbol{f}^s \\ \boldsymbol{g}^r \\ \boldsymbol{g}^s \end{pmatrix}, \tag{4}$$

where P is an $N \times N$ evolutionary matrix and

$$\mathrm{d}\omega(t) = \mathrm{Diag}\left[I_m \mathrm{d}t, I_{N-m}\mathrm{d}t, I_m \circ \mathrm{d}W(t), I_{N-m} \circ \mathrm{d}W(t)\right].$$

The goal is then to block diagonalize the matrix P iteratively to split the fast and slow dynamics from each other, which is done by a procedure of basis refinement (BE).

The main tool used for BE is based on algebraic Gaussian elimination (GE) on the matrix P. As for CSP, basis refinement can start from an arbitrary set of basis vectors. Each BE iteration for SCSP consists of two steps. The first weakens the coupling of fast modes from the slow (by a column GE), and the second weakens the coupling of the slow mode from the fast (by a row GE). A good choice for the initial set of basis are the eigenvectors of the vector field, especially when the system (1) is not strongly non-linear.

III. Main results

The main results of this work include: (1) splitting the drift $\boldsymbol{f}$ and the volatility $\boldsymbol{g}$ of the stiff SDE (1) into fast and slow components; (2) constructing the stochastic slow manifold and deriving simplified dynamics along the manifold; and (3) developing an efficient explicit time-scale splitting algorithm to integrate the stiff SDE (1).

IV. Application

The SCSP algorithm is applied to the stochastic Davis-Skodje system

$$\begin{aligned} \mathrm{d}x(t) &= -x(t)\mathrm{d}t + \mu x(t) \circ \mathrm{d}W(t), \\ \mathrm{d}y(t) &= \left(-\gamma y(t) + \gamma \frac{x(t)}{1+x(t)} - \frac{x(t)}{(1+x(t))^2}\right)\mathrm{d}t \\ &\quad + \sigma\sqrt{\gamma} y(t) \circ \mathrm{d}W(t), \end{aligned}$$

where $x(t)$ and $y(t)$ are stochastic processes, μ and σ are small positive numbers, and $W(t)$ is a one-dimensional Wiener process. Two different initial sets of basis vectors are examined, one with arbitrary vectors and one with eigen vectors. For the set with arbitrary vectors the SCSP shows its robustness in reducing the order of magnitude of the deterministic and stochastic fast modes, as well as reducing the stiffness of the simplified system. For the set with eigen vectors, the effect of refinements is not significant. This is because that the eigen vectors are close to the ideal vectors as the system is not strongly nonlinear, and hence a simplified system with no stiffness can be obtained even without refinements.

We illustrated the algorithm using the stochastic Davis-Skodje system. The construction follows the structure of the CSP time integrator for stiff ODEs. With decoupled fast/slow dynamics, the numerical simulation of a stiff SDE can be done by first approximating the fast dynamics with a stochastic algebraic relation, then integrating the system according to the slow dynamics. Since the stochastic algebraic relation describing the fast dynamics does not depend on the step length of time integration, and the subsequent time integration of the slow processes is non-stiff, the construction allows stable integration with large explicit time steps. Selected results are shown below.

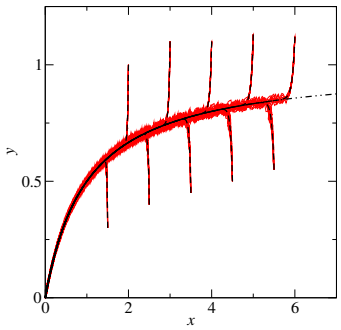

Fig. 1. Solution trajectories starting from a number of initial conditions, computed with both the deterministic and stochastic DS system, using explicit time integration of the stiff system. Also shown is the deterministic manifold. Parameter values are: $\sigma = \mu = 0.02$, $h = 10^{-4}$, $\gamma = 100$.

V. Acknowledgement

This work is partially supported by the National Science Foundation (grant number DMS1620027), National Natural Science Foundation of China (grant numbers 11471310 & 11071251), and the U.S. Department of Energy, Office of Basic Energy Sciences, Division of Chemical Sciences, Geosciences and Biosciences. Sandia National Laboratories is a multi-program laboratory managed and operated by Sandia Corporation, a wholly owned subsidiary of Lockheed Martin Corporation, for the U.S. Department of Energy Nuclear Security Administration under contract DE-AC04-94-AL85000.

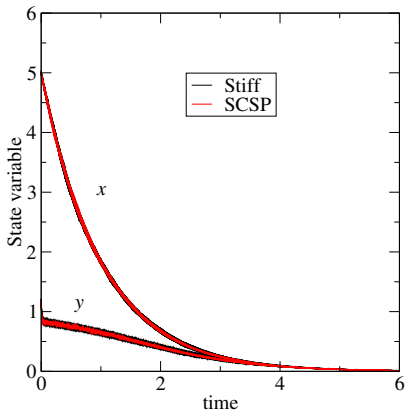

Fig. 2. Time evolution of (x, y), starting at $(5, 1.2)$, based on computations of the stochastic DS system with both the original stiff formulation and with SCSP, with no refinement. Baseline case, with the same (σ, μ, γ) as in Fig. 1, and with $h_{\text{stiff}} = 10^{-4}$ and $h_{\text{SCSP}} = 10^{-2}$.

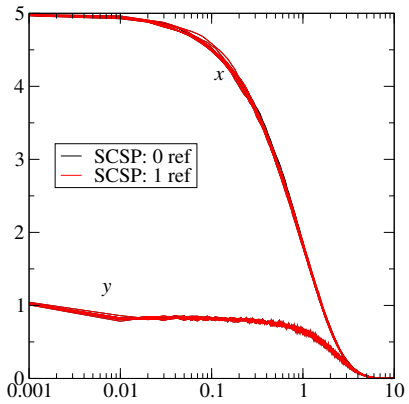

Fig. 3. A comparison of the time trajectories of the stochastic DS system using the SCSP integrator including both no-refinement and one refinement cases, for the baseline conditions, and plotted on a logarithmic time axis.

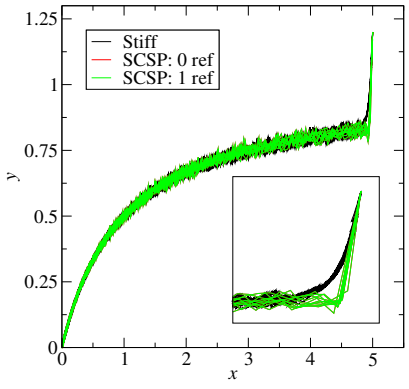

Fig. 4. Evolution of (x, y) in the phase plane, showing the fast evolution towards the manifold, and subsequent motion in the manifold basin, with both the stiff integration and SCSP, including cases with 0 and 1 refinements, for baseline conditions.

Ignition delay control through additives in DME/air and EtOH/air mixtures

Efstathios A. Tingas[*‡], Dimitrios C. Kyritsis[†] and Dimitris A. Goussis[*†]
[*] Department of Mechanics, School of Applied Mathematical and Physical Sciences, NTUA, Athens, Greece
[†] Khalifa University of Science and Technology, Abu Dhabi, UAE
[‡]Current address: Clean Combustion Research Center (CCRC), King Abduallah University of Energy and Technology (KAUST), Thuwal, Jeddah 23955-6900, Kingdom of Saudi Arabia

Abstract—**Computational Singular Perturbation (CSP) tools were used in order to determine algorithmically additives that can affect ignition delay in DME/air and EtOH/air mixtures. Identification through CSP is not a necessary condition for additives to be effective. Additives that are not pointed by CSP can also have a substantial effect on ignition delay, provided that they drastically alter the prevailing chemistry. Chemically stable, relatively light species were determined that can drastically affect ignition delay, such as hydrogen peroxide, formaldehyde and acetaldehyde.**

I. Introduction

The potential advantages of low-temperature combustion have been demonstrated through a long line of experimental and computational works [1,2]. However, industrial application of these technologies has so far been hindered by the lack of reliable mechanisms for the control of ignition delay and subsequent heat release. This caveat has recently motivated Reactivity-Controlled Combustion Ignition (RCCI) [3]. The so far dominant application of the technology has been to mix fuels of low and high octane numbers. Alcoholic additives have also been used for emission reduction and octane number control [4], and cetane-number enhancers have been proposed. This raises the question whether an algorithmic process can be established, through which additives can be identified for ignition delay control. The CSP method provides an algorithm for the decomposition of fast and slow dynamics of the chemical kinetics source term and introduces tools that can identify reactions and species, which contribute substantially to the dynamics of the oxidation [5,6]. In this paper, we apply CSP tools in order to determine species that can affect ignition delay for the combustion of two biofuels, namely ethanol (EtOH) and dimethylether (DME). Interestingly, the two are isomers, which means that they have similar thermochemistry but different kinetics.

II. Physical problem and CSP tools

The isochoric and adiabatic ignition of EtOH- and DME-air mixtures was studied for initial temperatures 700 K$<T_0<$ 1500 K, pressures 0.1 MPa$<p_0<$ 5 MPa and equivalence ratios $0.7<\phi<1.3$. The system of species evolution and energy conservation equations was solved and ideal gas behavior was assumed for all species. The chemical kinetics was modeled with the mechanism of [7], which utilizes 253 species, 6 elements and 1542 elementary reactions. Of particular importance are two diagnostic tools that were utilized for the algorithmic identification of additives, namely the Time Participation Index (TPI) J_k^n, which measures the contribution of the k-th reaction to the n-th eigenvalue of the system (or equivalently the n-timescale), and the CSP pointer (Po) D_k^e, which measures the contribution of the k-th scalar (i.e. species mole fraction or temperature) to the time scale and amplitude of the explosive mode of the system. Precise mathematical definitions of TPI and Po are provided in [8,9].

III. Additive selection and effect on ignition delay

Additive selection was mainly based on the determination of species that exhibited large values of Po in the so-called explosive stage, i.e. the time interval that precedes the steep temperature rise. TPI and Po data were calculated for all possible combinations of ϕ= 0.7, 1, and 1.3, p_0 = 0.1, 1, 3, and 5 MPa, T_0 = 700, 900, 1100, 1300 and 1500 K.

For the EtOH case, it was established that the set of reactions and species that exhibited large values of TPI and Po respectively did not vary drastically with initial conditions. Hydrogen chemistry plays an important role during the explosive stage. The reactions HO_2+EtOH → sC_2H_4OH+H_2O_2 and H_2O_2+M → 2OH+M are strongly pointed by TPI, whereas HO_2 and H_2O_2 consistently have the largest values of Po.

For the DME case, the situation is more complicated. Initial pressure does not have a major effect on the reactions/species with the largest TPI/Po values, but with increasing temperature, the heavy unstable intermediates such as $CH_3OCH_2O_2$ and HO_2CH_2OCHO that are strongly pointed for low temperatures subside and, for T_0>900 K, CH_3O_2 is strongly pointed. This is produced through the reaction CH_3+O_2+M→ CH_3O_2+M, which acquires a high TPI value. This transition is related to the NTC behavior that DME demonstrates in the range 900 K$<T_0<$ 1100 K. When the initial temperature exceeds 1300 K in the DME case, CH_2O acquires a high value of Po and the destruction of CH_2O through CH_2O+O_2→HCO+HO_2 has a major contribution to the fast explosive mode. Typical results for

the evolution of Po for several species during the explosive stage are provided in Fig. 1.

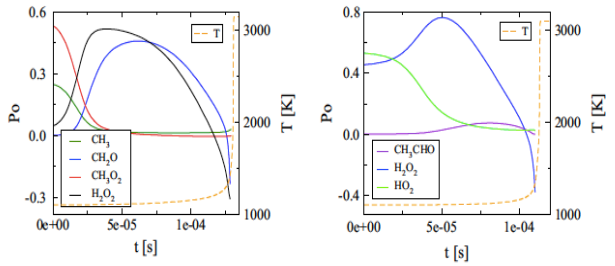

Fig. 1. The largest CSP Pointers (Po) of the fastest explosive mode during the explosive stage of a DME/air (left) and a EtOH (right) mixture, along with the temperature; To = 1100 K, po = 5 MPa, ϕ=1.

The large values of Po point to species that can be considered as additives for ignition delay control. It is, of course, realized that several of the pointed species with large values of Po are unstable radicals, but it is also noted that among the pointed species there are simple and relatively cheap chemicals such as H_2O_2 and CH_2O. It should be stressed that a high value of Po is a sufficient, but not a necessary condition for an additive to have an effect of ignition delay. A non-pointed species might have a small or a large impact on ignition delay, depending on whether it alters sufficiently enough the set of reactions that generate the explosive time scale.

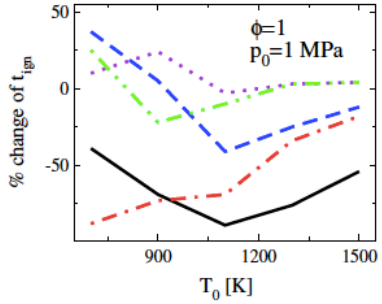

Fig. 2: Percentage change of ignition delay that is caused by insertion of 10% molar of selected additives to DME fuel as a function of initial temperature. H_2O_2: black, CH_3O_2: red, CH_3CHO: green, CH_2O: blue, C_2H_6: violet

This is shown in the results of Figs. 2 and 3, which present the percentage of decrease in ignition delay that is achieved through the insertion of several additives with a mole fraction of 10% in the fuel blend. It can be seen e.g. that CH_3CHO, which was not pointed for either the EtOH or the DME case, has a non-negligible effect on ignition delay, whereas CH_3O_2, which is pointed for the DME case, but not for EtOH, has a drastic effect on ignition delay for both DME and EtOH. Clearly, the algorithmic approach can be complemented by "educated" guesses such as species that have the same characteristic group (like the non-pointed CH_3CHO with the pointed CH_2O) or species that are pointed for isomers of the fuel under consideration (or possibly even fuels of approximately equal molecular weight). However, it is noted that these guesses are also indirectly guided by the results of the CSP algorithm.

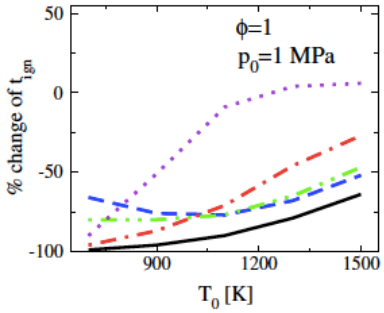

Fig. 2: Percentage change of ignition delay that is caused by insertion of 10% molar of selected additives to EtOH fuel as a function of initial temperature. CH_3O_2H: black, CH_3O_2: red, HO_2: green, H_2O_2: blue, CH_3CHO: violet

IV. Conclusions

CSP tools can identify the intermediate species that relate the most to the characteristic time scale that leads the system to ignition and can therefore be used as additives for the purpose of ignition-delay control. For DME and EtOH, several of the additives that were determined were radicals, addition of which in practical fuels is impossible (CH_3O_2, CH_3O_2H, HO_2). However, several stable and relatively light additives that can affect ignition delay were also identified, such as H_2O_2, CH_2O, and CH_3CHO. Species that are not identified by the CSP pointer can also affect ignition delay, provided that they can alter the prevailing chemical dynamics when added to the fuel.

References

[1] T.L. Hendricks, D.A. Splitter, J.B. Ghandhi, "Experimental investigation of piston heat transfer under conventional diesel and reactivity-controlled compression ignition combustion regimes" *Int. J. Engine. Res.* vol.15 (6), pp. 684–705, 2014.

[2] S. Saxena and I.D. Bedoya "Fundamental phenomena affecting low temperature combustion and HCCI engines, high load limits and strategies for extending these limits", *Prog. Energy Combust. Sci.* vol. 39 (5), pp. 457–488, 2013.

[3] R.D. Reitz and G. Duraisamy, "Review of high efficiency and clean reactivity controlled compression ignition (RCCI) combustion in internal combustion engines" *Prog. Energy Combust. Sci.,* vol 46, pp. 12–71, 2015.

[4] S.M. Sarathy, P. Oßwald, N. Hansen, and K. Kohse-Höinghaus "Alcohol combustion chemistry", *Prog. Energy Combust Sci.* vol. 44, pp. 40–102, 2014.

[5] S.H. Lam and D.A. Goussis, "Understanding complex chemical kinetics with Computational Singular Perturbation" *Proc. Combust. Inst.* vol. 22, pp. 931–941, 1988.

[6] S.H. Lam and D.A. Goussis, "CSP method for simplifying kinetics" *Int. J. Chem. Kinet.,* vol 26(4), pp. 461–86, 1994.

[7] W.K. Metcalfe, S.M. Burke, S.S. Ahmed, and H.J. Curran, "A hierarchical and comparative kinetic modeling study of C1- C2 hydrocarbon and oxygenated fuels". *Int. J. Chem. Kinet*. vol. 45 (10), pp. 638–75, 2013.

[8] E.A. Tingas, D.C. Kyritsis, and D.A. Goussis, "Algorithmic determination of the mechanism through which H_2O-dilution affects autoignition dynamics and NO formation in CH_4/air mixtures", *Fuel*, vol. 183, pp. 90-98, 2016.

[9] E.A. Tingas, D.C. Kyritsis, and D.A. Goussis, "Autoignition dynamics of DME/air and EtOH/air homogeneous mixtures", *Combustion and Flame*, vol. 162, pp. 3263-3276, 2015.

Extinction and Re-ignition Predictions of a Time-Evolving Turbulent Non-premixed Flame: Sensitivity to Chemical Kinetics Models

Suo Yang *, Reetesh Ranjan *, Vigor Yang *, Wenting Sun *, and Suresh Menon *
* School of Aerospace Engineering, Georgia Institute of Technology, Atlanta, USA

***Abstract*—To investigate the sensitivity of simulation predictions to chemical kinetics, GRI-Mech 3.0 and an 11-species syngas model, are compared by performing 3D finite-rate kinetics-based DNS of temporally evolving turbulent non-premixed flames. Significant deviations indicate high sensitivity to the chemical kinetics. This sensitivity is magnified relative to a 1D steady laminar simulation by the effects of unsteadiness and turbulence, with the deviations in species concentrations, temperature, and reaction rates forming a nonlinear positive feedback loop under the considered reacting flow conditions. The deviations between the two models majorly caused by: (a) GRI-Mech 3.0 contains more species than the 11-species model; (b) reaction rate coefficients are different for the same reactions. Both (a) and (b) are sensitive to unsteadiness and other turbulence effects. However, (b) is the dominant part and is more sensitive.**

I. Introduction

Most existing chemical kinetics models offer similar predictions of ignition and extinction in 0D/1D finite-rate simulations of laminar combustion processes. Is it appropriate, therefore, to extend this observation to a 3D turbulent combustion environment? In order to answer this question, two chemical kinetics models are used to simulate a temporally evolving turbulent non-premixed syngas flame, and the results are compared.

II. Numerical Methods

In this study, the well-established reacting flow solver AVF-LESLIE [1] has been used. The solver uses the 2nd-order accurate MacCormack finite volume scheme on generalized curvilinear coordinates, and an explicit 2nd-order accurate scheme for time-integration. For reasons of both accuracy and computational speed, point-implicit stiff ODE (ODEPIM) solver is selected for the integration of chemical source term. DAC generates locally reduced kinetics for each spatial location and time step. Only the reaction rates of active species are calculated. To reduce the computational overhead for mechanism reduction, a correlation technique [2-5] is introduced to share the reduced kinetics among time-space points with similar thermochemical states. Using the similar correlation technique but different grouping criteria [3-6], the calculation of mixture-averaged transport coefficients can be reduced significantly without computational overhead.

III. Results and Discussion

In this study, we consider a canonical temporally evolving non-premixed flame. The characteristic jet velocity is 100 m/s, and the pressure is 1 atm. The configuration comprises an inner fuel jet (50% CO, 10% H_2, and 40% N_2 by volume) and an outer oxidizer stream (25% O_2 and 75% N_2 by volume), which are counter-flowing in the streamwise direction. The jet has a Reynolds number (Re_{jet}) of 2315 and a Damkohler number (Da) of 0.01. The computational domain is $L_x \times L_y \times L_z \equiv 12H \times 14H \times 8H$, where H = 0.96 mm is the initial width of the fuel jet. The simulations in this study employ about 18 uniform spaced points along H. The characteristic transient jet time is defined as $t_j = H/U$, and the simulations are conducted up to $40\ t_j$ to capture both extinction and re-ignition. Two chemical kinetics models are compared. The 1st model, GRI-Mech 3.0 [7], comprises 325 steps and 53 species, and serves as a detailed stiff mechanism. The 2nd is a 21-step, 11-species non-stiff mechanism [8] developed by Hawkes *et al.*

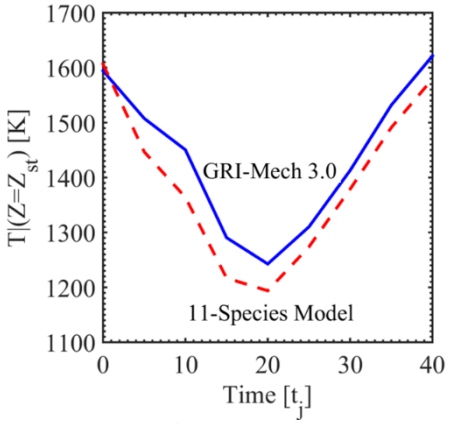

Fig. 1. Temporal evolution of mean temperature on the stoichiometric surface obtained from GRI-Mech 3.0 and 11-species model.

Figure 1 compares the temporal evolution of the temperature field on the stoichiometric surface obtained from simulations using GRI-Mech 3.0 and the 11-species model. Although the starting temperature and the trend are the same, the prediction from the 11-species model gradually deviates from that of GRI-Mech 3.0. The deviation reaches its peak of 86 K (6%) near $20t_j$, but decreases slightly afterwards, stabilizes at ~50 K, and remains stable to the end of the simulation.

TABLE I.
CONTRIBUTION FROM (A) TO THE MAXIMAL (OVER TIME) ABSOLUTE DEVIATIONS; ABSOLUTE DEVIATION MAGNIFICATION FACTORS FOR (A) GLOBAL REDUCTION OF REACTION PATHWAYS, (B) DIFFERENT REACTION RATE COEFFICIENTS, AND TOTAL – BASED ON $T|Z_{st}$ AND $Y_k|Z_{st}$

Contribution from (a) to total deviation (%)	T	Y_{H_2}	Y_{O_2}	Y_H	Y_{H_2O}
1D steady laminar	32.98	16.5	25.00	10.57	>100
3D turbulent	13.01	20.0	30.77	05.08	11.11
Magnification factor of deviation	T	Y_{H_2}	Y_{O_2}	Y_H	Y_{H_2O}
(a) Reduced pathways	2.79	12.12	2.67	08.11	0001.38
(b) Different RR coeff.	9.18	09.58	2.00	17.89	1329.36
Total	7.08	10.00	2.17	16.86	0012.55

The differences between the two models include two major parts: (a) GRI-Mech 3.0 contains 42 more species than the 11-species model; (b) for those reactions included by both models, their reaction rate coefficients are different. Table 1 shows the contribution of (a) to the total absolute deviations between the two chemical kinetics models, and the absolute deviation magnification factors for (a), (b), and total. Both (a) and (b) are sensitive to unsteadiness and other turbulence effects for all quantities. With only (a), the magnification is up to 12 times, but the deviations are within ~4%. For temperature and all species with more than 10 times total deviation magnification, (b) is more sensitive, which results in the rise of its contribution to total deviations from 1D steady laminar case to 3D turbulent case. Essentially, (a) means the reaction rates of those globally reduced pathways are linearly removed. In contrast, (b) the difference in reaction rate coefficients (e.g. activation energy) can be nonlinearly (e.g. exponentially) enlarged. In summary, (b) is the dominant part and is more sensitive to unsteadiness and other turbulence effects.

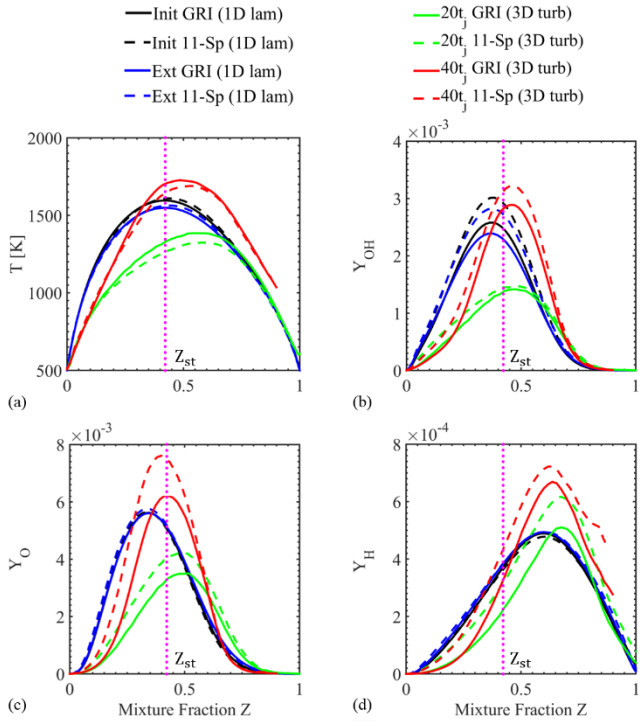

Fig. 2. Comparison of GRI-Mech 3.0 (solid line) and 11-species model (dashed line) in 1D steady laminar solutions (initial data and laminar flamelet values at extinction) and 3D turbulent simulations (at $20t_j$ and $40t_j$): the conditional means of (a) T, (b) Y_{OH}, (c) Y_O, and (d) Y_H.

The mixture-fraction conditioned mean values of T, and mass fractions of OH, O, and H at local extinction ($20\ t_j$) and re-ignition ($40\ t_j$), are shown in Fig. 2. Although the predictions from the two chemical kinetics models show the same trends, the 11-species model predicts a lower radicals-to-products conversion rate for release heat. As a result, the 11-species model predicts more local extinction (mean $T|Z_{st}$ is 49 K smaller) but less re-ignition (mean $T|Z_{st}$ is 42 K smaller). All deviations in the 3D turbulent simulations are significantly larger than those in the 1D steady laminar solutions, except for the OH. There are only minor deviations between GRI-Mech 3.0 and its globally reduced version in the same comparison (not shown here).

IV. CONCLUSIONS

To study the sensitivity of predictions to chemical kinetics models, GRI-Mech 3.0 and an 11-species syngas model, are compared in the 3D finite-rate simulation of a temporally evolving turbulent non-premixed syngas flame. The prediction of the 11-species model gradually deviates from that of GRI-Mech 3.0. In general, the deviations of the two chemical kinetics models increase sharply from 1D steady laminar to 3D unsteady laminar to 3D turbulent simulations for most quantities. Thus, the absolute deviation in turbulent combustion simulations is larger than that in 1D steady laminar solutions by up to 7 times for temperature, up to 12 times for CO, up to 13 times for H_2, up to 7 times for O_2, up to 5 times for CO_2, and up to 13 times for H_2O.

ACKNOWLEDGMENT

This work was funded partly by NASA (Grant NNX15AU96A), and partly by the William R.T. Oakes Endowment of the Georgia Institute of Technology.

REFERENCES

[1] W.-W. Kim, S. Menon, Numerical modeling of turbulent premixed flames in the thin-reaction-zones regime, Combust. Sci. Technol. 160 (1) (2000) 119-150.

[2] W. Sun, X. Gou, H.A. El-Asrag, Z. Chen, Y. Ju, Multi-timescale and correlated dynamic adaptive chemistry modeling of ignition and flame propagation using a real jet fuel surrogate model, Combust. Flame 162 (4) (2015) 1530-1539.

[3] S. Yang, V. Yang, W. Sun, S. Nagaraja, W. Sun, Y. Ju, X. Gou, Parallel On-the-fly Adaptive Kinetics for Non-equilibrium Plasma Discharges of C2H4/O2/Ar Mixture, 54th AIAA Aerospace Sciences Meeting (Jan. 2016), AIAA Paper 2016-0195.

[4] S. Yang, R. Ranjan, V. Yang, S. Menon, W. Sun, Parallel On-the-fly Adaptive Kinetics in Direct Numerical Simulation of Turbulent Premixed Flame, Proc. Combust. Inst. 36 (2) (2017) 2025–2032.

[5] S. Yang, X. Wang, V. Yang, W. Sun, H. Huo, Comparison of Flamelet/Progress-Variable and Finite-Rate Chemistry LES Models in a Preconditioning Scheme, 55th AIAA Aerospace Sciences Meeting (Jan. 2017), AIAA Paper 2017-0605.

[6] W. Sun, Y. Ju, Multi-timescale and Correlated Dynamic Adaptive Chemistry and Transport Modeling of Flames in n-Heptane/Air Mixtures, 53rd AIAA Aerospace Sciences Meeting (Jan. 2015), AIAA Paper 2015-1382.

[7] G.P. Smith, D.M. Golden, M. Frenklach, N.W. Moriarty, B. Eiteneer, M. Goldenberg, C.T. Bowman, R.K. Hanson, S. Song, W.C. Gardiner Jr., V.V. Lissianski, Z. Qin http://www.me.berkeley.edu/gri_mech/

[8] E.R. Hawkes, R. Sankaran, J.C. Sutherland, J.H. Chen, Scalar mixing in direct numerical simulations of temporally evolving plane jet flames with skeletal CO/H 2 kinetics, Proc. Combust. Inst. 31 (1) (2007) 1633-1640.

Machine Learning to Predict Combustion Chemistry Phenomenon

Vincent van Oudenhoven*, and S. Mani Sarathy*
* King Abdullah University of Science and Technology, Clean Combustion Research Center, Thuwal, Saudi Arabia

***Abstract*—Amongst the most complex chemical reaction networks are those involving free radical driven oxidation and pyrolysis, which take place through a series elementary reactions connecting the initial reactants with final products under certain initial conditions (temperature, pressure, composition, etc.). Theoretically, these complex processes can be predicted using a chemical kinetic model comprising a series of elementary reactions with corresponding kinetic rate parameters and species thermodynamic data. Such models are capable of predicting various combustion relevant phenomenon, such as ignition delay time, flame structure, and various pollutant emissions, as well as oxidation of pollutants in the atmosphere, and the pyrolysis of heavy hydrocarbon mixtures in chemical refineries. These models are useful for engine design, but their computational cost often exceeds available resources. In this work, we present three case studies to demonstrate the power of applying machine learning algorithms for the prediction of important combustion properties properties. These include determining critical compression ratio for autoignition, fuel octane numbers, and fuel/air mixture ignition delay time.**

I. INTRODUCTION

Machine learning has revolutionized the approach to multitudinous areas of research and industry, as well as affected countless aspects of our lives. One of the most notable machine learning tools is known as deep learning or the application of neural networks, which allows for complex relationships to be found, if present, between parameters of interest for numerous kinds of data. This may allow for an alternative way to quantify, qualify, and analyze data within the field of combustion chemistry, as has been recently demonstrated in other chemically reacting systems [1]. Our eventual goal is to make highly accurate and robust models for the prediction of relevant attributes such as, ignition delay time, octane and cetane numbers, laminar flame speed, critical compression ratio, heat release, etc. [2][3][4][6], which will in turn contribute to fuel and engine design.

II. METHODS AND RESULTS

A. Compression Ratio

The first study is concerned with predicting the critical Compression Ratio (CR) for autoignition of primary reference fuels (PRFs) blended with ethanol, when provided with initial conditions for inlet temperature, revolutions per minute (rpm), and mixture composition. Ethanol has a nonlinear relationship when blended with other fuels with respect to their octane number, which can be directly related to critical CR [5]. Therefore, machine learning was of interest for this problem. An artificial neural network (ANN) was developed to predict the experimentally measured critical compression ratio for various fuel blends. Overall, an average percentage error of 1% was achieved, which is within the experimental uncertainty of the study. Examples from the test set are shown in Fig. 1, where the trend line indicates the desired result. This same principle could be extended to other fuels, and to wider ranges of the studied parameters, allowing for a general model able to substitute, or at the least supplement the corresponding experiments.

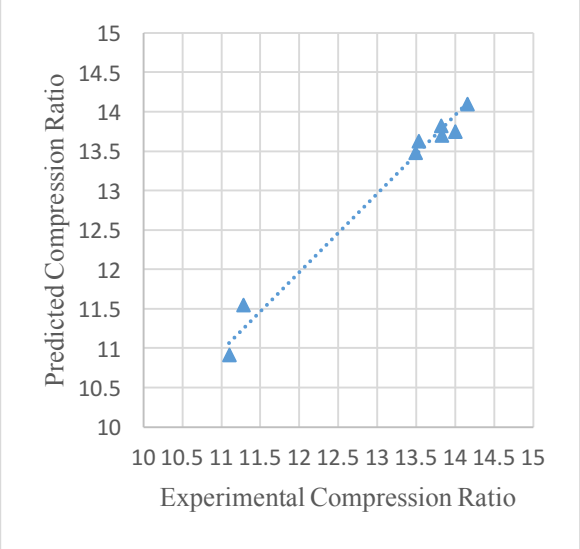

Figure 1, Predicted Compression Ratio vs. Experimental

B. Octane Numbers

The second study of interest is with regards to the prediction of the Research and Motor Octane Numbers (RON and MON) for various hydrocarbon fuels. Here, we simplify the fuel composition to s set of functional group descriptors; for example, the weight % of CH3, CH2, CH, olefins, naphthenes, aromatics, and ethanol, the average molecular weight, and the Branching Index (BI). In order to relate these independent features to the compound's RON and MON, ANN were used. To improve the ANN model, a genetic algorithm was applied to evolve against a randomly chosen training set. The final model achieved an overall average percentage error of 1.3%, proving both that fuel molecular parameters are indeed related to the octane number of a fuel, and that using deep learning for such problems can provide a trustworthy model. Results from the test set are presented in Fig. 2.

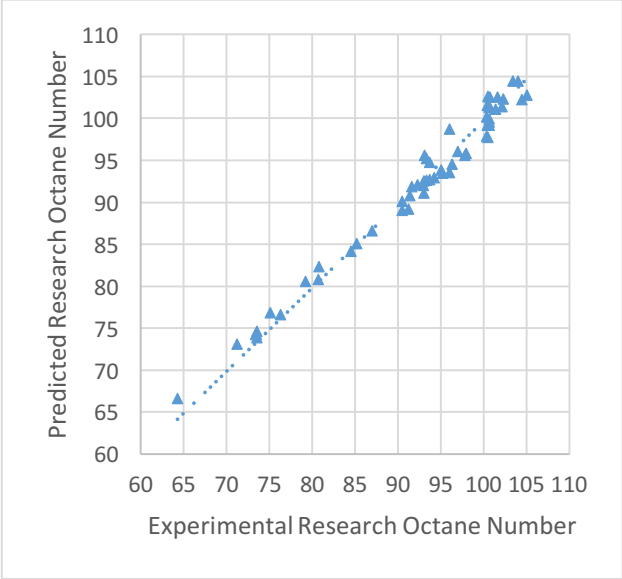

Figure 2, Predicted Research Octane Number vs. Experimental

C. Ignition Delay

Lastly, an ANN model was developed for the prediction of ignition delay time (IDT) for fuels composed of ethanol, iso-octane, n-heptane, and toluene, as a function of mixture composition, initial temperature, and initial pressure. Unlike previous case studies, the training dataset was obtained from simulations with a detailed chemical kinetic model using CANTERA. This will allow for a more general and extensive model. The model was able to predict complex pressure and temperature dependent ignition phenomenon, including negative temperature coefficient (NTC) behavior, with an average percentage errors of ~3%.

III. CONCLUSIONS

Chemical kinetic modeling is a useful tool for understanding combustion phenomenon, but computational expense limits its application in practical design processes. In this work, ANNs were used due to their ability to effectively capture non-linear and complex relationships between input features and the output of interest. As shown in the above case studies, valuable models can be produced from previously collected data, such as from individual experiments, literature, and simulations. We are currently extending the machine learning approach to predict combustion emissions using a computational brewing approach to predict chemical reactions, kinetics, and product distributions.

REFERENCES

[1] Baldi, Matthew A. Kayala and Pierre. "ReactionPredictor: Prediction of Complex Chemical Reactions at the Mechanistic Level Using Machine Learning." Journal of Chemical Information and Modeling, 2012.

[2] Hadi Taghavifara, Hamid Taghavifarb, Aref Mardanib, Arash Mohebbib, Shahram Khalilaryaa, Samad Jafarmadar. "Appraisal of Artificial Neural Networks to the Emission Analysis and Prediction of CO2, Soot, and NOx of n-heptane Fueled Engine." Journal of Cleaner Production, 2016.

[3] Jabir H. Al-Fahemi, Nahla A. Albis, and Elshafie A. M. Gad. "QSRP Models for Octane Number Prediction." Hindawi, 2014.

[4] M.V. Maylin, M.V. Kirgina, E.V. Sviridova, and B.V. Sakhnevitch. "Calculation of Gasoline Octane Numbers Taking into Account the Reaction Interaction of Blend Components." Procedia Chemistry, 2014.

[5] Muhammad Waqas, Nimal Naser, and Mani Sarathy. "Blending Octane Number of Ethanol in HCCI, SI and CI Combustion Modes." SAE International, 2016.

[6] Ramón Piloto-Rodrígueza, Yisel Sánchez-Borrotoa, Magin Lapuertab, Leonardo Goyos-Péreza, and Sebastian Verhelstc. "Prediction of the Cetane Number of Biodiesel using Artificial Neural Networks and Multiple Linear Regression." Energy Conversion and Management, 2013.

Invited Talk

Chair: C. K. Law

Title: “Model Reduction” by Singular Perturbation
Authors: Prof. S. H. Lam

"Model Reduction" by Singular Perturbation

S. H. Lam*
Department of Mechanical and Aerospace Engineering
Princeton University, Princeton, NJ 08544, U. S. A.

May 4, 2017

Abstract

These are lecture notes for my presentation in the 2017 IWMRRF conference at Princeton university.

Some obviously non-controversial statements

1. All terms in any governing equations have physically meaningful **dimensional** physical units. (e.g.

   kilograms, **meter**, **seconds, moles**, meters per second, Kelvin degrees, moles/volume, ... etc.)

2. terms can be added or subtracted **only if they have the same dimensional physical units**.

3. The dimensional physical unit of a **product** of two variables, is the product of the dimensioal physical units of the two variables .

4. The dimensional physical unit of a **ratio** of two variables, is the **ratio** of the dimensioal physical units of the two variables.

5. All equations have an equal sign "=" The dimensional physical units of the left and right sides of the equal sign **must** be the same.

*Professor emeritus. Email: lam@princeton.edu

6. A **dimensionless** parameter is **always** a ratio of two variables (or two terms) with the **same** physical units. The reciprocal of a dimensionless number is also dimensionless.

The challenging and "fun" job of doing perturbation analysis on a class of practically interesting problems is the identification of dimensionless parameters which can be "negligibly" small.

How small is "neglegibly" small?

- Let's denote the identified **dimensionless** parameter by ϵ, it is considered "neglegibly" small when it is very "small" in comparison to **unity**.
- the "largeness/smallness" of the magnitude of **any** dimensional number is meaningless unless it is compared to something with the same dimentional physical unit.

Why do we call some perturbation analysis "singular perturbation" ?

The short answer is: When the methodology used to exploit the "smallness of ϵ" is not "uniformly" valid in the space of dependent/independent variables.

Notations for the "order of magnitude" of a function of ϵ.

If the value of $f(\epsilon \to 0)$ is **neither** very small **nor** very large in comparison to unity, Then $f(\epsilon)$ is said to be an O(1) function in the small ϵ limit. If $g(\epsilon)/\epsilon)$ is O(1), then $f(\epsilon)$ is said to be an O(ϵ) function. If ϵ g(ϵ) is O(1), then $g(\epsilon)$ is said to be an O($1/\epsilon$) function.

1 How to do any perturbation analysis?

1. Normalize all dependent and independent variables of interest, so that all are **intuitively** expected to be O(1) dimensionless numbers. **This**

is the hard part. Because the investigator needs "experience and knowledge" on the subject matter (and **smart intuitions**).

2. Write the governing equations in terms of these domensionless variables. Some dimensionless parameters (i. e. **ratio** of two terms with **same** physical units.) will automatically show up.

3. Next, estimate the nominal order of magnitude of these dimensionless parameters for the class of problems of you are interested in. The one with the smallest nominal values is a good ϵ candidate for your problems.

4. Now, neglect all O(ϵ) terms, **this is the easy part**. You have just derived a "leading-order" simplified reduced model for your problems, provided that it is "consistent" with the original intuitive normalizations of the dependent/independent variables.

What is the physical meaning of $\epsilon << 1$?

- This is the fun part. It obviously means the value of the numerator in the ratio formula for ϵ is much smaller than the value of the denominator. You can now write an insightful paragraph in the discussion section of your paper! You next need to find out whether your reduced model so derived is "uniformly" valid.

What are some of the famous dimensionless parameters?

Mach number, **Reynold's** number, **Froude** number, **Knudson** number, Quantum number, ...

Session: Attractive Manifold 2

Chair: D. Lebiedz

Title: Covariant Geometric Characterization of Slow Invariant Manifolds: New Concepts and Viewpoints
Author: D. Lebiedz

Title: Slow Manifolds Localization from Canonical Formats of the Evolution Law
Authors: A. Ceccato, P. Nicolini, D. Frezzato

Covariant geometric characterization of slow invariant manifolds: New concepts and viewpoints

Dirk Lebiedz*
*Institute for Numerical Mathematics, Ulm University, Germany

***Abstract*— We point out a new view on slow invariant manifolds (SIM) in dynamical systems which departs from a purely geometric covariant characterization implying coordinate independency. The fundamental idea is to treat the SIM as a well-defined geometric object in phase space and elucidate characterizing geometric properties that can be evaluated as point-wise analytic criteria. For that purpose, we exploit curvature concepts and formulate our recent variational approach in terms of coordinate-independent Hamiltonian mechanics. Finally, we combine both approaches and conjecture a differential geometric definition of slow invariant manifolds. For the Davis-Skodje model the latter can be completely expatiated.**

I. Introduction

The analysis of slow invariant manifolds (SIM) for singularly perturbed dynamical systems goes back to Fenichel's geometric singular perturbation theory (GSPT). It formulates by help of perturbation techniques for the critical manifold (singular perturbation parameter $\varepsilon = 0$) the classical SIM existence theorem involving non-uniqueness similar to center manifold theory. A coordinate-specific graph representation of the slow manifold (mapping slow to fast variables) allows for a Taylor-series in the singular perturbation parameter ε whose coefficients can be determined successively by matched-asymptotic expansion from the invariance equation.

Our aim is to avoid the technical asymptotic local analysis as a first step to address the issue of bundling of trajectories near slow invariant manifolds to be rigorously defined as mathematical objects. Instead, we propose a purely geometric approach that uses global analysis in terms of coordinate-independent differential geometric concepts. The first step into that direction goes back to 2004 [3] when we suggested to formulate a trajectory-based variational principle distinguishing the SIM trajectories - parameterized by fixed reaction progress variables (*rpv*) initial values - from other trajectories. The objective functional for this problem formulation has been developed from entropy production [3] to curvature in time-parametrization [4] over the years. As in many other computational techniques for point-wise slow manifold approximation, a numerical grid for the *rpv* is chosen and the non-reaction progress variables (*non-rpv*) are computed on each grid point such that the resulting point in phase space is close to the SIM [5].

Most of these numerical SIM approximation methods, in particular the practical ones commonly used in applications, suffer from coordinate-dependency, they yield (at least slightly) different results depending on the chosen coordinate system (*rpv*) for the SIM (see Fig. 1). We conjecture that a covariant formulation of SIM criteria, coordinate-indepedency, i.e. invariance of the evaluation result under the *rpv* permutation group, should be at the root of a geometric characterization of an object in phase space that is reasonably related to the Fenichel SIM.

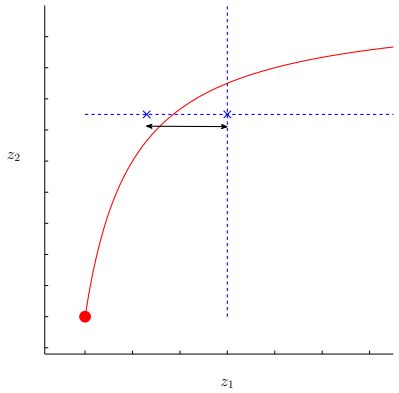

Fig. 1. Schematic illustration of the dependency of computational SIM (red curve) approximation (blue crosses) on *rpv* choice for the Davis-Skodje example model (1).

We follow two roads to address this issue, the first one [6] is analogy reasoning to analytic mechanics with its coordinate independent general structure allowing to easily figure out conserved properties in the time evolution of a dynamical system. The second one [2] is rooted in differential geometry as the theoretical framework for covariant analysis and coordinate-independent formulation of local geometric properties of manifolds and exploits curvature concepts.

We develop and illustrate our reasoning on the background of the benchmark problem (Davis-Skodje model)

$$\begin{aligned} \dot{z}_1 &= -z_1, \\ \varepsilon\dot{z}_2 &= -z + \frac{z_1}{1+z_1} - \frac{\varepsilon z_1}{(1+z_1)^2} \end{aligned} \tag{1}$$

as an example for a singularly perturbed two time-scale system with analytically known SIM $z_2(z_1) = \frac{1}{1+z_1}$.

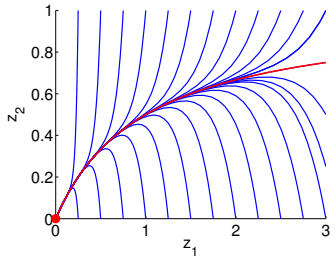

Fig. 2. Some solution trajectories (blue) and SIM (red) for the Davis-Skodje model (1) in phase space (time as curve parametrization), $\varepsilon = 10^{-2}$.

II. Analytic Mechanics

Inspired by an obvious local symmetry in the attraction behaviour of solution trajectories to the SIM (see Fig. 2, contraction rate ratio of vectors in normal versus tangent bundle of the SIM locally becomes extremal [1]) we formulate our variational problem for SIM approximation [4] in a Hamiltonian context [6] in order to be able to identify a conserved property that is related to a symmetry of the Lagrangian by the famous Noether-theorem.

We find an objective functional that allows analytical computation of the exact SIM of the Davis-Skodje model in terms of the solution of a variational boundary value problem [6]:

$$\min_{z(t)} \int_{t_0}^{t_f} k_1 \left\| \frac{\mathrm{d}}{\mathrm{d}t} z(t) \right\|_2^2 - k_2 \|z(t)\|_2^2 \, \mathrm{d}t \qquad (2)$$

subject to

$$\begin{aligned} \dot{z}_1 &= -z_1, \\ \varepsilon \dot{z}_2 &= -z + \frac{z_1}{1+z_1} - \frac{\varepsilon z_1}{(1+z_1)^2}, \; z_1(t_f) = z_1^{t_f} \end{aligned}$$

with constants $k_1, k_2 \in \mathbb{R}$. Chosing $k_1 = 1, k_2 = \frac{\varepsilon^{-1}}{z_1(t)+1}$, the solution of problem (2) on arbitrary time horizon $[t_0, t_f]$ yields exactly the SIM $z_2(z_1) = \frac{1}{1+z_1}$.

In the Hamiltonian viewpoint model reduction via projection to the SIM can be interpreted as partial integration of the dynamical system flow on the basis of the existence of a first integral (the Hamiltonian is conserved along the flow!).

III. Differential Geometry

One of the most famous examples of a covariant physical theory is Albert Einstein's general theory of relativity based on a space-time manifold with appropriate metric tensor derived from the gravitational field equation. The appropriate mathematical framework is Riemannian geometry.

By analogy reasoning with respect to general relativity we construct the extended phase space by adding to the phase space of a dynamical system the time as a fully equivalent state variable. A particular solution of the differential equation model is then a geometric curve in extended phase space. The SIM is a state-space-time manifold. We conjecture that an appropriate metrization (definition of a Riemannian metric) of the solution manifold in extended phase space will allow a complete geometric characterization of the SIM. The force-curvature relation from general relativity can be transferred to chemical kinetics.

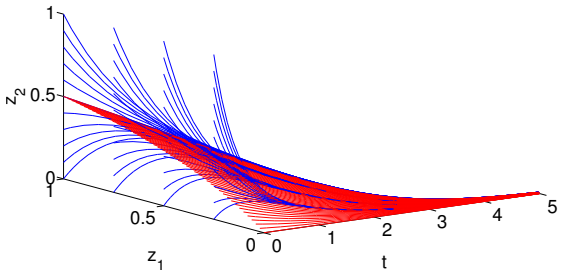

Fig. 3. Extended phase space with some solution trajectories (blue) and SIM (red) for the Davis-Skodje model (1), $\varepsilon = 10^{-2}$.

A. Curvature and Invariance: Necessary Condition for SIM

We demonstrated [2] that the SIM invariance property can in general be covariantly formulated as vanishing time-sectional curvatures of the extended-phase-space graph of the SIM $z_2(z_1, t)$ transporting in time along the flow an initial value manifold $z_2(z_1, 0)$. Vanishing curvature can be formulated point-wise as a root finding analytic criterion providing a necessary condition for the SIM.

B. Sufficient Condition for SIM: Davis-Skodje Model

Specifically for the Davis-Skodje model (1), the evaluation of the time-sectional curvature criterion yields a differential equation that can be analytically solved to a parameterized solution of the model equation. In this case the analytic mechanical approach and the covariant differential geometric viewpoint can be combined to formulate a sufficient criterion for the SIM [2].

References

[1] A. Adrover, F. Creta, M. Giona and M. Valorani. *Stretching-based diagnostics and reduction of chemical kinetic models with diffusion.* Journal of Computational Physics 225 (2007), 1442–1471

[2] P. Heiter and D. Lebiedz. Towards differential geometric characterization of slow invariant manifolds in extended state space: Sectional curvature and flow invariance. arXiv:1612.01308 [math.DS]

[3] D. Lebiedz, *Computing minimal entropy production trajectories: An approach to model reduction in chemical kinetics*, Journal of Chemical Physics, 120 (2004), 6890–6897.

[4] D. Lebiedz, J. Siehr and J. Unger, *A variational principle for computing slow invariant manifolds in dissipative dynamical systems*, SIAM Journal on Scientific Computing, 33 (2011),703–720.

[5] D. Lebiedz and J. Siehr, *A continuation method for the efficient solution of parametric optimization problems in kinetic model reduction.* SIAM Journal on Scientific Computing 35 (2013), A1584–1603 (2013)

[6] D. Lebiedz and J. Unger, *On unifying concepts for trajectory-based slow invariant attracting manifold computation in kinetic multi-scale models*, Mathematical and Computer Modelling of Dynamical Systems, 22 (2016), 87–112.

Slow Manifolds Localization from Canonical Formats of the Evolution Law

Alessandro Ceccato*, Paolo Nicolini †, Diego Frezzato*
* Dipartimento di Scienze Chimiche, Università degli Studi di Padova, via Marzolo 1, I-35131, Padova, Italy.
† Department of Control Engineering - K335, Faculty of Electrical Engineering,
Czech Technical University in Prague, Karlovo náměstí 13, 121 35, Prague 2, Czech Republic.

***Abstract*— Recasting the ordinary differential equations of chemical kinetics into universal "canonical" formats offers the possibility of investigating some general traits, like the low-dimensional slow manifolds which lie at the heart of dimensional reduction strategies. Here we outline our perspectives along this line of investigation.**

I. Introduction

The identification of slow invariant manifolds (here simply termed "slow manifolds", SMs) is a key step towards the dimensional reduction in the description of complex chemical kinetics. Although the formal definition of SM is rooted in Fenichel's geometrical singular perturbation technique [1] based on the partition between fast-slow evolution modes, the algorithmic implementation of the mathematical definition poses several issues due to the fact that for nonlinear kinetics the timescale separation is a *local* property. In the past decades, a number of heterogeneous but somehow related tools have been devised to work out approximations of the SM. Among them, we just mention the computational singular perturbation technique [2], the construction of intrinsic- and attracting- low-dimensional manifolds (respectively, ILDM [3] and ALDM [4]), and variational strategies like the trajectory-based methods [5].

In such a scenario, our idea is that the SM, being a general expected trait, should emerge, at least for the simplest class of mass-action chemical kinetics, from the properties of system-independent and universal "canonical" formats of the evolution law. In a series of articles ([6], [7], [8]) we derived and studied a *quadratic* canonical format of ordinary differential equations (ODEs) into which the polynomial rate equations of mass-action-based kinetics can be recast by adopting an extended set of mutually interrelated dynamical variables. A definition of SM naturally emerged. Interestingly, such a kind of transformation was already known as "embedding into Lotka-Volterra format" and was even rediscovered several times by various authors before us [9].

II. Canonical formats of ODEs

Here we shall focus on the simplest situation of N species involved in M elementary reactions taking place in a perfectly stirred medium under isothermal conditions. Let $\mathbf{x}$ be the N-dimensional array of the volumetric concentrations. The application of the mass-action law yields the following N-dimensional ODE system

$$\frac{dx_j}{dt} = \sum_{m=1}^{M} \left(\nu_{P_j}^{(m)} - \nu_{R_j}^{(m)} \right) r_m(\mathbf{x}) \quad , \quad r_m(\mathbf{x}) = k_m \prod_{i=1}^{N} x_i^{\nu_{R_i}^{(m)}} \tag{1}$$

where k_m is the kinetic constant of the m-th elementary reaction with rate $r_m(\mathbf{x})$, and $\nu_{R_j}^{(m)}$ and $\nu_{P_j}^{(m)}$ are the stoichiometric coefficients of species j as reactant and product, respectively, in that reaction. Let us consider the $N \times M$ new dynamical variables $h_{jm}(\mathbf{x}) = r_m(\mathbf{x})/x_j$, each associated with a pair species-reaction. Their physical dimension is inverse-of-time, and they evolve according to

$$\frac{dh_{jm}}{dt} = -h_{jm} \sum_{j',m'} M_{jm,j'm'} h_{j'm'} \tag{2}$$

with the matrix $M_{jm,j'm'} = (\nu_{P_{j'}}^{(m')} - \nu_{R_{j'}}^{(m')})(\delta_{j,j'} - \nu_{R_{j'}}^{(m)})$ where δ is the Kronecker delta. Notably, *any* mass-action based kinetics can be embedded into (2) regardless of the degree of non-linearity of the original rate equations. The interrelations among the new variables make the transformation invertible, i.e., the physical state $\mathbf{x}$ can be retrieved from the set of functions h_{jm} [6]. In practice, *general* features of the evolution in the extended space are mirrored by *specific* features of the dynamics in the concentration space (and vice versa). Eq. (2) represents the fundamental canonical form in our work.

By turning to the $(N \times M)^2$ dynamical variables $V_{jm,j'm'}(\mathbf{x}) = M_{jm,j'm'} h_{j'm'}(\mathbf{x})$, one gets the further extended set of ODEs

$$\frac{dV_{jm,j'm'}}{dt} = -V_{jm,j'm'} \sum_{j'',m''} V_{j'm',j''m''} \tag{3}$$

in which the details of the specific system are entirely borne on the initial conditions. Finally, by introducing the cumulative index $J \leftrightarrow (jm, j'm')$, the system's state can be expressed in a "hyper-spherical representation" where the new dynamical variables are the positive-valued rate $S = \sqrt{\mathrm{Tr}\{\mathbf{V}^T\mathbf{V}\}}$ (the "radial" variable) and the unit-norm vector $\boldsymbol{\psi}$ with $(N \times M)^2$ components $\psi_J \equiv V_{jm,j'm'}/S$. By inspecting the evolution law of S and $\boldsymbol{\psi}$ [8], we have

shown the existence of fixed subspaces (of the hyper-spherical space) that temporarily attract, one at a time, the vector $\boldsymbol{\psi}(t) \equiv \boldsymbol{\psi}(\mathbf{x}(t))$ while the reactive system follows a trajectory $\mathbf{x}(t)$ in the concentration space.

III. Candidate points to the SM proximity

From (2) and (3), it follows that the rate functions

$$z_{jm}(\mathbf{x}) = \sum_{j',m'} V_{jm,j'm'}(\mathbf{x}) \qquad (4)$$

control the evolution of the system in the extended space of the new dynamical variables. The heuristic analysis made in [6] and [7] allowed us to infer a close connection between the location of the zeros of the state-dependent time derivatives $z_{jm}^{(n)}(\mathbf{x})$ for $n \to \infty$ (with $z_{jm}^{(n)}(\mathbf{x}(t)) \equiv d^n z_{jm}(\mathbf{x}(t))/dt^n$ along a trajectory) and the SM. The subsequent analysis in the hyper-spherical representation [8] led us to justify the usage of low-order time derivatives to produce points which likely fall in the neighborhood of the SM. Namely, the scalar functions

$$Z_n(\mathbf{x}) = \sqrt{(NM)^{-1} \sum_{j,m} z_{jm}^{(n)}(\mathbf{x})^2} \quad , \quad n \geq 0 \qquad (5)$$

were proposed as "guiding potentials" to localize the candidate points via minimization strategies. Since Z_0 roughly quantifies the slowness of the system's evolution, and Z_1 catches the persistence of the slowness [8], a two-step minimization (of Z_0 and Z_1), in which the concentration of one species is held fixed, is expected to localize a point near the SM. Such a low-computational-cost method, recently illustrated in [10] and implemented in the DRIMAK ("Dimensional Reduction of Isothermal Mass-Action Kinetics") package [11], proved to be efficient in benchmark cases. Selected results for a basic hydrogen combustion model [12] are shown in Fig. 1. We stress that this strategy does not compete with other consolidated ones, rather it may be useful to provide initial points from which a more refined search of the SM can be performed.

IV. Perspectives

On methodological grounds, recasting the ODEs into canonical formats may reveal a powerful means to discover and characterize *general* traits (not only the slow manifold feature) which underlie the given class of dynamical systems. At the practical level, it would be interesting to test our "guiding potentials" $Z_n(\mathbf{x})$, with low order n, as objective functions in minimization strategies like the trajectory-based methods [5], in addition to the assessment of DRIMAK's performance on schemes involving a critical number of elementary steps and/or chemical species.

Acknowledgment

This work has been funded by Università degli Studi di Padova through "Progetti di Ricerca di Ateneo" - PRAT2013.

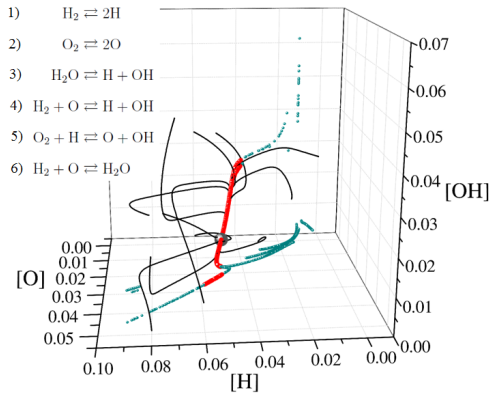

Fig. 1. Projection on the radical species subspace for the fictional hydrogen combustion scheme in [12] under the stoichiometric constraints $2[H_2] + 2[H_2O] + [H] + [OH] = 2$, $2[O_2] + [H_2O] + [O] + [OH] = 1$. All quantities are dimensionless; see [12] for the values of the kinetic constants. The green dots are candidate points produced by DRIMAK; the larger red marks are the points "filtered" by an ILDM-based post-production screening. The grey circle corresponds to the equilibrium point.

References

[1] C. K. R. T. Jones, in *Dynamical Systems, Lecture Notes in Mathematics*, vol. 1609, pp. 44-118 (L. Arnold Ed., Springer-Verlag, 1994).

[2] S. H. Lam and D. A. Goussis, "The CSP method for simplifying kinetics", *Int. J. Chem. Kinet.*, vol. 26, p. 461, 1994.

[3] U. Maas and S. B. Pope, "Simplifying chemical kinetics: Intrinsic low-dimensional manifolds in composition space", *Combust. Flame*, vol. 88, pp. 239-264, 1992.

[4] R. T. Skodje and M. J. Davis, "Geometrical simplification of complex kinetic systems", *J. Phys. Chem. A*, vol. 105, 1035610365, 2001.

[5] D. Lebiedz and J. Unger, "On unifying concepts for trajectory-based slow invariant attracting manifold computation in kinetic multiscale models", *Math. Comput. Model. Dyn.*, vol. 22, pp. 87-112, 2016.

[6] P. Nicolini and D.Frezzato, "Features in chemical kinetics. I. Signatures of self-emerging dimensional reduction from a general format of the evolution law", *J. Chem. Phys.*, vol. 138, 234101, 2013.

[7] P. Nicolini and D. Frezzato, "Features in chemical kinetics. II. A self-emerging definition of slow manifolds", *J. Chem. Phys.*, vol. 138, 234102, 2013.

[8] A. Ceccato, P. Nicolini, and D. Frezzato, "Features in chemical kinetics. III. Attracting subspaces in a hyper-spherical representation of the reactive system", *J. Chem. Phys.*, vol. 143, 224109, 2015.

[9] $^{(a)}$ J. L. Gouzé, "Transformation of polynomial differential systems in the positive orthant", Research Report RR-1308, INRIA. 1990, pp.10. $^{(b)}$ L. Brenig and A. Goriely, "Universal canonical forms for time-continuous dynamical systems", *Phys. Rev. A*, vol. 40, pp. 4119-4122, 1989. $^{(c)}$ B. Hernández-Bermejo and V. Fairén, "Nonpolynomial vector fields under the Lotka-Volterra normal form", *Phys. Lett. A*, vol. 206, pp. 3137, 1995. $^{(d)}$ V. Fairén and B. Hernández-Bermejo, "Mass action law conjugate representation for general chemical mechanisms", *J. Phys. Chem.*, vol. 100, pp. 19023-19028, 1996.

[10] A. Ceccato, P. Nicolini, and D. Frezzato, "A low-computational-cost strategy to localize points in the Slow Manifold proximity for isothermal chemical kinetics", *Int. J. Chem. Kinet.* vol. 49, pp. 477-493, 2017.

[11] DRIMAK is distributed under the General Public License v2.0. Software and documentation are available at: `http://www.chimica.unipd.it/licc/software.html`.

[12] A. N. Gorban, I. V. Karlin, and A. Y. Zynovyev, "Constructive methods of invariant manifolds for kinetic problems", *Physics Reports*, vol. 396, pp. 197-403, 2004.

Session: Reaction Diffusion System 2

Chair: T. Lu

Title: Reduced Models for Mixture-Averaged Diffusion
Authors: Y. Gao, J.-W. Park, T. Lu

Title: Identification of Low-Order Dynamics in Turbulent Premixed Flames with Dynamic Mode Decomposition
Authors: T. Grenga, J. F. MacArt, M. E. Mueller

Title: Multi-scale Adaptive Reduced Chemistry Solver (MARCS) for High-Dimensional Combustion Modeling with Detailed Chemical Kinetics
Authors: W. Sun, L. Wang, T. Grenga, Y. Ju

Title: Computation of supersonic reacting mixing layers with detailed and reduced kinetic mechanisms
Authors: C. Qian, Z. Huiqiang, Z. Weijiang, B. Peng, Y. Yunjun

Reduced Models for Mixture-Averaged Diffusion

Yang Gao, Ji-Woong Park and Tianfeng Lu*
Department of Mechanical Engineering, University of Connecticut
191 Auditorium Road Unit 3139, Storrs, CT, 06269 USA

***Abstract*—Different approaches to obtaining efficient and accurate reduced models for mixture-averaged diffusion (MAD) are proposed. The first approach is extended from the previous diffusive species bundling, in which species with similar binary diffusion coefficients are bundled to reduce the size of the binary diffusion coefficient matrix. To further improve the computational efficiency, the entries in the bundled binary diffusion coefficient matrix with non-negligible contribution to species MAD coefficients are identified based on sampled reaction states, and the other entries can be ignored. The second approach is based on the observation that, in the premixed fuel/air combustion, species MAD coefficients can be approximated with their binary diffusion coefficients with respect to N_2 while only inducing small errors. Therefore, the computational cost of evaluating MAD can be reduced from a quadratic to a linear function of the number of species. This approach can be further combined with species bundling to achieve even higher efficiency. These approaches are tested in 1D stretched and unstretched laminar flames under various conditions. *A posteriori* validation is performed using turbulent premixed DNS data. The results show good accuracy and significantly improved efficiency compared with the detailed MAD model.**

I. Introduction

Accurate modeling of molecular diffusion is important to predict many combustion problems such as near-limit flame behaviors and premixed flame propagation [1-3]. The mixture-averaged diffusion (MAD) model using the Curtiss-Hirschfelder approximation [4] has been widely used in flame simulations due to the relatively low computational cost and good accuracy in many cases compared with the multi-component models [5]. The computational cost of the MAD model is typically dominated by the evaluation of the binary diffusion coefficient matrix, which scales as a quadratic function of the number of species. To reduce the computational cost of the MAD model for large reaction mechanisms, Lu & Law [6] developed a method to bundle the diffusive species with similar diffusivities, such that the computational cost of evaluating binary diffusion coefficients can be reduced to a quadratic function of the number of diffusive groups. In the present study, the species bundling method is extended, such that the computational cost associated with the MAD model can become mostly negligible in CFD simulations.

II. Methodology

A. A reduced MAD model based on species bundling

The species diffusion velocity, $\boldsymbol{V}$, evaluated with the bundled MAD model without thermal diffusion and other correction effects can be written as [6]

$$\boldsymbol{V}_i = -\overline{D}_i \frac{\nabla X_i}{X_i}, \overline{D}_i = \frac{1-Y_i}{Q_{\mathrm{g}(i)} - \frac{X_i}{DG_{\mathrm{g}(i),\mathrm{g}(i)}}}, \quad (1a)$$

$$Q_n = \sum_{m=1}^{KG} Q_{n,m}, Q_{n,m} = \frac{XG_m}{DG_{n,m}}, XG_m = \sum_{\mathrm{g}(l)=m} X_l, \quad (1b)$$

where $\overline{D}_i$, Y_i and X_i are the MAD coefficient with bundling, mass fraction and mole fraction for the *i*th species, respectively. $\mathrm{g}(i)$ is the group number of the *i*th species. *KG* is the number of species groups. $DG_{n,m}$ is the binary diffusion coefficient between the representative species of group *n* and *m*. XG_m is the summation of species mole fractions in group *m*. For clarity, a matrix $\boldsymbol{Q}$ is defined with $Q_{n,m}$ being the entry at the *n*th row and *m*th column. Q_n is the summation of the *n*th row of matrix $\boldsymbol{Q}$.

It is seen from (1b) that the binary diffusion coefficients, $DG_{n,m}$, for some species may only have negligible contribution to $\overline{D}_i$ of the other species, e.g. if these species always stay in low concentrations. The binary diffusion coefficients involving such unimportant species can therefore be ignored. To quantify the importance of $Q_{n,m}$ to Q_n, an important index, $I_{n,m}$, is defined as

$$I_{n,m} \equiv \frac{|Q_{n,m}|}{\max_{j=1,KG} |Q_{n,j}|}, \quad (2)$$

and compared with a user-specified threshold value, such that the unimportant entries can be eliminated from (1) for reduced computational cost.

B. A linear-time reduced MAD model for premixed fuel/air combustion

For premixed fuel/air combustion, where N_2 is typically abundant, the species MAD coefficient can often be approximated with its binary coefficient with respect to N_2:

$$\boldsymbol{V}_i = -\overline{D}_i \frac{\nabla X_i}{X_i}, \overline{D}_i = D_{i,N_2}. \quad (3)$$

Compared with the detailed MAD model, the computational cost of evaluating species diffusivities is reduced from the quadratic function $O(K^2)$ to a linear function $O(K)$, where *K* is the number of species. This method can be further combined with species bundling, i.e.

$$\boldsymbol{V}_i = -\overline{D}_i \frac{\nabla X_i}{X_i}, \overline{D}_i = DG_{\mathrm{g}(i),g(N_2)}, \quad (4)$$

such that the computational cost is reduced to $O(KG)$.

III. Results and Discussions

A 24-species reduced model for *n*-dodecane [7] is used to demonstrate the performance of the reduced MAD models in

1D laminar premixed flames. The species are first bundled into 14 groups and the unimportant entries in (2) are eliminated using an error threshold of 0.1. Fig. 1(a) shows the sparse pattern of the matrix $\boldsymbol{Q}$, with the black pixels indicating the important entries identified based on reaction states sampled over a wide range of conditions with equivalence ratio of 0.5-1.5, pressure of 1-10 atm, and inlet temperature of 300 K for perfectly stirred reactors (PSR) and initial temperature of 1000-1600 K for auto-ignition. It is observed that, the 14-group bundled MAD model can be reduced to a 3-group reduced MAD model, i.e. only 3 important columns are retained in $\boldsymbol{Q}$. Fig. 1(b) compares laminar flame speed and global extinction strain rate of premixed counterflow flames as a function of equivalence ratio, calculated with different MAD models. It is seen that the results from the reduced models agree tightly with the detailed MAD model.

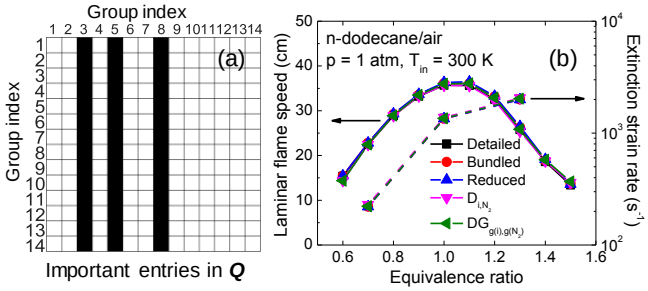

Fig. 1 (a) Sparse pattern of $\boldsymbol{Q}$ for the 3-group reduced MAD model. (b) Laminar flame speed and global extinction strain rate as a function of equivalence ratio, calculated with different MAD models. "Detailed" indicates the results calculated with the detailed MAD model without any simplification. "Bundled" and "Reduced" indicate the 14-group bundled and 3-group reduced models given in (1) and (2), respectively. "D_{i,N_2}" and "$DG_{\mathrm{g}(i),\mathrm{g}(N_2)}$" represent the linear-time reduced model and combined with species bundling given in (3) in (4), respectively.

To further demonstrate the accuracy of the reduced models, a 2D strongly turbulent premixed DNS flame of *n*-butane/air [7] is used for a *posteriori* validation. The DNS simulated a premixed flame propagating into fresh mixture at temperature of 500 K with an equivalence ratio of 0.6 and pressure of 5 atm. The solution at the time of 0.4 ms is used for current analysis, and the temperature field is plotted in Fig. 2(a). With an error threshold of 0.1, 25 species are first bundled to 10 groups. 3 important groups are further identified based on reaction states sampled over the parameter range with equivalence ratio of 0.6-0.9, pressure of 1-5 atm, and inlet temperature of 300 K for PSR and initial temperature of 1000-1600 K for auto-ignition. For each grid point, the species diffusivities are calculated with different MAD models using the local condition. The detailed MAD model is taken as the base model, and relative errors in species diffusivities are measured for different reduced models and plotted in Fig. 2(b). The worst-case error at each grid indicates the maximum error in diffusivities for all the species. The worst-case errors for the 10-group bundled and 3-group reduced models (red and blue) are effectively controlled by the error threshold. The worst-case errors for the linear-time reduced model with or without species bundling (olive, magenta and cyan) are within about 10%. Note that the worst-case error is less than 5% if excluding the errors in the diffusivity of N_2 (cyan).

The speedup factors of the reduced models for *n*-dodecane and *n*-butane are summarized in Table I. The speedup factors are measured by comparing the CPU time of one time evaluation of species diffusivities using the reduced MAD models with that of the detailed MAD model. Significant speedup is observed for all the cases, particularly for the linear-time reduced model combined with species bundling.

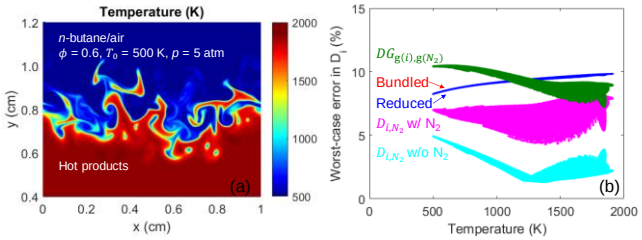

Fig. 2 (a) Temperature contour for the 2D DNS of *n*-butane/air at time of 0.4 ms. (b) Worst-case errors in species diffusivities as functions of temperature, calculated with different reduced MAD models.

TABLE I. Speedup factors of different MAD models

MAD models	Speedup factors	
	n-dodecane	*n*-butane
Bundled	2.5 (14 groups)	4.4 (10 groups)
Reduced	3.8 (3 groups)	5.6 (3 groups)
D_{i,N_2}	31.7	32.3
$DG_{\mathrm{g}(i),\mathrm{g}(N_2)}$	44.5	61.6

IV. Conclusions

Approaches to obtaining efficient and accurate reduced MAD models are proposed and tested for laminar flame speed and extinction of 1D premixed counterflow flames of *n*-dodecane/air. A *posteriori* validation of species diffusivities evaluated with different reduced MAD models is performed using 2D DNS data for *n*-butane/air, showing the worst-case errors of less than about 10%. CPU time is measured for the reduced MAD models and compared with the detailed MAD model. Speedup factors of ~45-60 are observed for the linear-time reduced model combined with species bundling for *n*-dodecane and *n*-butane, respectively.

Acknowledgment

This work was supported by NASA NRA NNX15AU96A under the technical monitoring of Dr. Jeff Moder.

References

[1] C. K. Law, *Combustion physics*, Cambridge University Press, New York, 2006.

[2] R. Hilbert, F. Tap, H. El-Rabii, D. Thevenin, Impact of detailed chemistry and transport models on turbulent combustion simulations, *Prog. Energy Combust. Sci.* 30 (1) (2004) 61-117.

[3] T. Lu, C. K. Law, Toward accommodating realistic fuel chemistry in large-scale computations, *Prog. Energy Combust. Sci.* 35 (2) (2009) 192-215.

[4] R. B. Bird, W. E. Stewart, E. N. Lightfoot, *Transport Phenomena*, Wiley, New York, 1960.

[5] M. D. Smooke, The computation of laminar flames, *Proc. Combust. Inst.* 34 (1) (2013) 65-98.

[6] T. Lu, C. K. Law, Diffusion coefficient reduction through species bundling, *Combust. Flame* 148 (3) (2007) 117-126.

[7] Y. Gao, R. Shan, S. Lyra, C. Li, H. Wang, J. H. Chen, T. Lu, On lumped-reduced reaction model for combustion of liquid fuels, *Combust. Flame* 163 (2016) 437-446.

Identification of Low-Order Dynamics in Turbulent Premixed Flames with Dynamic Mode Decomposition

Temistocle Grenga *, Jonathan F. MacArt*, Michael E. Mueller*
*Department of Mechanical and Aerospace Engineering, Princeton University, USA

***Abstract*— Dynamic Mode Decomposition (DMD) has emerged as a promising tool for the investigation of unsteady and dynamic phenomena. In this work, DMD is applied to the investigation of broadband phenomena in turbulent premixed flames using large-scale DNS data. A new, efficient parallel implementation of DMD has been developed for analysis of large-scale DNS databases. This is then used to identify coherent modes in turbulent premixed flames and provide insights into the dynamical features of such flames.**

I. Introduction

DMD, first developed by Schmid [1], is a powerful method for analyzing the dynamics of nonlinear systems using data generated from either computations or experiments. In its application to fluid dynamics and combustion, DMD is able to identify the low-order dynamics describing the flow field described by the infinite-dimensional Navier-Stokes equations. DMD modes are a numerical approximation to Koopman modes, which represent nonlinear, finite-dimensional dynamics without linearization. The identified flow structures are unbiased by energy, so they are particularly well suited to probing dynamic processes at scales smaller than the largest, energy-containing scales. The eigenvalues corresponding to the DMD modes are the Ritz values, and they provide a characteristic frequency and growth/decay rate for each mode, which allows for understanding the role of nonlinear structures in turbulent combustion. These coherent structures, spanning multiple time and length scales, are locally transient and non-linear, may not obey Taylor's hypothesis of frozen turbulence, and cannot be identified with statistical analysis.

In this work, DMD is used as a tool to analyze three-dimensional DNS of a low Mach number spatially-evolving turbulent planar hydrogen/air premixed jet flame. The focus of this investigation will be on the practical use of DMD for analyzing large datasets as well as the identification of the dominant modes and their characteristics in broadband turbulent premixed flames.

II. DMD Algorithm

Consider a sequence of data vectors $\mathbf{x}_k \in \mathbb{R}^n$ containing the variables in a multidimensional domain at a single snapshot in time, where m is the number of snapshots forming the sequence of data and n is the dimension of the vector. These vectors are arranged into a matrix of dimension $n \times m$, $X = [\mathbf{x}_1, \ldots, \mathbf{x}_{m-1}]$. It is assumed that a linear tangent approximation, or rather that an unknown linear mapping A, relates a snapshot to the next one $\mathbf{x}_{k+1} = A\mathbf{x}_k$. The DMD modes and Ritz values are an approximation of the eigenvectors and eigenvalues of A, which, to this point, remains unknown.

The original DMD algorithm [1] is strongly related to Koopman operator theory. An approximation of A, $\tilde{A}$, is constructed through the SVD of X, which is then decomposed further to determine the DMD modes and Ritz values. For very large systems, this algorithm is inefficient or even computationally intractable since the size of the data snapshot vectors can be tens of millions and hundreds or thousands of snapshots could be considered.

Tu *et al.* [2] created a memory efficient algorithm that requires the loading in memory of only two snapshots at a time, so the algorithm can be applied to very large datasets. Moreover, they computed the SVD of X using the method of snapshots introduced by Sirovich [3]. This algorithm, in the version used in this work, has been further improved by Belson *et al.* [4], eliminating unnecessary inner products and linear combinations.

In this algorithm, the correlation matrix is defined as the inner product of the various snapshot having elements $[H]_{i,j} =< \mathbf{x}_i, \mathbf{x}_j >$, where the indices i and j have the range $1, \ldots, m-1$. The eigenvectors of the correlation matrix are computed $HW = W\tilde{\Sigma}$ in order to define $\tilde{A}$ as $\tilde{A} = \tilde{\Sigma}^{1/2} W^* [H^{'} H^{''}] W \tilde{\Sigma}^{1/2}$, where $H^{'} = [H]_{1:m-1,2:m-1}$ and $H^{''} =< \mathbf{x}_m, \mathbf{x}_j >$, with $j = 1, \ldots, m-1$. After solving the eigensystem for $\tilde{A}$, $\tilde{A}\tilde{V} = \Lambda\tilde{A}$, the scaled DMD modes are given by

$$\phi_j = \sum_{i=1}^{m} \lambda_i^{m-1} \mathbf{x}_i [T]_{i,j} \tag{1}$$

where $T = W^* \tilde{\Sigma}^{1/2} \tilde{V} D$ and D is a diagonal matrix having diagonal $\mathbf{d} = (\tilde{V}^* \tilde{V})^{-1} \tilde{V}^* \tilde{\Sigma}^{1/2} \tilde{V}^* [H]_{1:m-1,1}$.

The algorithm has been implemented in two codes in order to maximize the computational efficiency. The first code is devoted to the the evaluation of H and $H^{''}$, which is distributed over a large number of cores, ideally one

element per core. Due to the size of the snapshots, it is not possible to load in memory more than two snapshots nor is redistribution of the data through all-to-all communication. Therefore, the second code evaluates the eigensysytem of H and $\tilde{A}$, as well as the DMD modes. The evaluation of the eigensystems is computationally inexpensive because of small dimensions of the matrices. However, evaluation and output to disk of the DMD modes (Eq. 1) requires large I/O bandwidth.

III. Results

To generate the DNS database, the Navier-Stokes equations are solved in the low Mach number limit using a semi-implicit iterative algorithm of Desjardins *et al.* [5], implemented in the code NGA, and recently updated for the solution of the species equation [6]. The numerical simulations include spatially-developing coflowing Cartesian planar jets at $Re = 5000$, in a domain having dimensions $12D \times 24D \times 3D$ in the streamwise (x), cross-stream (y) and spanwise (z) directions, respectively. The boundary conditions are inflow on the $-x$ face, outflow on $+x$ one, free slip on $\pm y$ faces, and periodic in the z-direction. A central jet of height $D = 4.32$ mm is separated from two coflow jets by thin walls. The central jet consist of a stoichiometric hydrogen-air mixture at a temperature of 300 K, diluted 80% by mass with nitrogen at 23.35 m/s. The coflow jets have heights $4.5D$ and consist of equilibrium products of combustion at 116.42 m/s. A slow bulk flow of equilibrium products at 10 m/s is placed near the top and bottom boundaries. A nine species hydrogen chemical kinetic model [7] is used.

The subdomain considered for the DMD analysis has dimensions $7D \times 4D \times 1D$ in the x-, y-, and z- direction, respectively. The subdomain contains almost five million grid points, so the snapshot dimension is $n \approx 3 \times 10^7$ since six variables (the three velocity components, the temperature, and the mass fractions of OH and H_2O) are considered. The number of snapshots considered is up to $m = 400$, spaced in time with $\Delta t = 2\mu$s. In total, for this DMD analysis, 12 billion data values are used. This amount of data makes the standard DMD algorithm impossible to perform, but an efficient parallel implementation of the snapshot algorithm presented above requires approximately 25,000 CPU-hours to perform the analysis.

Figure 1(a) shows that all the Ritz values for the case $m = 400$ are close to the unit circle, while the values for $m = 20$ are inside the unit circle. The eigenvalues lying outside the circle would identify unstable modes, while the ones lying inside identify stable modes, with the distance from the circle a measure of the explosive/dissipative nature of the modes. The Ritz eigenvalues are further transformed into the complex stability plane through the logarithmic transformation $\mu_i = \log(\lambda_i)/\Delta t$. The real part of μ_i is the exponential growth or decay rate of the i-th mode,

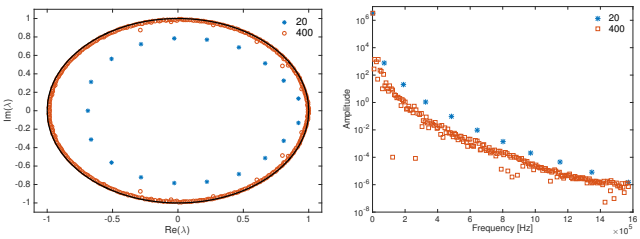

Fig. 1. (a) Ritz values on the complex plain, and (b) L_2-norm of the amplitude of the modes.

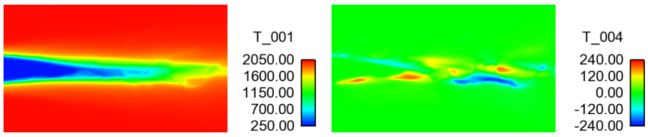

Fig. 2. Example of DMD modes: (a) mode 1 and (b) mode 4.

while the imaginary part represents the temporal frequency. Figure 1(b) shows the amplitude of each mode (L_2-norm) versus the temporal frequency. For both dataset sizes, the mode amplitude decays rapidly with increasing temporal frequency. The smaller dataset is qualitatively similar to the larger dataset, but the frequencies are not exactly the same, as anticipated from the fact that the Ritz values did not lie on the unit circle. Moreover, the smaller number of modes do not allow adequate resolution of the dominant reacting flow structures.

Figure 2(a) shows mode 1, having $\mu_1 = 0$, which represents the time-averaged flow and captures the steady flow structures. Mode 4 in Fig. 2(b) is a low-frequency mode containing the large scale turbulence structures resulting from a combination of shear and chemical reaction.

References

[1] Schmid, P. J., "Dynamic mode decomposition of numerical and experimental data," *Journal of Fluid Mechanics*, 656 (2010) 5–28

[2] Tu, J.H., Rowley, C.W., "An improved algorithm for balanced POD through an analytic treatment of impulse response tails," *Journal of Computational Physics* 231.16 (2012) 5317-5333.

[3] Sirovich, L., "Turbulence and the dynamics of coherent structures. I. Coherent structures," *Quarterly of Applied Mathematics* 45.3 (1987) 561-571.

[4] Belson, B.A., Tu, J.H., Rowley, C.W., "Algorithm 945: modred-A parallelized model reduction library," *ACM Transactions on Mathematical Software (TOMS)* 40.4 (2014) 30.

[5] Desjardins, O., Blanquart, G., Balarac, G., Pitsch, H., "High order conservative finite difference scheme for variable density low Mach number turbulent flows," *Journal of Computational Physics* 227.15 (2008) 7125-7159.

[6] MacArt, J.F., Mueller, M.E., "Semi-implicit iterative methods for low Mach number turbulent reacting flows: Operator splitting versus approximate factorization," *Journal of Computational Physics* 326 (2016) 569-595.

[7] Davis, S.G., Joshi, A.V., Wang, H., Egolfopoulos, F., "An optimized kinetic model of H2/CO combustion," *Proceedings of the Combustion Institute* 30.1 (2005) 1283-1292.

Multi-scale Adaptive Reduced Chemistry Solver (MARCS) for High-Dimensional Combustion Modeling with Detailed Chemical Kinetics

Weiqi Sun[1], Liang Wang[1,2], Temistocle Grenga[1] and Yiguang Ju[1,*]
[1] Princeton University, Mechanical and Aerospace Engineering, Princeton, USA
[2] Tsinghua University, School of Aerospace Engineering, Beijing, China

***Abstract*—A Multiscale Adaptive Reduced Chemistry Solver (MARCS) is developed by integrating the Correlated Dynamic Adaptive Chemistry and Transport (CO-DACT) method and Hybrid Multi-Timescale (HMTS) and G-Scheme method together to conduct the efficient combustion modeling with detailed chemical kinetics. The in-house Full Speed Fluid code are further utilized to compute convection fluxes and transport processes. The preliminary results of ignitions and flame propagations in this paper demonstrate that the computational efficiency can be improved by orders of magnitude using CO-DACT method with HMTS and G-Scheme methods. In the final presentation, simulations of a two-dimensional jet flame and an oblique shock induced auto-ignition with detailed mechanisms will be conducted to validate the present algorithm.**

I. Introduction

The large and detailed chemical kinetics have been challenges in combustion modeling for decades. The first challenge comes from the stiff ODE system which govern the chemical reactions. In a chemical reaction system, the characteristic time of different species can vary from millisecond to picosecond and even beyond. In order to integrate the stiff ODE system efficiently, advanced time integration methods are required. Several chemical solvers have been developed in last decades, among them, the HMTS method[1] and the G-Scheme method[2,3] have the potential to be integrated together and provide an efficient integration for detailed chemical kinetics.

The second challenge of utilizing detailed chemistry in simulations is the size of chemical mechanism that proportionally increases number of degrees of freedom of the problem. In order to reduce the number of species and reactions in simulations, several methods have been developed. Among these methods, the Correlated Dynamic Adaptive Chemistry (CO-DAC) method[4] can provide locally reduced mechanism on-the-fly without generating overhead CPU time cost.

Another challenge comes from the accurate calculation of transport properties for a large number of species. Indeed, these needs to be evaluated in all the cells and at each time step because they vary significantly across the temporal and spatial coordinates due to the rapid species and temperature variations caused by chemical reactions. Both the traditional multi-component diffusion model and mixture-averaged model become inefficient to be used when a large chemical mechanism is involved. The CO-DACT method[5] makes the computation cost of transport properties calculation negligible by conducting the transport properties calculation in phase space, and reducing the computational cost of two orders of magnitude.

The goal of this paper is to present the MARCS method for an efficient numerical computation of combustion simulations by integrating the CO-DACT method, HMTS and G-Scheme method together with an in house Full Speed Fluid Solver. MARCS method will be here validated solving an oblique shock induced auto-ignition with detailed mechanisms.

II. Methodology

A. CO-DACT method

In a combustion simulation, one cell in adjacent time steps or two different cells in the same time step may have similar thermodynamic conditions, which results in the same local reduced chemical mechanism and/or transport properties. Therefore, detailed calculations in similar cells are redundant. Based on this idea, the CO-DACT method examines computational cells in correlated space spanned by a few phase parameters. Similar cells in the correlated space will be grouped so that the detailed calculation for chemical reduction and transport properties is performed only once.

B. HMTS and G-Scheme method

Based on the locally reduced mechanism from the CO-DACT method, the chemical reactions are integrated by HMTS or G-Scheme method. The solver automatically determines which method to use based on the combustion regime and the size of mechanism.

C. Full Speed Fluid Solver

The HMTS and G-Scheme methods are implemented into an in-house parallelized code, Full Speed Fluid Solver to simulate unsteady, compressible and reactive flows. The convection and diffusion terms are discretized with 3rd-order AUSMPW+ and central difference schemes respectively. A modified fully implicit lower-upper symmetric Gauss-Seidel (LU-SGS) scheme with Newton-like sub-iterations in pseudo time is taken as time marching method for solving the Navier-Stokes equations.

III. Results and Discussion

The preliminary results presented in this section are used to demonstrate the capability of the Full Speed Fluid Solver, CO-DACT and HMTS methods, respectively. The results of the 2D jet flame and oblique shock induced ignition will be included in the final presentation.

Fig 1 shows the density contours in a double Mach reflection case calculated by the Full Speed Fluid Solver with AUSM+ (left) and AUSMPW+ (right) respectively. The computational domain is [0, 4] × [0, 1]. The lower boundary is set to be reflecting wall starting from x = 1/6. At t = 0, a right-moving 60° inclined Mach 10 shock is positioned at [1/6, 0]. The upper boundary is set to describe the exact motion of the Mach 10 shock. The left boundary at x = 0 is assigned with post-shock values. An outflow condition with zero gradients is set at x = 4. It is seen from this figure that the shock waves as well as the small structures near the up-rolling region are well captured by both schemes. However, only the AUSMPW+ scheme adopted in the present solver can resolve structures along the contact line, which implies that the Full Speed Fluid Solver with AUSMPW+ scheme is more accurate and less dissipative near discontinuities.

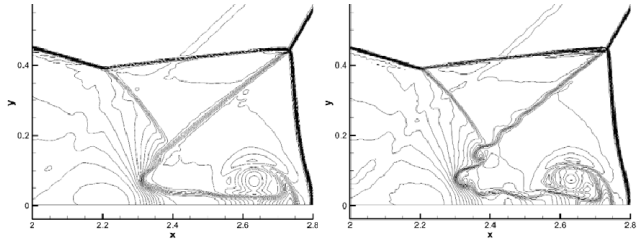

Fig. 1. Density contours of the double Mach reflection problem calculated by AUSM+ (left) and AUSMPW+ (right) schemes respectively.

In order to demonstrate the computational efficiency of the CO-DACT method, the CPU time comparisons between VODE, HMTS, HMTS/CO-DAC and HMTS/CO-DACT methods in a premixed spherical propagating flame calculation is plotted in Fig. 2. It shows that for the VODE method the computational cost is mostly due to the chemistry integration cost. This cost is reduced by one order of magnitude using HMTS and even further using HMTS/CO-DAC. In this latter case the evaluation of the transport properties is larger than the chemistry integration cost, however, using HMTS/CO-DACT this becomes negligible.

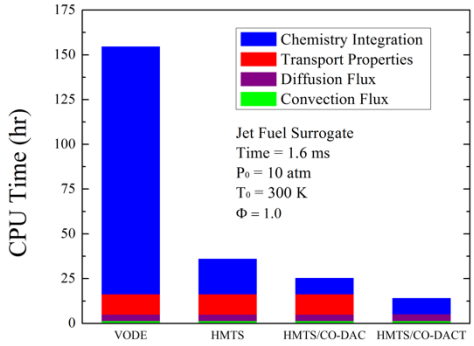

Fig. 2. CPU time comparisons for CO-DACT.

Fig. 3 shows the comparison of the computational cost between HMTS (blue) and G-Scheme (red) methods with different chemical mechanisms. It demonstrates that the dependency of CPU time on the mechanism size is first order and third order, respectively for HMTS and G-Scheme method. Therefore, the solver automatically switches to G-Scheme method when the local reduced mechanism is smaller than 40 species and select HMTS method when the mechanism is larger, so that it can be more efficient.

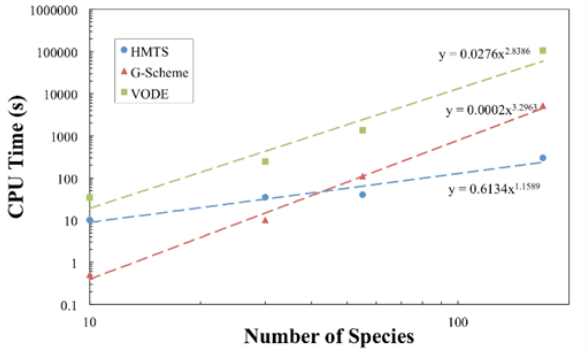

Fig. 3. CPU time comparison between HMTS and G-Scheme.

IV. Conclusion

The capability of the in-house Full Speed Fluid Solver and the efficiency of the CO-DACT, HMTS and G-Scheme methods are demonstrated in the preliminary results. The parallel Full Speed Fluid Solver can handle large scale and multi-dimensional simulations. The CO-DACT, HMTS and G-Scheme methods are able to accelerate the combustion modeling by orders of magnitude. Therefore, by integrating them together, the proposed MARCS method has the promising potential to conduct combustion modeling in large domain and multi-dimensional geometry with detailed chemical kinetics in order to investigate complicated coupling between chemistry and transport.

Acknowledgment

The authors would like to thank the grant support from the Army Research Office with grant number W911NF-16-1-0076.

References

[1] X. Gou, W. Sun, Z. Chen, and Y. Ju, "A dynamic multi-timescale method for combustion modeling with detailed and reduced chemical kinetic mechanisms," *Combust. Flame*, vol. 157, no. 6, pp. 1111–1121, Jun. 2010.

[2] M. Valorani and S. Paolucci, "The G-Scheme: A framework for multi-scale adaptive model reduction," *J. Comput. Phys.*, vol. 228, no. 13, pp. 4665–4701, 2009.

[3] T. Grenga, S. Paolucci, and M. Valorani, "G-Scheme-based simplification and analysis methodology for hydrocarbon ignition," in *Eastern States Section of the Combustion Institute*, 2016.

[4] W. Sun, X. Gou, H. a. El-Asrag, Z. Chen, and Y. Ju, "Multi-timescale and correlated dynamic adaptive chemistry modeling of ignition and flame propagation using a real jet fuel surrogate model," *Combust. Flame*, vol. 162, no. 4, pp. 1530–1539, 2015.

[5] W. Sun and Y. Ju, "Multi-timescale and Correlated Dynamic Adaptive Chemistry and Transport Modeling of Flames in n-Heptane/Air Mixtures," *53rd AIAA Aerosp. Sci. Meet.*, 2015.

Computation of supersonic reacting mixing layers with detailed and reduced kinetic mechanisms

Chen Qian*, Zhang Huiqiang†, Zhou Weijiang*, Bai Peng*, Yang Yunjun*
* China Academy of Aerospace Aerodynamics, Beijing 100074, China
† School of Aerospace Engineering, Tsinghua University, Beijing 100084, China

***Abstract*—Numerical simulations of supersonic reacting mixing layers using high-order numerical schemes with detailed and reduced kinetic mechanisms were conducted. Two interesting differences between the instantaneous fields based on the two mechanisms are observed, which implies the necessity of a reasonable mechanism in computations.**

I. INTRODUCTION

The flow and combustion of supersonic reacting mixing layer are typical phenomena in the combustion chamber of hypersonic air-breathing propulsion system. Understanding the mechanisms involved is of great importance for the human beings to overcome the problems encountered. In the past three decades, a number of researches on flow and combustion of supersonic reacting mixing layers were conducted computationally using different methods [1-12]. Some of them utilized laminar simulation [1-6] while others used turbulent simulation [7-12]. The reaction mechanisms employed in these works included global mechanism [1, 7], reduced mechanism [2, 4] and detailed mechanism [3, 5-12].

Generally, the global mechanism is not accurate enough for the prediction of ignition process [7], although recent simulations of combustion in scramjets often adopt this kind of mechanism. The reduced mechanism is able to identify some characteristics of ignition process [4], while the reduction method should base on reasonable assumptions [2]. The detailed mechanism is the most accurate choice, but a large amount of computational resource is needed.

The present work attempts to conduct high-accuracy numerical simulations of supersonic reacting mixing layers, using both reduced and detailed reaction mechanisms. High-accuracy numerical simulations are now useful methods to investigate the mechanisms involved in flow and combustion, and are also effective means to compare the performances of various reaction mechanisms. In the following, physical and mathematical models as well as computational methods are described briefly in section II. After that, results and discussions are given in section III. Finally, conclusions are drawn in section IV.

II. MODELS AND METHODS

The physical model in this study is a supersonic H2/air reacting mixing layer. Near the interface of the two freestreams, physical interactions will happen and lead to a turbulent shear layer region. After the fluids mix on a molecular scale, there may be chemical reactions in the turbulent shear layer region [13].

The basic equations for such supersonic reacting mixing layer are multi-component Navier-Stokes equations [14]. The reduced H_2-O_2 reaction mechanism consists of 8 elementary reaction steps [15] while the detailed mechanism consists of 19 elementary reaction steps [16].

The initial vorticity thickness $\delta_{\omega 0}$ for the flow is taken as 4×10^{-4}m. The sizes of computation domain in streamwise, transverse and spanwise directions are $600\delta_{\omega 0}$, $100\delta_{\omega 0}$ and $50\delta_{\omega 0}$, respectively. The computational grid is uniform in streamwise and spanwise directions, but is refined in transverse direction in the turbulent shear layer region. The number of grid points is about 6000000 and the streamwise, transverse and spanwise minimum spacing are $0.74\delta_{\omega 0}$, $0.50\delta_{\omega 0}$ and $0.72\delta_{\omega 0}$, respectively. This spacing is small enough compared with the recent DNS of supersonic reacting mixing layer [17].

The convective term is discretized by a fifth-order compact-WENO hybrid scheme [18]. The diffusion term is discretized by a sixth-order compact scheme [19]. The source term is treated with point-implicit scheme [20]. The unsteady term is integrated with Runge-Kutta scheme [18].

III. RESULTS AND DISCUSSIONS

Based on the above models and methods, instantaneous fields of various properties are obtained. Two key phenomena will be analyzed briefly in this extended abstract.

The first key phenomenon is about combustion patterns. Fig. 1 compares the rate of heat release per unit volume in the two cases. It shows that the combustion happens earlier in the case based on detailed mechanism. The O_2 mass fraction in Fig. 2 and the H_2 mass fraction in Fig. 3 together show that in both cases the turbulent shear layer regions are fuel-rich but in the case based on detailed mechanism the O_2 are consumed away earlier. Different combustion patterns (premixed, partially premixed and diffusion combustion) appear in the two cases. This phenomenon may due to the difference of ignition delay times between the reduced and detailed mechanisms.

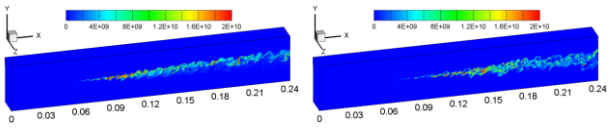

(a) Detailed mechanism (b) Reduced mechanism

Fig. 1 Distribution of rate of heat release per unit volume at $t=6.4\times10^{-4}$s

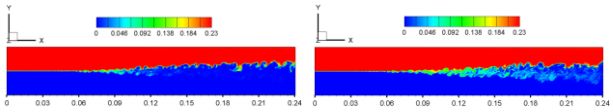

(a) Detailed mechanism (b) Reduced mechanism

Fig. 2 Distribution of O_2 mass fraction on z_{max} plane at t=6.4×10^{-4}s

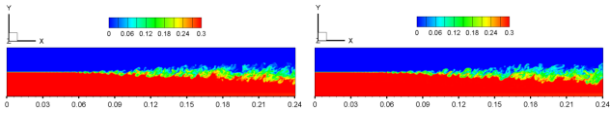

(a) detailed mechanism (b) reduced mechanism

Fig. 3 Distribution of H_2 mass fraction on z_{max} plane at t=6.4×10^{-4}s

The second key phenomenon is about combustion induced shock-wave. Fig. 4 and Fig. 5 compare the pressure and density in the two cases. It is shown that the freestream pressure and density distributions before the ignition position in the two cases are similar. However, after the ignition position, large differences appear. The freestreams pressures and density rise earlier in the case based on detailed mechanism. This pressures and density rise is caused by shock waves which are shown in Fig. 6 using the iso-surfaces of normal Mach number. This is the phenomenon of combustion induced shock-wave in supersonic mixing layer [12].

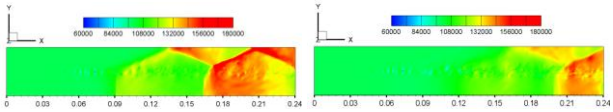

(a) Detailed mechanism (b) Reduced mechanism

Fig. 4. Distribution of pressure on z_{max} plane at t=6.4×10^{-4}s.

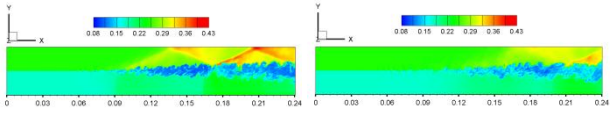

(a) Detailed mechanism (b) Reduced mechanism

Fig. 5. Distribution of density on z_{max} plane at t=6.4×10^{-4}s.

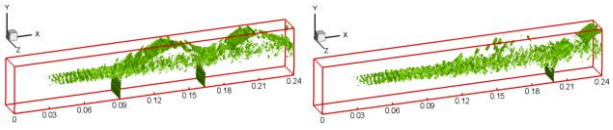

(a) Detailed mechanism (b) Reduced mechanism

Fig. 6. Iso-surfaces of normal Mach number at t=6.4×10^{-4}s.

In all, the instantaneous fields in the case based on detailed kinetic mechanism are much different from that base on reduced kinetic mechanism.

IV. Conclusions

Since the effect of kinetic mechanisms on the results of computation is nontrivial, the importance of adoption of a proper kinetic mechanism in the high-accuracy numerical simulations of supersonic reacting mixing layers should be emphasized. A reasonable kinetic mechanism is necessary for the understanding of flow and combustion of supersonic reacting mixing layer through numerical simulations.

References

[1] C. E. Gosch, and T. L. Jackson, "Ignition and structure of a laminar diffusion flame in a compressible mixing layer with finite rate chemistry," *Phys. Fluids A*, vol. 3, pp. 3087-3097, December 1991.

[2] Y. Ju, and T. Niioka, "Reduced kinetic mechanism of ignition for nonpremixed hydrogen/air in a supersonic mixing layer," *Combust. Flame*, vol. 99. pp. 240-246, February 1994.

[3] Y. Ju, and T. Niioka, "Ignition simulation of methane/hydrogen mixtures in a supersonic mixing layer," *Combust. Flame*, vol. 102, pp. 462-470, April 1995.

[4] C. Treviño, and A. Liñán, "Mixing layer ignition of hydrogen," *Combust. Flame*, vol. 103, pp. 129-141, February 1995.

[5] M. Nishioka, and C. K. Law, "A numerical study of ignition in the supersonic hydrogen/air laminar mixing layer," *Combust. Flame*, vol. 108, pp. 199-219, February 1997.

[6] J. H. Tien, and R. J. Stalker, "Release of chemical energy by combustion in a supersonic mixing layer of hydrogen and air," *Combust. Flame*, vol. 131, pp. 329-348, March 2002.

[7] D. Chakraborty, H. V. Nagarai Upadhyaya, and P. J. Paul, "A thermo-chemical exploration of a two-dimensional reacting supersonic mixing layer,". *Phys. Fluids*, vol. 9, pp. 3513-3522, November 1997.

[8] K. Luo, "Combustion effects on turbulence in a partially premixed supersonic diffusion flame," *Combust. Flame*, vol. 119, pp. 417-435, April 1999.

[9] A. M. Starik, N. S. Titova, L. V. Bezgin, and V. I. Kopechnov, "The promotion of ignition in a supersonic H_2-air mixing layer by laser-induced excitation of O_2 molecules: Numerical study," *Combust. Flame*, vol. 156, pp. 1641-1652, August 2009.

[10] J. O'Brien, J Urzay, M. Ihme, P. Moin, and A. Saghafian, "Subgrid-scale backscatter in reacting and inert supersonic hydrogen–air turbulent mixing layers," *J. Fluid Mech.*, vol. 743, pp. 554-584, January 2014.

[11] Q. Chen, B. Wang, H. Q. Zhang, Y. L. Zhang, and W. Gao, "Numerical investigation of H_2/air combustion instability driven by large scale vortex in supersonic mixing layers," *Int. J. Hydrogen Energy*, vol. 41, pp. 3171-3184, January 2016.

[12] Q. Chen, *Numerical Investigation of Combustion in Three Dimensional Spatially Developing Supersonic Mixing Layers*. Ph. D Dissertation, Beijing: Tsinghua University, 2016.

[13] Q. Chen, H. Q. Zhang, B. Wang, W. J. Zhou, Y. J. Yang, "A compatible inlet condition for supersonic reacting mixing layers," unpublished.

[14] T. Poinsot, and D. Veynante, *Theoretical and Numerical Combustion*, 2nd ed., Philadelphia: Edwards Inc., 2005.

[15] S. R. Lee, C. K. Law. "Asymptotic analysis of ignition in nonpremixed counterflowing hydrogen versus heated air," *Combust. Sci. Technol.*, 1994.

[16] R. A. Yetter, F. L Dryer, and H. A. Rabitz, "Comprehensive Reaction Mechanism for Carbon Monoxide/Hydrogen/Oxygen Kinetics," *Combustion Sci. Technol.*, vol. 79, pp. 97-128, 1991.

[17] P. J. M. Ferrer, G. Lehnasch, and A. Mura, "Direct Numerical Simulations of High Speed Reactive Mixing Layers," *J. Phys.: Conference Series*, vol. 395, N012004, pp. 1-8, 2012.

[18] Y. X. Ren, M. E. Liu, and H. X. Zhang, "A characteristic-wise hybrid compact-WENO scheme for solving hyperbolic conservation laws," *J. Comput. Phys.*, vol. 192, pp. 365-386, February 2003.

[19] S. K. Lele, "Compact Finite Difference Schemes with Spectral-Like Resolution," *J. Comput. Phys.*, vol. 103, pp. 16-42, January 1992.

[20] T. R. A. Bussing, and E. M. Murman, "Finite Volume Method for the Calculation of Compressible Chemically Reacting Flows," *AIAA J.*, vol. 26, pp. 1070-1078, September 1988.

Session: Mechanism Simplification 2

Chair: M. Valorani

Title: A Novel Strategy for Analysis and Reduction of Uncertain Chemical Kinetic Models
Authors: R. Malpica Galassi, M. Valorani, H. N. Najm, C. Safta, M. Khalil, P. P. Ciottoli

Title: LES for Turbulent Non-Premixed Jet Flame with CODAC Reduction
Authors: Z. Liu, W. Han, W. Kong, Y. Ju

Title: Automated Construction, Reduction, and Optimization of Chemistry for Reactive Flow Modelling
Authors: X. Gou, Z. Chen, W. Sun, Y. Ju

Title: Propagation of Kinetic Uncertainty thregh Surrogate Subspace in Combustion Simulations
Authors: W. Ji, J. Wang, B. Yang, Z. Ren, C. K. Law

A novel strategy for analysis and reduction of uncertain chemical kinetic models

Riccardo Malpica Galassi*, Mauro Valorani*, Habib N. Najm†, Cosmin Safta†,
Mohammad Khalil†, Pietro Paolo Ciottoli*
*Sapienza University of Rome, Dipartimento di Ingegneria Meccanica e Aerospaziale, Rome, Italy
†Sandia National Laboratories, Livermore, CA 94551, USA

***Abstract*— We outline a strategy for chemical kinetic model reduction under uncertainty. We present highlights of our existing deterministic model reduction strategy, and describe the extension of the formulation to include parametric uncertainty in the detailed mechanism. We discuss the utility of this construction, as applied to hydrocarbon fuel-air kinetics, and the associated use of uncertainty-aware measures of error between predictions from detailed and simplified models.**

I. Introduction

Chemical model reduction strategies generally start from a detailed chemical kinetic mechanism as the reference or baseline gold-standard. Given this standard, a specified range of operating conditions or set of state vectors, a select set of Quantities of Interest (QoIs), and a requisite error threshold, a model reduction strategy produces a simplified mechanism of associated size/complexity [1], [2].

This strategy, despite its effectiveness, nonetheless relies on the quality of the starting mechanism. Yet, there is typically significant uncertainty in both the structure of available detailed mechanisms for hydrocarbon fuels, and their thermodynamic and chemical kinetic rate parameters. Therefore, in principle, the analysis/reduction processes that provide simplified mechanisms starting from the detailed mechanism, and the measures of quality of a simplified mechanism relative to the detailed mechanism, need to account for both model and parametric uncertainties in both mechanisms. This is a challenging, yet highly relevant topic. Overconfidence in the detailed mechanism can lead to a misplaced focus on tight error tolerances in the simplified model, relative to a faulty/uncertain baseline. Simplified-model errors ought to be handled along with detailed-model uncertainties in the same error budget. Any error norm between simplified and detailed models ought to be weighted appropriately with attendant uncertainties. Moreover, the fact that both the detailed and simplified mechanisms are burdened with uncertainty suggests that any measures of distance between their predictions be done in a probabilistic context. This line of reasoning highlights the need for rethinking model analysis/reduction strategies for uncertain chemical kinetic models.

The above is a significant undertaking with a range of technical challenges. There has been some work addressing model reduction under uncertainty in the context of proper orthogonal decomposition (POD) [3], albeit for small degrees of uncertainty. The dynamical analysis of uncertain ordinary differential equation (ODE) systems has also received some attention [4], [5], in a full probabilistic setting. However the challenge of dynamical analysis and uncertain chemical model simplification in hydrocarbon kinetics of relevance to combustion has yet to receive significant attention.

We lay out in the following a general strategy for analysis and reduction of uncertain chemical kinetic models, and describe its utilization in the context of ignition of hydrocarbon fuel-air mixtures. The construction is fully probabilistic, allowing for an arbitrary uncertainty structure. It is based on an existing analysis and reduction strategy, using computational singular perturbation (CSP) analysis [6], [7], that has been used extensively for deterministic models of hydrocarbon fuels [1], [2].

II. Method

Consider a detailed chemical mechanism $\mathcal{M}^*(\lambda)$, defined by a set of species $\mathcal{S}^* = \{S_1, \ldots, S_N\}$ and elementary reactions $\mathcal{R}^* = \{R_1, \ldots, R_M\}$, where λ is the relevant vector of uncertain parameters, *e.g.* the Arrhenius rate parameters of all reactions. Consider the auto-ignition process of a hydrocarbon fuel-air system in a constant pressure batch-reactor, for a range of initial temperature and stoichiometry, which is used to compute a set of ignition trajectories, providing a database of states $D = \{X^{(1)}, \cdots, X^{(K)}\}$, where $X^{(k)} \in \mathbb{R}^{N+1}$ is the k-th state vector, composed of temperature and the N mole fractions, in the database, with $k = 1, \ldots, K$. Given that λ is uncertain, let D_λ denote the database computed for a given value of λ.

For any given D_λ, and considering a given set of QoIs - such as the set of target species - and a tolerance τ on Importance Indices, the CSP-based analysis and simplification strategy provides a simplified mechanism $\mathcal{M}_\tau(\lambda)$, being a subset of the starting mechanism with species $\mathcal{S}_\tau(\lambda)$ and reactions $\mathcal{R}_\tau(\lambda)$. In fact, given the starting model specification, the simplified model can be specified compactly in terms of a vector of M binary indicators $\alpha^\tau(\lambda) = (\alpha_1^\tau(\lambda), \ldots, \alpha_M^\tau(\lambda))^T$, where

$$\alpha_r^\tau(\lambda) = \begin{cases} 1 & \text{for reaction } R_r \in \mathcal{R}_\tau(\lambda) \\ 0 & \text{otherwise.} \end{cases}, \qquad r = 1, \ldots, M \quad (1)$$

In fact, $\alpha^\tau(\lambda)$ is a multi-index that specifies 2^M models. We can view the process of database generation, analysis, and model simplification as an input-output map:

$$f_\tau(\lambda) : \lambda \to \alpha^\tau(\lambda), \quad (2)$$

which provides a convenient abstraction for the use of uncertainty quantification (UQ) methods to account for uncertainty in λ in the process of simplified model selection.

Generating n random samples from $p(\lambda)$, $\{\lambda^{(1)},\cdots,\lambda^{(n)}\}$, the input-output map of Eq.(2) provides corresponding samples $\{\alpha^{\tau j}\}_{j=1}^{n}$, where $\alpha^{\tau j}=\alpha^{\tau}(\lambda^{(j)})$, so that we can estimate, $\forall\alpha=(\alpha_1,\cdots,\alpha_M)$, the joint probabilities,

$$P_\tau(\alpha)\approx\frac{1}{n}\sum_{j=1}^{n}\delta_{\alpha^{\tau j}\alpha} \tag{3}$$

where $\delta_{\alpha^{\tau j}\alpha}$ is the Kronecker delta, which is equal to 1 if $\alpha=\alpha^{\tau j}$ and 0 otherwise. Thus, the contribution of each sample j to the sum for $P_\tau(\alpha)$ in Eq. (3) is 1 if $\alpha^{\tau j}=\alpha$, and 0 otherwise. Further, we have

$$\delta_{\alpha^{\tau j}\alpha}=\prod_{i=1}^{M}\delta_{\alpha_i^{\tau j}\alpha_i}. \tag{4}$$

The joint probabilities provide a wealth of information on the coupling among reactions. For example, marginalizing over $M-2$ reactions, provides the 2-way joint probabilities for any two given reactions (p,q),

$$P_\tau(\alpha_p,\alpha_q)\approx\frac{1}{n}\sum_{j=1}^{n}\delta_{\alpha_p^{\tau j}\alpha_p}\delta_{\alpha_q^{\tau j}\alpha_q}. \tag{5}$$

This provides information on the relevance of two reactions p and q being included/excluded jointly or separately in the model. Similarly, this analysis can be generalized to any subset of reactions forming a pathway of interest. Moreover, extending the scope to a full sub-mechanism, the joint picture provides a statement concerning the probability of any given mechanism that is a subset of the detailed model. One can thus select the model with the highest $P(\alpha)$ as the one most supported by the reduction strategy.

However, the complexity of the joint-picture can raise the need for large numbers of samples to establish multivariate statistics, in which case we may confine ourselves to the marginal probabilities for individual reactions,

$$P_\tau(\alpha_i)\approx\frac{1}{n}\sum_{j=1}^{n}\delta_{\alpha_i^{\tau j}\alpha_i},\qquad i=1,\ldots,M. \tag{6}$$

With this, and since $\delta_{\alpha_i^{\tau j}1}\equiv\alpha_i^{\tau j}$, the marginal probability that a reaction is included in the simplified mechanism for a given τ, is given by

$$\mathcal{P}_i^\tau=P_\tau(\alpha_i=1)\approx\frac{1}{n}\sum_{j=1}^{n}\alpha_i^{\tau j}. \tag{7}$$

In this way, we arrive at a proposed marginal strategy for model reduction under uncertainty, whereby a reaction is included in the simplified mechanism for a given τ, when its marginal probability satisfies $\mathcal{P}_i^\tau>\theta$, where $0<\theta<1$ is a user-specified threshold.

III. Discussion

We have used the above construction for simplification of uncertain methane-air and n-butane-air mechanisms with specified uncertainty in pre-exponential rate constants, based on constant pressure homogeneous ignition computations. We have explored convergence of the results as a function of the size of the database, as well as the number of random samples. We also explored requisite means of error estimation, relying e.g. on the uncertain prediction of lumped quantities such as ignition-time, or on the comparison of uncertain time-trajectories, given the detailed mechanism and a simplified mechanism. In this last context, whether comparing nominal predictions weighted with uncertainty, or relying on probabilistic measures of difference between uncertain predictions, we employ error estimates that are informed by uncertainty. We examined the advantage that a general user, who might not be necessarily interested in uncertain predictions but rather in deterministic predictions from robust reduced mechanisms, can derive from the use of a simplified mechanism generated through the proposed probabilistic approach. Lastly, we explored the outcomes of the models with the highest $P(\alpha)$, as an alternative to the strategy relying on marginal probabilities only. We will present the above construction, and illustrate its use in the simplification of uncertain detailed kinetics of n-butane.

Acknowledgment

HNN & MK acknowledge the support of the US Department of Energy (DOE), Office of Basic Energy Sciences (BES) Division of Chemical Sciences, Geosciences, and Biosciences. CS acknowledges the support of the US DOE Advanced Scientific Computing Research (ASCR) Scientific Discovery through Advanced Computing (SciDAC) program. Sandia National Laboratories is a multi-program laboratory managed and operated by Sandia Corporation, a wholly owned subsidiary of Lockheed Martin Corporation, for the U.S. Department of Energys National Nuclear Security Administration under contract DE-AC04-94AL85000. MV, PPC, and RMG acknowledge the support of CCRC/KAUST and of the Italian Ministry of University and Research (MIUR).

References

[1] M. Valorani, F. Creta, D. Goussis, J. Lee, H. Najm, Chemical Kinetics Simplification via CSP, Combustion and Flame 146 (2006) 29–51.

[2] M. Valorani, F. Creta, F. Donato, H. Najm, D. Goussis, Skeletal Mechanism Generation and Analysis for *n*-heptane with CSP, Proc. Comb. Inst. 31 (2007) 483–490.

[3] C. Homescu, L. R. Petzold, R. Serban, Error estimation for reduced-order models of dynamical systems, SIAM Review 49 (2) (2007) 277–299.

[4] B. Sonday, R. Berry, H. Najm, B. Debusschere, Eigenvalues of the Jacobian of a Galerkin-Projected Uncertain ODE System, SIAM J. Sci. Comp. 33 (2011) 1212–1233.

[5] M. Salloum, A. Alexanderian, O. Le Maître, H. Najm, O. Knio, Simplified CSP Analysis of a Stiff Stochastic ODE System, Computer Methods in Applied Mechanics and Engineering 217-220 (2012) 121–138.

[6] S. Lam, D. Goussis, Conventional Asymptotics and Computational Singular Perturbation for Simplified Kinetics Modelling, in: M. Smooke (Ed.), Reduced Kinetic Mechanisms and Asymptotic Approximations for Methane-Air Flames, no. 384 in Springer Lecture Notes, Springer Verlag, 1991, Ch. 10, pp. 227–242.

[7] D. Goussis, S. Lam, A study of homogeneous methanol oxidation kinetic using csp, Proc. Comb. Inst. 24 (1992) 113–120.

LES for Turbulent Non-premixed Jet Flame with CODAC Reduction

Zaigang Liu[†,‡], Wenhu Han[†], Wenjun Kong[*,†,‡], Yiguang Ju[§]
[†] Key Laboratory of Light-Duty Gas-Turbine, Institute of Engineering Thermophysics, Chinese Academy of Sciences, Beijing 100190, China
[‡] University of Chinese Academy of Sciences, Beijing 100049, China
[§] Department of Mechanical and Aerospace Engineering, Princeton University, 08544, United States

***Abstract*—Large eddy simulations (LESs) for turbulent flames with detailed mechanisms have received growing interest. However, a direct implementation of detailed mechanisms requires a vast amount of computational resources which limits the use of detailed mechanism in large-scale LESs. An on-the-fly mechanism reduction method named Correlated Dynamic Adaptive Chemistry (CODAC) is proposed to overcome this issue. A LES for Sandia Flame-D was conducted. An appropriate reduction threshold for CODAC was determined a priori based on 1-D freely propagating premixed methane-air flames. This reduction threshold was then used in the LES. The chemical mechanism used in the LES is GRI-Mech 3.0 with 53 species and 325 reactions. Predictions obtained with the LES are in good agreement with the experimental data. Results obtained by using CODAC are similar to those obtained by using the detailed mechanism without reduction procedures and the computational time is reduced by 33%, demonstrating the accuracy and efficiency of CODAC in LES. In particular, the CODAC method provides reliable predictions of intermediate species and radicals.**

I. INTRODUCTION

Large eddy simulations (LESs) for turbulent flames with detailed mechanisms have received growing interest. However, using detailed mechanisms in LESs requires significant computational resources which limits the use of detailed mechanisms in large-scale LESs. Therefore, [1]mechanism reduction methods are needed.

For decades now, a large number of methods have been developed to reduce combustion mechanism models. Among the different methods, the dynamic adaptive chemistry (DAC) method [1, 2] is one of the most promising methods to be used in the LES. DAC is an on-the-fly reduction method that generates reduced mechanisms instantaneously and locally. Based on PFA reduction, the correlated DAC (CODAC) method [3, 4] was developed to avoid the redundant computation for similar grid points. CODAC method was found to be not only computationally efficient but also robust and accurate when it was applied to real jet fuel flame ignition and propagation problems. The PFA based DAC and CODAC have not been tested in such configuration. The performance of the correlation and PFA algorithm has to be investigated in turbulent conditions.

Therefore, in order to validate the CODAC method in flame LES, a simulation for the Sandia Flame-D is performed. The results of simulation are compared with the experimental data and with LES calculations involving the detailed mechanism without reduction procedure.

II. NUMERICAL METHODS

The turbulent flame tested in the present work is the well-defined Sandia flame-D [5]. The flame is a piloted no-premixed methane-air jet flame with Re = 22400.

The LES runs on an in-house FORTRAN code designed for the low Mach number combustion simulations. The second order fully conservative finite difference scheme [6] is employed. Pressure and velocity is decoupled using the fractional step approach. The third order WENO scheme is applied for the scalar transport equation. Temporal advancement is solved using the second order semi-implicit Crank-Nicolson scheme. The thermal and transport properties and chemical reactions are solved coupled with Chemkin and Transport package. The sub-grid scale model is the dynamic Smagorinsky model. The turbulent combustion model is the PaSR model [7, 8]. The ODE solver of reaction source term is VODE. The computational domain is a cylinder with 300 mm in diameter and 600 mm in length. The grids resolution is $280\times64\times133$ (x, φ, r) and there are 2.38 million points in total.

Full GRI-Mech 3.0 [9] with 53 species and 325 reactions is used in the present LES study. The DAC method used in the present study is based on the PFA calculation [10]. Key radicals OH, HO_2, CO and NO are preselected as important species. The reduction threshold is set as 0.1 *a priori* based on 1-D freely propagating premixed methane-air flame calculations. The correlation technic proposed by Sun et al. [3] is used in the present work to reduce further the computational time. The corresponding set of correlation thresholds $\boldsymbol{\varepsilon_c}$ is then defined as 10K for the temperature and 0.01 for the mass fractions.

III. RESULTS AND DISCUSSIONS

Figure 1 shows instantaneous contours of temperature and number of species and reaction in the locally reduced mechanism. The size of the reduced mechanism is positively

*Corresponding author, E-mail: wjkong@iet.cn

This work was supported by the National Natural Science Foundation of China under Grant Nos. 91441131, 91441119.

correlated to the local reactivity. The numbers of selected species and reactions are large in the flame region near the central line demonstrating the active creation and destruction of intermediate species and radicals in this region. On the other hand, these numbers are small in the region away from the flame as there is mainly the post-burning production and the air co-flow. The average computational time per step without CODAC reduction is 26902 s, while that with CODAC can be reduced to 18054 s, which is about a 33% reduction.

Figure 2 shows the comparison of simulated results with conditional averaged experimental data with respect to the mixture fraction at x =15d. The comparisons indicate a good agreement between the simulated results and the experimental data for temperature and species. The distribution of scatters is in a broad region without unphysical conglomeration or void region. The simulated heat release rates are also plotted. The results without reduction agree well with the results obtained with CODAC, which demonstrates the accuracy of the CODAC reduction. The results of H_2 are generally in good agreement with the experimental data, in spite that the peaks are over-predicted. For OH radicals, the profiles are also well reproduced, demonstrating the capability of the detailed mechanism and the CODAC reduction to predict minor species.

IV. Conclusions

In this work, CODAC reduction method has been employed in a LES for Sandia Flame-D turbulent flame. The results are compared with both experimental data and simulations performed without mechanism reduction. Simulated results of the LES for Sandia Flame-D with detailed GRI-Mech 3.0 and CODAC reduction are in good agreement with experimental data and results obtained by using detailed mechanism without reduction, demonstrating

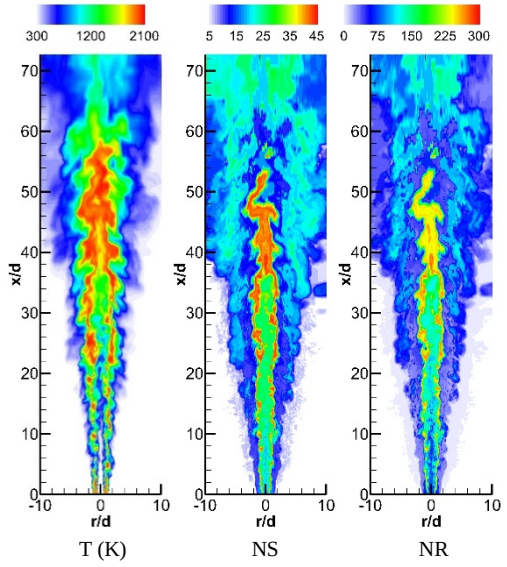

Fig. 1. Instantaneous contours of temperature (T in K), the number of activated species (NS) and the number of reactions (NR) in reaction mechanism for flame-D are plotted from the left to the right.

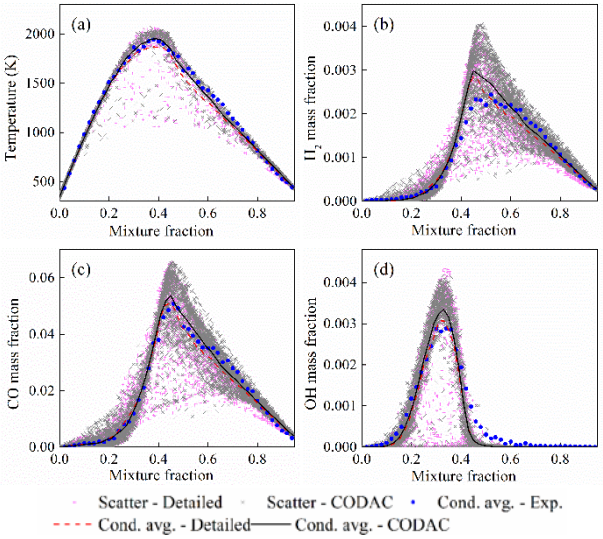

Fig. 2. Scatter and conditional mean of simulated results without reduction and with CODAC reduction as well as the conditional mean of the experiment data for temperature (T in K), H_2, CO and OH mass fractions at x = 15d.

the accuracy and efficiency of using CODAC for a detailed mechanism in the LES. The number of species and reactions of local reduced mechanism is concentrated in the vicinity of the flame zone. The computational time of simulations with CODAC is reduced about 33% as compared to the simulation without reduction. The results have accurately reproduced the distributions of the intermediate species and radicals.

References

[1] L. Liang, J.G. Stevens, J.T. Farrell, "A dynamic adaptive chemistry scheme for reactive flow computations", *P Combust Inst*; vol. 32, pp. 527-534, 2009.

[2] X.L. Gou, Z. Chen, W.T. Sun, et al., "A dynamic adaptive chemistry scheme with error control for combustion modeling with a large detailed mechanism", *Combust. Flame*; vol. 160, pp. 225-231, 2013.

[3] W.Q. Sun, X.L. Gou, H.A. El-Asrag, et al., "Multi-timescale and correlated dynamic adaptive chemistry modeling of ignition and flame propagation using a real jet fuel surrogate model", *Combust. Flame*; vol. 162, pp. 1530-1539, 2015.

[4] W.Q. Sun, S.H. Won, X.L. Gou, et al., "Multi-scale modeling of dynamics and ignition to flame transitions of high pressure stratified n-heptane/toluene mixtures", *P Combust Inst*; vol. 35, pp. 1049-1056, 2015.

[5] C. Schneider, A. Dreizler, J. Janicka, et al., "Flow field measurements of stable and locally extinguishing hydrocarbon-fuelled jet flames", *Combust. Flame*; vol. 135, pp. 185-190, 2003.

[6] Y. Morinishi, T.S. Lund, O.V. Vasilyev, et al., "Fully conservative higher order finite difference schemes for incompressible flow", *J Comput Phys*; vol. 143, pp. 90-124, 1998.

[7] E. Fedina, C. Fureby, "A comparative study of flamelet and finite rate chemistry LES for an axisymmetric dump combustor", *Journal of Turbulence*; vol. 12, pp. 1-20, 2011.

[8] C. Fureby, "A Comparative Study of Flamelet and Finite Rate Chemistry LES for a Swirl Stabilized Flame", *J Eng Gas Turb Power*; vol. 134, pp. 2012.

[9] G.P. Smith, D.M. Golden, M. Frenklach, et al., GRI-Mech 3.0, in, 1999, pp. http://www.me.berkeley.edu/gri_mech/.

[10] W.T. Sun, Z. Chen, X.L. Gou, et al., "A path flux analysis method for the reduction of detailed chemical kinetic mechanisms", *Combust. Flame*; vol. 157, pp. 1298-1307, 2010.

Automated Construction, Reduction, and Optimization of Chemistry for Reacting Flow Modelling

Xiaolong Gou*, Zheng Chen†, Wenting Sun‡, Yiguang Ju§
* School of Power Engineering, Chongqing University, Chongqing 400044, China
† SKLTCS, College of Engineering, Peking University, Beijing 100871, China
‡ School of Aerospace Engineering, Georgia Institute of Technology, Atlanta, GA 30332, USA
§ Department of Mechanical and Aerospace Engineering, Princeton University, Princeton, NJ 08544, USA

***Abstract*—An automated method for chemical kinetic model construction, reduction and optimization is developed to generate a reduced skeletal mechanism for the reacting flow modelling. Based on the database of chemical kinetics, the initial chemistry is created first. Then the model reduction and optimization are conducted to minimize the reduced mechanism to meet the pre-specified error requirements. The results show that this method can generate reduced kinetic models with high accuracy. An automated software, Automated Construction, Reduction and Optimization (ACRO), is developed for the application of this method on any reacting flow modelling.**

I. Introduction

In reacting flow modelling, the application of detailed chemistries with hundreds of species and thousands of elementary reactions would be limited by the computer memory and computation time. In order to simplify the chemistry, several effective reduction methods have been proposed in the literature to obtain reduced skeletal mechanisms from detailed ones [1, 2].

One of most efficient reduction approaches is the mapping/storage method, which uses the stored solution instead of the kinetics based differential equations during the simulation process, such as the application of orthonormal polynomials[3], in situ adaptive tabulation (ISAT) [4, 5] and piecewise implementation of solution mapping (PRISM)[6]. Another one is the lumping method which replaces the similar reactions or species with lumped ones, such as the non-linear lumping, constrained lumping [7], unconstrained lumping [8] and quasi-steady-state approximation (QSSA) based method. The mechanism reduction approach timescale analysis is also proved to be effective with accurately described slow subsystems which dominate the long-time behavior, such as QSSA [9], the partial equilibrium assumption (PEA), the computational singular perturbation (CSP) [10] and the intrinsic low dimensional manifold (ILDM) [11] methods. The reduction method which eliminate redundant species and reactions from detailed mechanisms based on the importance analysis to the parameters of interest are popularly used, such as the sensitivity analysis (SA) [12], optimization-based methods [13] and so on. The methods eliminating the redundant species according to the interaction coefficient analysis have been proved to have high efficiency, such as the directed relation graph (DRG) [14] and the path flux analysis (PFA) [15] method.

In this paper, an automated method and software ACRO is developed to conduct chemistry construction, reduction and optimization to obtain an optimized reduced mechanism efficiently.

II. Methodology

A. Initial Chemistry Construction

There are three basic datasets respectively for: chemical reaction mechanism, thermochemical properties, and transport properties. All the data are saved in CHEMKIN format.

The chemical kinetic reactions are divided into two groups: one for high temperature reactions and the other one is low temperature reactions [16]. For the high temperature reaction group, there are several classes of reactions like unimolecular fuel decomposition reaction, H-atom abstraction reaction and so on. For the low temperature reaction group, there is oxygen addition to alkyl radical reaction, alkyl peroxy radical isomerization and so on. There are two ways to construct an initial chemical kinetic reaction mechanism: using the detailed chemistry directly or creating from the basic chemical kinetic mechanism database.

B. Chemistry Reduction

The method integrating path flux analysis (PFA) and sensitivity analysis (SA) is used automatically to generate a skeletal chemistry [15, 17]. As a key parameter to generate the smallest reduced mechanism, the error threshold value is adjusted automatically to satisfy the requirements of the modelling.

C. Chemistry Optimization

Similar to Ref. [18], the optimization based on reaction rules is adopted. According to the difference between the numerical data from the skeletal mechanism based modelling and the data from experiments or modelling using detailed mechanism, the kinetic parameters of the related reaction class can be optimized in the range of the uncertainties of reaction constants.

D. Chemistry Evaluation

The accuracy of the reduced mechanism can be assessed through comparison with prediction from the detailed mechanism or with experimental data. Normally the concentrations of selected species, ignition delay times and laminar flame speeds with different weight values in different working conditions are taken as the evaluation parameters. Besides the accuracy, the numbers of species and elemental reactions are also used to evaluate the computation efficiency. The final reduced skeletal mechanism is obtained by continuously eliminating the species or reactions until all the parameters satisfy the error requirements.

E. Software Development

As an integrated tool, the software can complete all processes including: chemistry construction, reduction and optimization. In order to get the simplest skeletal mechanism efficiently, several processes are run in parallel.

The basic working algorithm for using this software is as follows:

a. Define the basic components of the chemistry, including the fuel, oxidizer and diluents. If an existing chemistry is chosen directly, the components definition is not required.

b. Define the key parameters and their error bounds. For example, the error bounds of ignition delay time, the adiabatic flame temperature, the laminar flame speed, and species can be specified.

c. Select the basic models and initial conditions for model reduction and validation.

d. Start the chemistry construction, reduction and optimization process, and the software will automatically generate an optimized skeletal mechanism with minimum number of species.

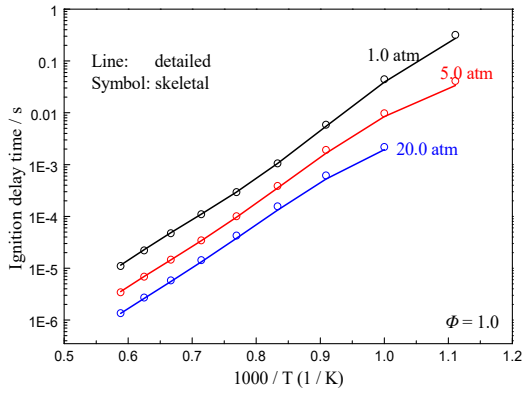

Fig. 1 Ignition delay time comparison between the detailed and skeletal mechanism

III. Results and Discussion

Several skeletal mechanisms were obtained using the automated mechanism construction, reduction and optimization system ACRO. The results show that this software can efficiently create different skeletal and detailed mechanisms to satisfy the error requirements of different reacting flow modelling.

The high temperature ignition delay time comparison between the detailed and skeletal mechanism of n-heptane is shown as Fig. 1. Using the software, the skeletal with 65 species and 254 reactions was obtained from the detailed one with 469 species and 1221 elemental reactions.

Acknowledgment

This work was supported by National Natural Science Foundation of China (No. 91441112).

References

[1] T. Lu and C.K. Law, "Toward accommodating realistic fuel chemistry in large-scale computations", *PROG ENERG COMBUST*, vol. 35, no. 2, 2009, pp. 192-215.

[2] S.B. Pope, "Small scales, many species and the manifold challenges of turbulent combustion", *P COMBUST INST*, vol. 34, no. 1, 2013, pp. 1-31.

[3] T. TURANYI, "PARAMETERIZATION OF REACTION-MECHANISMS USING ORTHONORMAL POLYNOMIALS", *COMPUTERS & CHEMISTRY*, vol. 18, no. 1, 1994, pp. 45-54.

[4] S.B. Pope, "Computationally efficient implementation of combustion chemistry using in situ adaptive tabulation", *COMBUST THEOR MODEL*, vol. 1, no. 1, 1997, pp. 41-63.

[5] B. Yang and S.B. Pope, "Treating chemistry in combustion with detailed mechanisms - In situ adaptive tabulation in principal directions premixed combustion", *COMBUST FLAME*, vol. 112, no. 1-2, 1998, pp. 85-112.

[6] S.R. Tonse, et al., "Computational economy improvements in PRISM", *INT J CHEM KINET*, vol. 35, no. 9, 2003, pp. 438-452.

[7] A.S. TOMLIN, et al., "A GENERAL-ANALYSIS OF APPROXIMATE NONLINEAR LUMPING IN CHEMICAL-KINETICS .2. CONSTRAINED LUMPING", *J CHEM PHYS*, vol. 101, no. 2, 1994, pp. 1188-1201.

[8] G.Y. LI, et al., "A GENERAL-ANALYSIS OF APPROXIMATE NONLINEAR LUMPING IN CHEMICAL-KINETICS .1. UNCONSTRAINED LUMPING", *J CHEM PHYS*, vol. 101, no. 2, 1994, pp. 1172-1187.

[9] T. TURANYI, et al., "ON THE ERROR OF THE QUASI-STEADY-STATE APPROXIMATION", *JOURNAL OF PHYSICAL CHEMISTRY*, vol. 97, no. 1, 1993, pp. 163-172.

[10] S.H. LAM, "USING CSP TO UNDERSTAND COMPLEX CHEMICAL-KINETICS", *COMBUST SCI TECHNOL*, vol. 89, no. 5-6, 1993, pp. 375-404.

[11] U. MAAS and S.B. POPE, "SIMPLIFYING CHEMICAL-KINETICS - INTRINSIC LOW-DIMENSIONAL MANIFOLDS IN COMPOSITION SPACE", *COMBUST FLAME*, vol. 88, no. 3-4, 1992, pp. 239-264.

[12] H. RABITZ, et al., "SENSITIVITY ANALYSIS IN CHEMICAL-KINETICS", *ANNU REV PHYS CHEM*, vol. 34, 1983, pp. 419-461.

[13] B. Bhattacharjee, et al., "Optimally-reduced kinetic models: reaction elimination in large-scale kinetic mechanisms", *COMBUST FLAME*, vol. 135, no. 3, 2003, pp. 191-208.

[14] T.F. Lu and C.K. Law, "A directed relation graph method for mechanism reduction", *P COMBUST INST*, vol. 30, no. 1, 2005, pp. 1333-1341.

[15] W. Sun, et al., "A path flux analysis method for the reduction of detailed chemical kinetic mechanisms", *COMBUST FLAME*, vol. 157, no. 7, 2010, pp. 1298-1307.

[16] S.M. Sarathy, et al., "Comprehensive chemical kinetic modeling of the oxidation of 2-methylalkanes from C-7 to C-20", *COMBUST FLAME*, vol. 158, no. 12, 2011, pp. 2338-2357.

[17] W. Wang and X. Gou, "An improved path flux analysis with multi generations method for mechanism reduction", *COMBUST THEOR MODEL*, vol. 20, no. 2, 2016, pp. 203-220.

[18] L. Cai and H. Pitsch, "Mechanism optimization based on reaction rate rules", *COMBUST FLAME*, vol. 161, no. 2, 2014, pp. 405-415.

Propagation of Kinetic Uncertainty through Surrogate Subspace in Combustion Simulations

Weiqi Ji [*], Jiaxing Wang [*], Bin Yang [*], Zhuyin Ren [*], Chung K. Law [*, †]

[*] Center for Combustion Energy, Tsinghua University, Beijing, China

[†] Department of Mechanical and Aerospace Engineering, Princeton University, NJ, USA

***Abstract*— In combustion simulations with uncertainty quantification, a large number of samples from the high-dimensional uncertainty parameter space are needed to propagate the kinetic uncertainty to global combustion characteristics such as the ignition delay time. Recognizing that it is computationally challenging to perform so many individual turbulent combustion simulations, a novel approach is proposed to propagate the kinetic uncertainty through a low-rank surrogate subspace as a replacement for the entire parameter space to reproduce the uncertainty on the quantity of interest. Specifically, the entire parameter space is projected onto the surrogate subspace via a transform matrix, which is optimized by using the generic algorithm, such that the projected samples can reproduce the uncertainty of the quantity of interest. We demonstrate the construction of the surrogate subspaces for a detailed hydrogen mechanism, with the probability distribution function of the ignition delay time, laminar flame speed and the extinction time in perfectly stirred reactor as the objective functions for the optimization.**

I. Introduction

The assessment of the predictive capabilities of turbulent combustion models requires extensive validation of the simulation results against experimental measurements. However, isolation of the errors incurred by the turbulent combustion models in the simulations is difficult due to the possible uncertainties in initial/boundary conditions as well as those in other model components such as the chemical kinetic mechanisms. While careful burner design for laboratory-scale flames and detailed measurements of inflow/initial flow and composition fields can help to mitigate the uncertainties in the boundary/initial conditions, few methods exist to quantify the uncertainties in turbulent combustion simulations due to the uncertainties in chemical kinetics.

For simple combustion problems such as homogeneous reactors and one-dimensional laminar flames [1-4], statistical methods have been developed to quantify the uncertainties in simulations arising from chemical kinetics. However, few works on chemical kinetic uncertainty quantification (UQ) for turbulent combustion simulations have been reported, while recognizing that it is computationally intractable to apply the above UQ procedure for simple combustion system to turbulent combustion simulations, as hundreds or thousands of samples are required to generate the output statistics. Mueller et al. [5] take advantage of the algorithm employed with the steady flamelet model by first propagating the kinetic uncertainty through the steady flamelet equations, producing a lower-dimensional joint distribution of the temperature, species mass fractions, and other derived quantities in the flamelet library. Then, only three 'active' quantities, i.e., density, molecular viscosity and molecular diffusivity, are needed to evolve the LES governing equations, of which only the uncertainty in the density is considered. Therefore, only few LES runs are required for its propagation. The algorithm is demonstrated with the Sandia flame D [6], and the results indicate that the uncertainty due to the kinetic rates is large enough to account for nearly all of the discrepancies between the LES results and experimental measurements. The approach, although efficient, is nevertheless limited to turbulent combustion simulations with flamelet-like combustion models.

In this work, a novel approach, compatible with various combustion models, is proposed to propagate the chemical kinetic uncertainty in turbulent combustion simulations, in which the simulation uncertainties are quantified through performing samples from a very low dimensional surrogate subspace of the kinetic parameters. Homogeneous reactors and laminar flames at the representative thermo-chemical conditions of target turbulent combustion applications are simulated prior for the identification of the surrogate subspace, which aim to reproduce the probability density function (PDF) of key combustion characteristics such as the ignition delay time, the flame speed as well as the extinction strain rate from the original high-dimensional parameter space. In the following, the methodology is presented and identification of the surrogate subspace is demonstrated using a 33-step detailed hydrogen mechanism [8].

II. Methodology

A. Propagation of kinetic uncertainty

Following previous works [1-3, 7, 8], the reaction rate coefficients are presumed to be independent and characterized by a lognormal distribution with a median value k_{j0} and a temperature-independent uncertainty factor U_j, which is interpreted as three times of the standard deviation:

$$\ln k_j \sim N(\ln k_{j0}, \left(\frac{1}{3}\ln U_j\right)^2)$$

in which $N(\mu, \sigma^2)$ reads a normal distribution with mean μ and standard deviation σ. The low discrepancy sequences proposed by Sobol [7] is used to generate random samples of reaction rate coefficients. Each sample corresponds to a set of rate coefficients and is then integrated into Cantera [8] to acquire the corresponding quantities of interest (QOIs).

B. Identification of surrogate subspace

Let f be a scalar-valued function of n variables $\mathbf{x} = [x_1, x_2, \dots, x_n]^T$.

$$y_0 = f_0(\mathbf{x}), \qquad \mathbf{x} \in \mathcal{X} \subseteq \mathbb{R}^n$$

where it is assumed without loss of generality that $\mathcal{X}$ is centered at the origin. For the UQ in combustion simulations, y are the QOIs such as the lift-length from the simulation of a turbulent lift flame, and $\mathbf{x}$ are the pre-factors of the elemental reaction rate constant. Let $\mathcal{X}$ be equipped with a bounded probability density function, $\rho_{\mathbf{x}}: \mathbb{R}^n \to \mathbb{R}_+$, where $\rho_{\mathbf{x}} > 0, \mathrm{x} \in \mathcal{X}$ and $\rho_{\mathbf{x}} = 0, \mathbf{x} \notin \mathcal{X}$. The goal is to achieve the PDF of y, denoted as ρ_y.

Existing dimension reduction methods [4, 9-11] can be applied to reduce the dimension of the input parameter space and the number of samples required for statistics. However, these methods suffer the issue that a lot of samples are required for identifying the low-dimensional subspace. Therefore, we propose to identify the subspace with the datasets from homogeneous reactors and laminar flames at the representative thermo-chemical conditions of target turbulent combustion applications. Then, each of such simple model, $y_i = f_i(\mathbf{x})$, will lead to a subspace spanned by one or several sensitive directions $\mathbf{u}_i$. Combine them together will lead to a comprehensive subspace, i.e., [$\mathbf{u}_1$, $\mathbf{u}_2$, …, $\mathbf{u}_m$], expected to work for the target turbulent combustion applications. However, the combination will result in a subspace whose dimension is higher than acceptance.

To tackle above challenge, we propose to use a low dimensional subspace to approximate the PDF of y_i, which contains less information than approximating the high dimensional function $f_i(\mathbf{x})$. The approximation formulated as

$$y_i = f_i(\mathbf{x}) \approx f_i(\mathbf{S}\boldsymbol{\Lambda}\mathbf{S}^T\mathbf{x}) \quad (1)$$

In which $\mathbf{S}$ is a $n \times r$ matrix with $r \leq n$, and $\mathbf{S}^T\mathbf{S} = \mathbf{I}_r$. $\boldsymbol{\Lambda}$ is a $r \times r$ diagonal matrix, whose diagonal component functions as a rescaling factors on the orthogonal projection operator $\mathbf{S}\mathbf{S}^T$. The intution for introducing $\boldsymbol{\Lambda}$ is to compensate the error due to applying same projection for all of y_i.

The identification of $\mathbf{S}$ and $\boldsymbol{\Lambda}$ is done by multi-object generitic evolution algorithm, subjected to following minimization problem,

$$\min_{S,\boldsymbol{\Lambda}} JSD\left(PDF\left(f_i(\mathbf{x})\right), PDF\left(f_i(\mathbf{S}\boldsymbol{\Lambda}\mathbf{S}^T\mathbf{x})\right)\right) \quad (2)$$

In which JSD is the Jensen-Shannon divergence [12] for measuring the difference between two PDF. The JSD between $p(y)$ and $q(y)$ is defined as

$$JSD(p,q) = \frac{1}{2}\int \left(p \log\frac{p}{M} + q \log\frac{q}{M}\right) dy \quad (3)$$

In which $M = (p+q)/2$.

III. Demonstration

The identification of one-dimensional surrogate subspace is demonstrated with a 33-step hydrogen mechanism with both the reaction rate and the uncertainty factor for the pre-factor A in the rate constant comes from Konnov. [13]. In such case, the matrix S is a column vector.

Figure 1 shows the PDFs of laminar flame speed for the stoichiometric mixture of H2/air at 300 K and one atmosphere. The solid line shows the PDF acquired by sampling from the entire parameter space, and it approximately follows a Gaussian distribution. The PDF acquired by sampling over the surrogate subspace is shown as dash line, and is very close to the one from the entire space. The difference on the standard deviations acquired by sampling the entire space and the surrogate subspace is 2%. In addition, the surrogate subspace shows similar performance on the ignition delay time and the extinction time for PSR, which are not shown here due to limited space.

In a summary, we have successfully demonstrated a one-dimensional surrogate subspace, which can dramatically reduce the number of samples for acquire the PDF of y_i. Further demonstration on the turbulent combustion simulation is under-going.

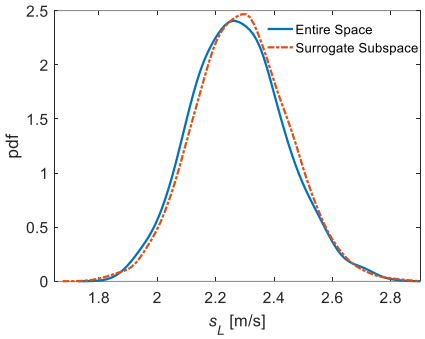

Fig.1. The PDFs of the laminar flame speed achieved by sampling the entire parameter space and the surrogate subspace.

Acknowledgment

This work was supported by the National Natural Science Foundation of China #91441202. W. Ji thanks Prof. Youssef Marzouk and Dr. Olivier Zahm at MIT for the helpful discussion.

References

[1] B.D. Phenix, J.L. Dinaro, M.A. Tatang, J.W. Tester, J.B. Howard, G.J. McRae, Incorporation of parametric uncertainty into complex kinetic mechanisms: Application to hydrogen oxidation in supercritical water, Combust. Flame 112 (1998) 132-146.

[2] M.T. Reagan, H.N. Najm, B.J. Debusschere, O.P. Le Maître, O.M. Knio, R.G. Ghanem, Spectral stochastic uncertainty quantification in chemical systems, Combust. Theor. Model. 8 (2004) 607-632.

[3] I.G. Zsély, J. Zádor, T. Turányi, Uncertainty analysis of updated hydrogen and carbon monoxide oxidation mechanisms, Proc. Combust. Inst. 30 (2005) 1273-1281.

[4] D.A. Sheen, H. Wang, The method of uncertainty quantification and minimization using polynomial chaos expansions, Combust. Flame 158 (2011) 2358-2374.

[5] M.E. Mueller, G. Iaccarino, H. Pitsch, Chemical kinetic uncertainty quantification for Large Eddy Simulation of turbulent nonpremixed combustion, Proc. Combust. Inst. 34 (2013) 1299-1306.

[6] R.S. Barlow, J.H. Frank, Effects of turbulence on species mass fractions in methane/air jet flames, Symposium (International) on Combustion 27 (1998) 1087-1095.

[7] I.y.M. Sobol', On the distribution of points in a cube and the approximate evaluation of integrals, Zhurnal Vychislitel'noi Matematiki i Matematicheskoi Fiziki 7 (1967) 784-802.

[8] H.K.M. David G. Goodwin, and Raymond L. Speth, Cantera: An object-oriented software toolkit for chemical kinetics, thermodynamics, and transport processes, Caltech: Pasadena, CA,, 2014.

[9] T.M. Russi, Uncertainty Quantification with Experimental Data and Complex System Models, Mechanical Engineering, UC Berkeley, 2010.

[10] P.G. Constantine, E. Dow, Q. Wang, Active subspace methods in theory and practice: applications to kriging surfaces, SIAM Journal on Scientific Computing 36 (2014) A1500-A1524.

[11] P.G. Constantine, Active subspaces: Emerging ideas for dimension reduction in parameter studies, SIAM2015.

[12] J. Lin, Divergence measures based on the Shannon entropy, IEEE Trans. Inf Theory 37 (1991) 145-151.

[13] A.A. Konnov, Remaining uncertainties in the kinetic mechanism of hydrogen combustion, Combust. Flame 152 (2008) 507-528.

Session: Mechanism Analysis 2

Chair: H. G. Im

Title: Dynamics of n-Heptane/Air Low Temperature Autoignition
Authors: E. A. Tingas, Z. Wang, S. Mani Sarathy, H. G. Im, D. A. Goussis

Title: Enhancements of the G-Scheme Framework
Authors: M. Valorani, P. P. Ciottoli, R. Malpica Galassi, S. Paolucci, T. Grenga, E. Martelli

Title: Using Global Pathway to Understand Chemical Kinetics
Authors: X. Gao, S. Yang, W. Sun

Dynamics of n-Hexane/Air Low Temperature Autoignition

Efstathios-Al. Tingas*, Zhandong Wang *, S. Mani Sarathy *, Hong G. Im *, Dimitris A. Goussis †‡
*King Abdullah University of Science and Technology, CCRC, Jeddah, Kingdom of Saudi Arabia
†Department of Mechanics, School of Applied Mathematical and Physical Sciences, NTUA, Athens, Greece
‡Department of Mechanical Engineering, Khalifa University of Science, Technology and Research, Abu Dhabi, UAE

***Abstract*— The ignition of n-hexane/air mixture, both at constant volume autoignition and variable volume engine conditions, is investigated using algorithmic tools generated from Computational Singular Perturbation (CSP), on the basis of two chemical kinetics mechanisms; one including and another one excluding third-stage O_2 addition reactions.**

I. Introduction

Cleaner and more efficient internal combustion engines have been the focus of industrial and academic research. One promising combustion technique to achieve such engines is homogenous charge compression ignition (HCCI), in which well-mixed fuel and oxidizer are compressed to the point of auto-ignition [1]. However, the combustion timing of the HCCI engines is hard to control, which requires a comprehensive understanding of the auto-ignition process [2].

The auto-ignition process is controlled by the low-temperature oxidation of hydrocarbons and detailed kinetic models have been developed to predict the ignition of the major components of liquid fuels [3]. The reaction framework for hydrocarbon oxidation is based on the classical low-temperature reaction mechanism, which involves two stages of O_2 addition and produces keto-hydroperoxides as the main chain-branching intermediates. Additional chain propagation pathways (via cyclic ethers) and chain termination pathways (via concerted HO_2 eliminations) compete with the main chain branching pathway (via keto-hydroperoxides), and thereby alter the ignition timing. However, recent work by Wang et al. [4] observed additional radical chain-branching intermediates in the low-temperature oxidation of alkanes, and they proposed a third-stage O_2 addition reaction scheme. The new proposed reaction mechanism predicts the formation of the additional radical chain-branching intermediates [4], which are found to promote the auto-ignition and advance the combustion phasing of HCCI engines at lower temperatures (e.g., 500-700 K), when n-hexane is considered as a surrogate fuel [5]. The promotion of auto-ignition from the new reaction scheme was also observed in simulations of 2-methylhexane ignition [4].

Based on these previous works, it is postulated that the third-stage O_2 addition reaction scheme alters the ignition process significantly.

Therefore, two kinetic models of n-hexane oxidation were adopted in this work; i.e., the model without third-stage O_2 addition reactions by Zhang et al. [6] and the model with third-stage O_2 addition reactions by Wang et al. [5].

Algorithmic tools derived from the CSP methodology were used in order to elucidate how the third-stage O_2 addition reaction scheme promotes the n-hexane auto-oxidation firstly in an ideal reactor (i.e., homogenous batch reactor) and secondly in HCCI engine [5].

II. Chemical kinetics models

Details of the two kinetic models of n-hexane oxidation, which were adopted in the 0-D auto-ignition and HCCI ignition simulation, can be found in the original papers by Zhang et al. [6] and Wang et al. [5]. The "Zhang model" consists of N=1118 species and K=4808 reversible reactions, while the "Wang model" (which includes additional O_2 reactions) consists of N=1188 species and K=4959 reversible reactions. In the following discussions, we refer to the "Zhang model" as the C6 model, while the "Wang model" is referred to as the C6+O2 model. Moreover, the symbols "f" and "b" when met in the reactions, stand for forward and backward directions, respectively.

III. Results

A. Autoignition in a Constant Volume Reactor

The adiabatic homogeneous isochoric autoignition of an n-hexane/air mixture was first studied at various initial temperature, pressure, and equivalence ratio conditions.

It was found that the ignition delay time provided by the C6+O2 mechanism is always smaller than that of the C6 mechanism, especially at low initial temperatures (T(0)=600 K) (min 39% and max 46%), regardless of the initial pressure (p(0)=20 and 60 atm) or the stoichiometry ($\phi = 0.4$ and 1) of the system. These findings suggest that it is mainly the low temperature radical chain branching chemistry that is different between the kinetic models.

Also, it was found that the fast explosive time scale $\tau_{e,f}$ of the extended C6+O2 kinetics mechanism has always a smaller value than $\tau_{e,f}$ of the C6 mechanism, throughout the *explosive stage*. This feature explains why

the C6+O2 mechanism has always a smaller t_{ign} than the C6 mechanism. In order to investigate further this finding, the Timescale Participation Index (TPI) was used and the reactions that contribute the most to the generation of $\tau_{e,f}$ were identified [7], [8].

The analysis revealed that reaction groups R_{18f}, R_{13f} and R_{12f}, included only in the extended mechanism, play important role favoring the explosive character of $\tau e, f$ and, therefore promoting ignition, from the very beginning and for the most part of the process. Reaction groups R_{14f} and R_{15f} (also included exclusively in the extended mechanism) provide quite small contributions, the first one opposing and the second favoring the explosive character of $\tau_{e,f}$. Moreover, the role of reaction groups R_{16f}, R_{11f}, R_{17f} and R_{10f}, the first four favoring and the latter opposing the explosive character of $\tau_{e,f}$, is considerably decreased in the extended mechanism case. Likewise, the contribution of R_{7f} is decreased but in much smaller scale, in the extended mechanism case. On the other hand, the effect of reaction group R_{4f} is increased, during the most part of the autoignition process, therefore contributing to the shorter ignition delay time in the extended mechanism case.

TABLE I

THE REACTION GROUPS PROVIDING SIGNIFICANT CONTRIBUTION TO THE GENERATION OF $\tau_{e,f}$; F: nC_6H_{14}, R: C_6H_{13}, Q: C_6H_{12}, Q': C_6H_{11}, P: $C_6H_{11}Q$. REACTION GROUPS IN BOLD ARE THOSE THAT ARE INCLUDED ONLY IN THE EXTENDED MECHANISM [5].

R_4	$RO_2 \leftrightarrow QOOH$	$\mathbf{R_{12}}$	$P(OOH)_2 + O_2 \leftrightarrow OOP(OOH)_2$
R_5	$RO_2 \leftrightarrow$ olefin + HO_2	$\mathbf{R_{13}}$	$OOP(OOH)_2 \leftrightarrow KDHP + OH$
R_6	$QOOH + O_2 \leftrightarrow O_2QOOH$	$\mathbf{R_{14}}$	$T(OOH)_3 \leftrightarrow ODHP + HO_2$
R_7	$O_2QOOH \leftrightarrow KHP + OH$	$\mathbf{R_{15}}$	$T(OOH)_3 \leftrightarrow DHPCE + OH$
R_8	$O_2QOOH \leftrightarrow OHP + HO_2$	R_{16}	$KHP \leftrightarrow OQ'=O + OH$
R_{10}	$P(OOH)_2 \leftrightarrow OHP + HO_2$	R_{17}	$HPCE \leftrightarrow$ products + OH
R_{11}	$P(OOH)_2 \leftrightarrow HPCE + OH$	$\mathbf{R_{18}}$	$KDHP \leftrightarrow$ products+OH

B. Autoignition in a Variable Volume HCCI Engine

In the constant volume autoignition simulations, only a single stage ignition event was observed. However, hydrocarbon fuels typically display two-stage ignition characteristics. Under HCCI engine conditions, it is common to observe a low temperature heat release (LTHR) that relates to a first-stage ignition delay time, followed by a high temperature heat release (HTHR) that relates to the second-stage ignition delay time.

The ignition of n-hexane/air mixture in HCCI environment was investigated using Chemkin-PRO in an adiabatic single-zone HCCI engine model. The input for the HCCI engine simulation was the same as that in Ref. [5], e.g., a mixture of n-hexane/air at an intake pressure p(0) of 1 atm, intake temperature T(0) of 336 K, and equivalence ratio ϕ of 0.4.

In the HCCI case, the process is characterized by a 2-step ignition. It was found that each step is characterized by a distinct set of explosive timescales τ_e and that the second stage is highly related to the thermal character of the system.

A comparison of the fast explosive timescales $\tau_{e,f}$ of both mechanisms reveals that $\tau_{e,f}$ in the case of the C6+O2 mechanism, is always faster than that of C6. This explains why the C6+O2 mechanism attains a shorter ignition delay time. Although the difference of $\tau_{e,f}$ between the two mechanisms appears more pronounced in the second rather than in the first stage, it is the first stage that relates to the chemical runaway of the process, and therefore it determines the evolution of the second stage that follows.

Therefore, the analysis during the first stage ignition revealed the following:

- Reaction groups R_{18f} and R_{12f}, which are included only in the C6+O2 mechanism, play significant role in promoting ignition, although their effect diminishes with time.
- The effect of reaction groups R_{16f} and R_{7f}, which both favor the explosivity of the mixture, diminishes in the C6+O2 mechanism. The same applies for reaction groups R_{10f} and R_{8f}, which both favor the dissipative nature of $\tau_{e,f}$, therefore tend to retard ignition.
- The effect of reaction groups R_{6f} and R_{5f} is increased in the C6+O2 mechanism, the first favoring and the second opposing the explosive character of $\tau_{e,f}$.
- The net effect of reaction group R_4 is always positive when using the C6+O2 mechanism, thus promoting ignition, and is much stronger when compared to the net effect in the case where the C6 mechanism is used; in the latter case the net effect is negative at the start of the process and then gradually becomes positive.

REFERENCES

[1] M. Yao, Z. Zheng, H. Liu, Progress and recent trends in homogeneous charge compression ignition (HCCI) engines, Progress in Energy and Combustion Science 35 (5) (2009) 398–437.

[2] X.-C. Lü, W. Chen, Z. Huang, A fundamental study on the control of the HCCI combustion and emissions by fuel design concept combined with controllable EGR. Part 1. The basic characteristics of hcci combustion, Fuel 84 (9) (2005) 1074–1083.

[3] C. K. Westbrook, F. L. Dryer, Chemical kinetic modeling of hydrocarbon combustion, Progress in Energy and Combustion Science 10 (1) (1984) 1–57.

[4] Z. Wang, S. Y. Mohamed, L. Zhang, K. Moshammer, D. M. Popolan-Vaida, V. S. B. Shankar, A. Lucassen, L. Ruwe, N. Hansen, P. Dagaut, et al., New insights into the low-temperature oxidation of 2-methylhexane, Proceedings of the Combustion Institute.

[5] Z. Wang, S. M. Sarathy, Third O_2 addition reactions promote the low-temperature auto-ignition of n-alkanes, Combustion and Flame 165 (2016) 364–372.

[6] K. Zhang, C. Banyon, C. Togbé, P. Dagaut, J. Bugler, H. J. Curran, An experimental and kinetic modeling study of n-hexane oxidation, Combustion and Flame 162 (11) (2015) 4194–4207.

[7] E.-A. Tingas, D. C. Kyritsis, D. A. Goussis, Comparative investigation of homogeneous autoignition of DME/air and EtOH/air mixtures at low initial temperatures, Combustion Theory and Modelling (2017) in press.

[8] D. J. Diamantis, E. Mastorakos, D. A. Goussis, H_2/air autoignition: The nature and interaction of the developing explosive modes, Combust. Theory and Modelling 19 (2015) 382–433.

Enhancements of the G-Scheme Framework

Mauro Valorani*, Pietro Paolo Ciottoli*, Riccardo Malpica Galassi*,
Samuel Paolucci†, Temistocle Grenga‡, Emanuele Martelli§
*University of Rome "La Sapienza," Rome, Italy
†University of Notre Dame, Notre Dame, IN, USA
‡Princeton University, New Jersey, USA
§Campania University "L. Vanvitelli", Aversa, Italy

I. Introduction

In our 2009 paper [1], we demonstrated the effectiveness of the *G-Scheme* framework with reference to a number of test models, together with an identification of the critical areas that were in need of further theoretical and computational refinements. In this communication, we report on enhancing the algorithm performance.

II. Problematics of the G-Scheme

To exploit the full potential of the G-Scheme, it is desirable that the fast subspace dimension be identified, all along the system evolution, in a stable and possibly maximal way because the time step at which the integration proceeds depends on this determination.

Futhermore, when the problem is nonlinear, the largest fraction of work load in the G-Scheme relates to the temporal update of the *CSP Basis**. This work load can be estimated for the calculation of the Jacobian matrix as being of $O(N^{1.5})$ and for the eigensystem (eigenvectors & eigenvalues) of $O(N^{2.5})$. It is therefore essential for the success of the solver to pursue all means to minimize the associated work load.

This communication will specifically address these two aspects, namely, (i) a criterion for the *identification of the fast subspace dimension*, and (ii) a criterion to *reuse* the *CSP Basis* as much as possible during the system evolution.

A. A stable criterion for the identification of the fast subspace dimension

In the CSP Method [2], the dimension, dim($\mathbb{T}$), of the fast subspace $\mathbb{T}$ is defined as the largest number of time scales that provides a negligible contribution δx^i_{fast} to the change of the state vector δx^i, within the limit of accuracy specified by the user δx^i_{error}, on a time period of the order of the fastest of the active time scale τ_T.

To make this statement computable, one has first to express the vector field $\boldsymbol{g}$ with respect to the frame of reference induced by the matrix A of the right eigenvectors of the Jacobian matrix, $J_{\boldsymbol{g}}$, of $\boldsymbol{g}$, that is, first (i) to cast $\boldsymbol{g} = A\boldsymbol{f}$, where the mode amplitude vector $\boldsymbol{f}$ is defined as $\boldsymbol{f} = A^{-1}\boldsymbol{g}$, and then (ii) to partition A in slow (h), active (a), and fast (t) subspace contributions: $\boldsymbol{g} = A_h\boldsymbol{f}^h + A_a\boldsymbol{f}^a + A_t\boldsymbol{f}^t$. Given that the modes vary with time, one has to estimate the overall contribution of the term $\boldsymbol{g}_t = A_t\boldsymbol{f}^t$ to check if it is indeed negligible over τ^T.

Operatively, one can define dim($\mathbb{T}$)=N-T, where T is the smallest integer lying between 1 and N, which satisfies the following inequality† for each component of the N-dimensional state vector $\boldsymbol{x}$:

$$\left\{Min\left\{T \in (1,N)\right\} : \delta x^i_{fast} \approx \tau^T \left|a^i_t f^t\right| < \delta x^i_{error} = True\right\} \tag{1}$$

where the error vector is defined as $\delta x^i_{error} = rtol^i|x^i| + atol^i$.

Implicit, in the criterion (1), is the approximation of keeping constant $\boldsymbol{g}_t = A_t\boldsymbol{f}^t$ over a time period of the order of τ^T. In contrast, both the mode direction A_t and its amplitude $\boldsymbol{f}^t$ vary with time. Leaving aside the variation of A_t, the evolution of $\boldsymbol{f}^t$ can be approximated, at any time t^n, as

$$\boldsymbol{f}^t(t = t^n + \tau) = e^{\tau\Lambda_t}\boldsymbol{f}^t_0(t^n). \tag{2}$$

Because of this result, the approximation of keeping constant the value of the fast mode amplitudes over a time period of the order of τ^T overestimates the contribution of the modes with large negative real parts.

As a consequence, criterion (1) might provide a too conservative estimate of the fast subspace dimension, which might be also affected by numerical noise since the fast mode amplitudes are typically small but not persistently so with time.

We recall that smaller values of dim($\mathbb{T}$) imply smaller integration time steps in the G-Scheme integration, i.e., in a larger number of time steps to cover a given time period of interest, with the associated extra cost.

A more accurate estimate of the fast mode contribution in (1) can be obtained by recasting it as an integral, where we retain the functional dependence of $\boldsymbol{f}^t$ with time, albeit

*We refer to the collection of mathematical objects involving the Jacobian, the eigenvectors, and the eigenvalues as the *CSP Basis*.

†In the application of the criterion defined by Eq. (1), a special care is required to manage the contribution of pairs of complex conjugate eigenvalues and eigenvectors.

neglecting a possible rotation of A_t, and then to replace $\boldsymbol{f}^t(t)$ with $\boldsymbol{f}_0^t e^{\Lambda^t t}$ according with Eq. (2), where $\boldsymbol{f}_0^t$ is set as the value of the fast mode amplitudes at the beginning of a time interval of duration τ^T, so that:

$$\delta x^i_{fast} \approx \int_0^{\tau^T} a_t^i f^t(t) dt \approx \int_0^{\tau^T} a_t^i f_0^t e^{\lambda^t t} dt. \qquad (3)$$

The last integral can be solved in closed form to provide the sought after form of the criterion:

$$\{Min\{T \in (1,N)\} : \\ \delta x^i_{fast} == \left| a_t^i f_0^t \frac{1 - e^{\lambda^t \tau^T}}{\lambda^t} \right| < \delta x^i_{error} = True\Bigg\}. \qquad (4)$$

B. Reuse of the basis vectors

It can be shown that the terms on the diagonal of the Jacobian matrix, $J_{\boldsymbol{g}}$, have the meaning of reciprocal of time scales, and thus their time rate of change is a manifestation of the action of nonlinearities. Therefore, we decided to update the *CSP Basis* only when the norm of the relative change of the diagonal of the Jacobian matrix of the vector field is larger than a prescribed threshold (typically equal to 10%). We do not allow the *CSP Basis* to stay frozen for more 10 than consecutive integration time steps.

III. Results

In the following we will refer to (i) the original form of the G-Scheme as M#0, (ii) the method with the new fast subspace dimension detection as M#1, and (iii) the method with the new fast subspace dimension detection and the reuse of the *CSP Basis* as M#2.

A. A stable criterion for the identification of the fast subspace dimension

A comparison of the new and old criterion for the identification of the fast subspace dimension is offered in Fig. 1 for a test case involving the auto-ignition of a stoichiometric n-heptane/air (T_0=900 K, p_0=1 atm) using the Curran mechanism for iso-octane oxidation [3] (561 species and 2538 reactions). Fig. 1 shows that the time evolutions of the fastest (red symbols) and slowest (green) of the active scales, with the new criterion are more stable than the ones provided by the old criterion. The temperature evolution (black solid line) is also smoother as a consequence of the smoother evolution of the fastest (red symbols) scale. Table I indicates that M#0 takes 672 steps to reach convergence while M#1 takes 455 steps for the same accuracy (as measured in term of ignition delay time, τ_{ign}). Because of the fewer integration time steps, the CPU time drops from 269s to 175s.

B. Reuse of the basis vectors

The effectiveness of reusing the *CSP Basis* has been verified for the same model problem and test case considered in the previous section. The test demonstrated that the time

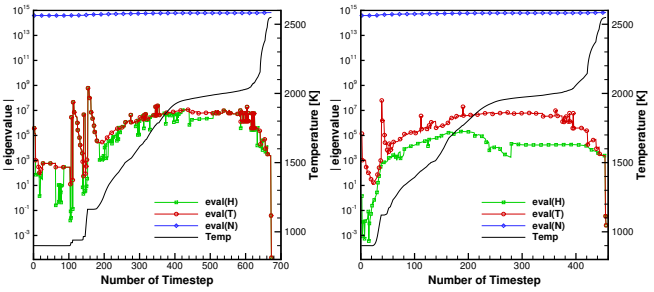

Fig. 1. M#0 (left) and M#1 (right). Evolution of the fastest (red symbols) and slowest (green) of the active scales, of the fastest (blue) scale, of the temperature (black line); x-axis is the time step counter.

evolutions of the slow and fast subspace dimension detection with the reuse of the *CSP Basis* are only slightly more noisy than when the *CSP Basis* is updated at each time step.

We note that the total number of integration time step of M#1 and M#2 is approximately the same, this implying that the reuse of the *CSP Basis* does not translate in a penalty on the number of integration time steps.

Table I indicates that M#0 takes 672 steps to reach convergence while M#2 takes 449 steps for the same accuracy (measured in term of ignition delay time τ_{ign}). The CPU time drops from 269s to 61s (a speed up factor of 4.4) . The profiling of the solver indicates that the calculation of the *CSP Basis* (although reused for 69% of the steps in this case) takes about 52s (85.2%) of the total CPU budget of 61s. These figures address both the remaining bottleneck of the solver but also the potential additional saving at hand whenever a smarter way to compute the *CSP Basis* is found.

TABLE I
PERFORMANCE SUMMARY OF THE THREE METHODS

Method	steps	τ_{ign} (s)	CPU time (s)
M#0	672 (0 reused)	0.28932	2.692E+02
M#1	455 (0 reused)	0.28776	1.751E+02
M#2	449 (310 reused)	0.28776	6.054E+01

IV. Acknowledgements

We acknowledge the support of MIUR, as well as that provided by KAUST 1975-03 CCF Subaward Agreement.

References

[1] M. Valorani, S. Paolucci, The G-Scheme: A framework for multi-scale adaptive model reduction, Journal of Computational Physics 228 (13) (2009) 4665–4701.
[2] S. H. Lam, D. A. Goussis, The CSP method for simplifying kinetics, International Journal of Chemical Kinetics 26 (4) (1994) 461–486.
[3] H. J. Curran, P. Gaffuri, W. J. Pitz, C. K. Westbrook, A comprehensive modeling study of iso-octane oxidation, Combustion and Flame 36 (129) (2002) 253–280.

Using Global Pathway to Understand Chemical Kinetics

Xiang Gao, Suo Yang and Wenting Sun
School of Aerospace Engineering, Georgia Institute of Technology, Atlanta, GA 30332, USA

Abstract— **A hierarchical framework, Global Pathway Analysis (GPA), is presented to understand complex chemical kinetics. The behavior of the reacting system at macro level is bridged to the elementary reaction level by Global Pathways, which are the chemical pathways from an initial reactant species to a final product species. For each Global Pathway, its dominancy and effect on the system, such as these on radical production or consumption, are quantified to understand its contribution to the system. The non-monotonic relation between auto-ignition delays and ratios of toluene in its mixture with n-decane is analyzed as a demonstration.**

I. Introduction

Numerical simulation plays an increasingly important role in the study of combustion. However, realistic chemical kinetic models describing the combustion process typically involve hundreds of species and thousands of reactions. Due to their large sizes and complicated coupled relations, it remains a formidable task to extract insights from the reaction system. Systematic and rigorous analytic tools are necessary to obtain useful information from massive simulation datasets.

The early stage of analysis of chemical kinetics may start from timescale decoupling. This includes Computational Singular Perturbation (CSP) [1], Intrinsic low-dimensional manifold (ILDM) [2], and Chemical Explosive Mode Analysis (CEMA)[3]. Recently, a Global Pathway Selection algorithm (GPS) [4] is proposed to identify important Global Pathways for reacting systems, which are the chemical pathways that convert initial reactants to final products, based on atomic flux analysis. GPS has been used for effective chemical kinetic mechanism reduction [4, 5]. In this study, Global Pathways is used to formulate an automatic and quantified framework to understand the complex chemical kinetics.

II. Methodology

As illustrated in Fig 1, a hierarchical model to analyze chemical kinetics is proposed. Other aspects such as transport are not focused in the present work. The objective is to find the elementary reactions controlling the phenomena of interest in a complex reacting system and underlying connections among different species. Therefore, it is necessary to formulate an interface between the behavior of the system and the elementary reactions. For this purpose, Global Pathways are identified using GPS algorithm [4] for considered source/sink pairs of species. The source species are usually components of the fuel or the oxidizer which are providing C, H, and O atoms, and the sink species are usually final products which are absorbing C, H, and O atoms. These Global Pathways provide a simplified representation of the reacting system, yet reflecting the key chemical information of species conversion. Each arrow (→) in a Global Pathway is called a conversion step.

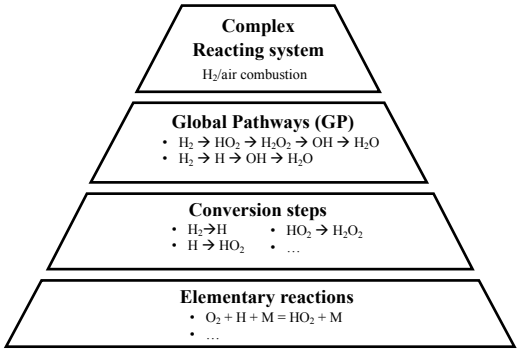

Fig 1. A hierarchical model to analyze complex chemical kinetics, using H_2/air combustion as a demonstration.

Then, for the identified Global Pathways, their dominancy and effects on radical production and consumption are quantified. The effects on other aspects such as heat release and entropy production can be quantified as well in a similar way but are not focuses of present work. These quantities provide an overview of each Global Pathway and explain that how these Global Pathways compete with each other and affect the reacting system differently. Three quantities are defined to analyze the system, where the detailed definition can be found in Ref. [6]. They are: (i) The dominancy of a Global Pathway, $D_{GP,e}$, represents the fraction of the *e*-th atoms (e.g., C atoms) that are going through this Global Pathway. It ranges from 0 to 1. (ii) The net radical production rate associated with a Global Pathway, R_{GP}, and (iii) the net radical production rate associated with the conversion step from the *i*-th species to the *j*-th species, $R_{i\to j}$. As this hierarchical framework is based on the analysis of Global Pathways, this methodology is hereafter referred as Global Pathway Analysis (GPA).

III. Results and Discussion

A demonstration is given in this section using simulation results of zero-dimensional reactors (from Cantera [7]) to illustrate the analysis process of complex chemical kinetics with GPA framework. The accuracy/validity of the kinetic mechanisms themselves (e.g., their possible discrepancies with experimental results) is not the concern of this work.

Instead, GPA provides insights to interpret behavior of the system shown in the simulation results in terms of the coupling relation between elementary reactions.

Normal-alkanes and aromatics are two common classes selected in surrogate fuel model. The mixture of n-decane ($C_{10}H_{22}$) and toluene ($C_6H_5CH_3$) is chosen as the fuel to be investigated in this section with a relatively compact kinetics model [8]. τ_{ign} of the stoichiometric mixture of fuel/air of different n-decane/toluene volume ratio at 1000 K is illustrated in Fig. 2. τ_{ign} of pure n-decane is shorter than that of pure toluene, as shown in Fig. 2. One may expect that τ_{ign} of the mixture of n-decane and toluene is in between, as in Fig. 2(a). However, this is not always the case according to the kinetic model by Chaos et al [8]. At 10 atm, τ_{ign} firstly decreases, then increases as the ratio of toluene increases, as shown in Fig. 2(b). These trends may depend on the kinetics model employed. However, this work only focuses on the interpretation of an existing kinetic model.

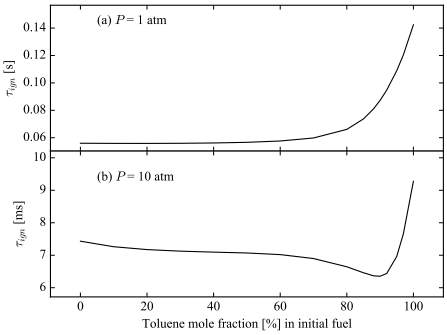

Fig. 2. τ_{ign} of stoichiometric n-decane/toluene/air mixture for different fuel compositions at (a) P = 1atm and (b) P = 10 atm.

To understand this non-monotonic relation between fuel composition and τ_{ign} shown in Fig. 2(b), Global Pathways are identified from simulation results. The most dominant Global Pathway identified from the auto-ignition of n-decane is GP-dec, and the one from the auto-ignition of toluene is GP-tol.

$C_{10}H_{22} \rightarrow C_{10}H_{21} \rightarrow C_6H_{13\text{-}1} \rightarrow C_6H_{13\text{-}2} \rightarrow C_3H_6 \rightarrow C_3H_5 \rightarrow C_3H_5O \rightarrow C_2H_3CHO \rightarrow C_2H_3 \rightarrow HCO \rightarrow CO \rightarrow CO_2$ (GP-dec)

$C_6H_5CH_3 \rightarrow C_6H_5CH_2 \rightarrow C_6H_5CH_2O \rightarrow C_6H_5CHO \rightarrow C_6H_5CO \rightarrow C_6H_6 \rightarrow C_6H_4O_2 \rightarrow C_5H_4O \rightarrow C_5H_5O \rightarrow$ n-C_4H_5 $\rightarrow C_4H_4 \rightarrow$ i-$C_4H_3 \rightarrow HCCO \rightarrow CO \rightarrow CO_2$ (GP-tol)

R_{GP} of these Global Pathways are illustrated in Fig. 3, for mixture n-decane/toluene with volume ratio of 1:9 at 10 atm, where τ_{ign} is close to the minimal in Fig. 2(b). It can be found that, GP-tol firstly produces radicals then consumes radicals. In contrast, GP-dec firstly consumes radicals then produces radicals. This means that, these two Global Pathways provide radicals for each other when the other is consuming radicals, and this coupling effect increases the overall reactivity. Therefore, the mixture of toluene and n-decane may autoignite faster than the neat fuel (pure toluene or n-decane).

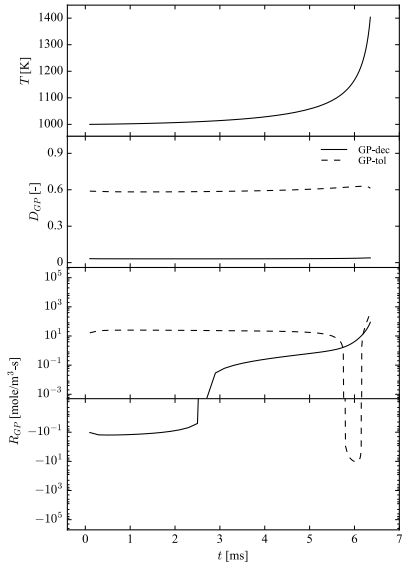

Fig. 3. Global Pathways during auto-ignition at 10 atm for mixture of n-decane/toluene (volume ratio = 1:9)

IV. Conclusion

A hierarchical framework, Global Pathway Analysis (GPA), to understand the chemical kinetics is proposed. The behavior of the reacting system at macro level is bridged to elementary reactions by Global Pathways. An explanation for the non-monotonic relation at high P between τ_{ign} and toluene ratio in its mixture with n-decane is provided using GPA. Two identified Global Pathways provide radicals for each other when the other is consuming radicals. This increases the overall reactivity for the mixture comparing to the neat fuels.

Reference

[1] Lam, S., and Goussis, D., "Understanding complex chemical kinetics with computational singular perturbation," *Symposium (International) on Combustion*, Vol. 22, Elsevier, 1989, 1.

[2] Maas, U., and Pope, S. B., "Simplifying chemical kinetics: intrinsic low-dimensional manifolds in composition space," *Combustion and flame* Vol. 88, No. 3, 1992, pp. 239-264.

[3] Lu, T., Yoo, C. S., Chen, J., and Law, C. K., "Three-dimensional direct numerical simulation of a turbulent lifted hydrogen jet flame in heated coflow: a chemical explosive mode analysis," *Journal of Fluid Mechanics* Vol. 652, 2010, pp. 45-64.

[4] Gao, X., Yang, S., and Sun, W., "A global pathway selection algorithm for the reduction of detailed chemical kinetic mechanisms," *Combustion and Flame* Vol. 167, 2016, pp. 238-247.

[5] Coogan, S., Gao, X., McClung, A., and Sun, W., "Evaluation of Kinetic Mechanisms for Direct Fired Supercritical Oxy-Combustion of Natural Gas," *ASME Turbo Expo 2016: Turbomachinery Technical Conference and Exposition*, 2016, pp. GT2016-56658.

[6] Gao, X., and Sun, W., "Using Global Pathway Selection Method to Understand Chemical Kinetics," *55th AIAA Aerospace Sciences Meeting*, 2017, pp. AIAA 2017-0836.

[7] Goodwin, D. G., Moffat, H. K., and Speth, R. L., "Cantera: An object-oriented software toolkit for chemical kinetics, thermodynamics, and transport processes. http://www.cantera.org/, 2016. Version 2.2.1.."

[8] Chaos, M., Kazakov, A., Zhao, Z., Dryer, F., and Zeppieri, S., "Reduced hightemperature mechanisms for large paraffins–n-hexadecane," *Eastern States Fall Technical Meeting of the Combustion Institute, Orlando, FL, USA*, 2005.

Session: Mechanism Simplification 3

Chair: F. Mauss

Title: Horizontal Species Lumping Using Structural Information from a Mechanism Generator
Authors: M. Hilbig, L. Seidel, F. Mauss

Title: Reduced High-Temperature Combustion Chemistry Models of Jet Fuels
Authors: Y. Gao, R. Xu, H. Wang, T. Lu

Horizontal species lumping using structural information from a mechanism generator

Martin Hilbig*, Lars Seidel*, Fabian Mauss*
*Brandenburg University of Technology, Cottbus, Germany

***Abstract*— In the present work we suggest an *a priori* lumping method for chemical species in an gas phase fuel oxidation scheme. In contrast to prior development we utilize structural information of individual species which originate from a mechanism generator. The suggested method yields a closer agreement to the detailed scheme than the previously suggested evaluation of thermodynamic properties.**

I. Introduction

As reported by Tomlin et. al. [1] due to strong nonlinear nature of chemically reactive systems it is quite tough to find a priori assumptions for an automatic lumping procedure. At the 5th Model Reduction Workshop the authors presented an a priori lumping approach based on the evaluation of thermodynamic data [2].

The idea behind that is that similar isomers have similar thermodynamic data. This method was successfully applied for the reduction of n-heptane mechanism [3].

One considerable drawback of this approach is that it heavily relies on the quality of the given thermodynamic data. It can be observed that the same thermodynamic data are often used for all isomers - which groups them into one lumped species. Further thermodynamic data carry no structural information. In the aforementioned lumping of the n-heptane scheme [3] it was found that lumping together different ring sizes of cyclic ether with the same sum formula and similar thermodynamic data leads to deviations from the detailed model.

This implies that the lumping procedure would strongly benefit if structural information would be available. In this work we evaluate the incorporation of species structure information into the lumping process. The structural information are obtained from a mechanism generator firstly presented in 2011 [4].

II. Mechanism Generator Overview

The mechanism generator developed by the present authors uses a rule based approach and operates on the graphical structure of chemical species.

The species structures are stored in the document database CouchDB [5]. The reactions and structures are iteratively and semi-automatically generated by applying 29 reaction class based on rules of the work of Ahmed [6], Mehl [7] and Blurock [8] and others including low-temperature kinetics. If those classes produce new species structures they are added to the database and we again apply our reaction rule classes until no new reactions are generated.

In order to generate an oxidation chemistry for a fuel, a base chemistry along with its structures needs to be provided by the user. This chemistry describes the combustion of smaller species (typically H2 and C1-C4/C5) which can not be described by classes.

The database is then exported into standard format mechanism file and a RMG [9] input file for it's group additivity based molecular and thermodynamic properties estimator in conjunction with MOPAC [10].

III. Structurally Guided Horizontal Chemical Species Lumping

After fully populating the Mechanism database and generating the corresponding molecular and thermodynamic properties, our lumping tool queries the database for all species structures (sorted by structural identifications) and groups those species according to their sum formula.

Afterwards adjusted thermodynamic and molecular properties are generated (for the lumped species) and a new mechanism file in standard format is written.

A. Identification and grouping

Using CouchDB's "Map/Reduce" feature a specific document in a mechanism database contains a view which returns all species structures, accompanied by an identifying structure describing string. CouchDB Map/Reduce views are referential-transparent functions, which are called for every document in a database and can return arbitrary key-value-pairs. For example one such function checks whether it's input is a chemical species and whether the species is a cyclic ether. If this is the case the function returns the species' document id, an identifier string (e.g. "cyclic-ether"), whether the cyclic-ether contains a primary carbon, the ring size of the ether and the sum formula of the ether. These key-value-pairs are then grouped together by sum formula and functional group identifiers. The group identifiers are based on: radical carbons, carbonyl, peroxy, hydroperoxy, oxi radical, alkenyl groups and combinations thereof. Further we take into account if the functional groups are on a primary or secondary carbon and the distance between them (if there is more than one group).

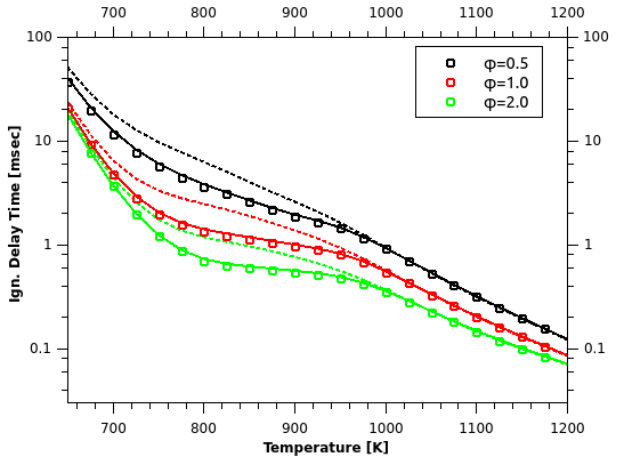

Fig. 1. Predicted ignition delay times for n-dodecane / air mixture at different fuel / equivalence ratios. Symbols: detailed scheme; Dashed line: lumping based on Gibbs free energy; Solid line: lumping based on structural information.

The list of species to be lumped into a representative specie is used to calculate new reaction rates and thermodynamic data as explained in [3].

IV. Results

A. Detailed scheme

The detailed scheme was generated with the rules outlined above and the NTUA [11] C1-C4 chemistry was chosen as base chemistry. The chemistry was chosen to underline that the method can be applied to any reaction scheme and is not limited to schemes developed by the author. The scheme consists of 720 species and 11917 reactions (backward and forward).

B. Lumped schemes

Both horizontal lumping strategies have been applied to the detailed scheme.

The lumping based on a maximum deviation of 1kJ in Gibbs free energy between 300 - 3000K identified 74 representative species resulting in a mechanism with 460 species and 11875 reactions (back and forward). This scheme shows a significant deviation from the detailed one in the low temperature regime (figure 1).

The lumping based on the evaluation of functional groups identified 74 representative species as well. But results in 493 species and 11821 (back and forward) reactions. This lumped scheme shows a much better agreement with the detailed scheme over the whole temperature range (figure 1).

The CPU time is reduced by about 25% for both lumped schemes.

Acknowledgment

We would like to thank Zisis Malliotakis at the NTUA HMCS for compiling the detailed mechanism with the generator outlined above.

References

[1] A.S. Tomlin, T. Turanyi, and M.J. Pilling. "Mathematical tools for the construction, investigation and reduction of combustion mechanisms", Low temperature Combustion and Autoignition. Comprehensive Chemical Kinetics. Elsevier, Amsterdam, vol. 35(4), pp. 293437, (1997)

[2] A. Matrisciano, L. Seidel, C. and Klauer, H. Lehtiniemi F. and Mauss, "An a priori thermodynamic data analysis based chemical lumping method for the reduction of large and multi-component chemical kinetic mechanisms", Proceedings of the 5th International Workshop on Model Reduction in Reaction Flows, (2015)

[3] L. Seidel, C. Netzer, M. Hilbig, F. Mauss, C. Klauer, M. Pasternak and A. Matrisciano. "SYSTEMATIC REDUCTION OF DETAILED CHEMICAL REACTION MECHANISMS FOR ENGINE APPLICATIONS". ASME. J. Eng. Gas Turbines Power. (2017) doi:10.1115/1.4036093.

[4] M. Hilbig, L. Seidel, X. Wang, F. Mauss, T. Zeuch. "Computer Aided Detailed Mechanism Generation for Large Hydrocarbons: n-Decane". Proceedings of 23rd ICDERS, pp. 24-27, (2011).

[5] http://couchdb.apache.org/

[6] S.S. Ahmed, F. Mauss, G. Moréac, T. Zeuch, "A comprehensive and compact n-heptane oxidation model derived using chemical lumping", Phys. Chem. Chem. Phys., vol 9 , pp. 1107-1126, (2007).

[7] M.Mehl, G.Vanhove, W.J. Pitz, E. Ranzi, "Oxidation and combustion of the n-hexene isomers: A wide range kinetic modeling study". Combustion and Flame, vol 155(4), pp. 756-772, (2008).

[8] E.S. Blurock, "Detailed mechanism generation. 2. Aldehydes, ketones, and olefins". Journal of Chemical Information and Computer Sciences, vol 44(4), pp. 134857, (2004).

[9] C.W. Gao, J.W. Allen, W.H. Green, R.H. West, "Reaction Mechanism Generator: automatic construction of chemical kinetic mechanisms". Computer Physics Communications, vol 203, pp. 212-225, (2016).

[10] MOPAC2016, James J. P. Stewart, Stewart Computational Chemistry, web: HTTP://OpenMOPAC.net

[11] G. Vourliotakis, G. Skevis, M. A. Founti, "Some aspects of combustion chemistry of C1C2 oxygenated fuels in low pressure premixed flames", Proceedings of the Combustion Institute, vol 35, pp. 437-445, (2015).

Reduced High-Temperature Combustion Chemistry Models of Jet Fuels

Yang Gao[1], Rui Xu[2], Hai Wang[2], Tianfeng Lu[1*]
[1] Department of Mechanical Engineering, University of Connecticut
191 Auditorium Road Unit 3139, Storrs, CT 06269-3139
[2] Department of Mechanical Engineering, Stanford University
452 Escondido Mall, Stanford CA 94305-3032

***Abstract*—In the present study, reduced kinetic models, including fuel-specific reduced models and a universal reduced foundational fuel chemistry model for jet fuel combustion, are developed based on the recently developed HyChem models. The HyChem approach takes advantage of the de-coupling between fuel pyrolysis and oxidation of the pyrolysis products that underlies the basic physics of real, liquid fuel combustion processes and the diagnostic capabilities currently available. The resulting HyChem model of real jet fuels is comprised of a "1-species" lumped model of a jet fuel and a detailed foundational reaction model for the pyrolysis and oxidation H_2/CO/C_{1-4}/one-ring aromatics, and is thus already substantially reduced in size. The foundational fuel chemistry model may be further reduced through skeletal reduction using directed relation graph (DRG) and sensitivity analysis, and timescale reduction using the linearized quasi-steady state approximations (LQSSA). This two-stage reduction approach is applied on one conventional and two alternative jet fuels, resulting in fuel-specific reduced models with 31, 26, and 31 species, respectively. A universal reduced model with 35 species is further proposed for the three fuels, which features programmable fuel thermodynamic and transport properties and fuel cracking reaction parameters, as well as a shared reduced oxidation core for the fuel cracking products. The fuel-specific and universal reduced models are validated against the detailed HyChem models for auto-ignition, perfectly stirred reactors (PSR), 1-D laminar premixed flame speed, and extinction of premixed and non-premixed counterflow flames.**

I. Introduction

Jet fuels are comprised of a large number of components with different chemical and physical properties. In addition, combustion of jet fuels results in myriad intermediate species during the pyrolysis and oxidation processes. As such it is highly challenging to model the chemical kinetic behaviors of real jet fuels. Recently, a hybrid approach, "HyChem," was proposed to model high-temperature combustion of practical jet fuels [1, 2], and HyChem models have been developed for multiple real jet fuels. The HyChem approach takes advantage of the de-coupling between fuel pyrolysis and oxidation of the pyrolysis products that underlies the basic physics of real, liquid fuel combustion processes and the diagnostic capabilities currently available. The resulting HyChem model of real jet fuels is comprised of a lumped model of fuel pyrolysis and a detailed foundational reaction model for the pyrolysis and oxidation of the primary intermediates of jet fuel pyrolysis and oxidative pyrolysis. Key species include hydrogen, methane, ethylene, propene, *iso*-butene, 1-butene, benzene and toluene. Because the lumped model is essentially a 1-species model, the HyChem models are already extremely compact. In essence, the approach uses the physical phenomenon to derive the lower-dimension model, rather than starting at a higher complexity (e.g., using the surrogate and detailed reaction mechanism approach).

The HyChem model for each fuel consists of 119 species and 843 reactions, in which seven lumped reaction steps are used to describe the fuel pyrolysis, and the oxidation kinetics of the fuel pyrolysis products is described by USC Mech II [3]. The kinetic parameters of the HyChem model were determined though time-history data of shock-tube and flow-reactor experiments. The HyChem models have been validated against a variety of experiments, including ignition delay, laminar flame speed, and counterflow extinction [1, 2].

The emphasis of the current work is the reduction of the foundational fuel chemistry model. In particular, compact reduced models are developed based on the HyChem models for three target fuels to obtain CFD-amenable models for more efficient simulations. The three target fuels include a conventional petroleum-derived Jet-A fuel (POSF10325, Cat A2), and two alternative jet fuels: one (POSF11498, Cat C1) features a low derived cetane number (DCN) and is composed of highly branched *iso*-alkanes, and the other (POSF12345, Cat C5) features similar chemical properties but vastly different physical properties (flat boiling curve) with Cat A2. More details of the fuels can be found in Refs. [4, 5].

II. Methodologies and Results

A. Fuel-specific reduced HyChem models

The reduction is based on reaction states sampled from auto-ignition and perfectly stirred reactors (PSR). The reduction parameter range covers pressure of 0.5-30 atm, equivalence ratio of 0.5-1.5, initial temperature of 1000-1600 K for auto-ignition, and inlet temperature of 300 K for PSR. Skeletal reduction with directed relation graph (DRG) [6] and sensitivity analysis [7] is first applied to eliminate unimportant species and reactions from the detailed HyChem models. In DRG, H radical is selected as the starting species and an error threshold of 0.3 is specified for all the three target fuels. After the skeletal reduction with DRG, the resulting skeletal models are further reduced with sensitivity analysis

with ignition delay and extinction residence time of PSR as target parameters. Fig. 1 shows the accumulative worst-case relative error in the target parameters as function of the number of retained species in sensitivity analysis for Cat A2, with the vertical dashed line indicating the error threshold. The error threshold for each fuel in sensitivity analysis is chosen where the rapid increase in worst-case error of target parameters starts to occur, that is 20% for A2 and C5, and 35% for C1, respectively. The final skeletal models consist of 41, 34, and 41 species for Cat A2, C1, and C5, respectively. As the last step in the skeletal reduction, reactions unimportant for all the remained species are eliminated by comparing the contribution of each reaction to each remained species using an error threshold of 20% [8]. In the second-stage of the reduction, linearized quasi-steady-state approximations (LQSSA) [9] are further applied on 10, 8, and 10 global QSS species for Cat A2, C1, and C5, respectively. The QSS species are removed from the transport equations and are analytically solved using internal algebraic equations with a graph-based method [9]. Table I provides the summary of the detailed, skeletal and reduced models for the three target fuels.

Fig. 2 shows selected validations of the reduced and skeletal models against the detailed HyChem models for Cat A2, C1, and C5 for ignition delay and laminar flame speed. The reduced and skeletal models agree well with the detailed models over a wide range of conditions. Fig. 3 compares the maximum temperature of the flame as function of the reciprocal strain rate for non-premixed and premixed flames. The reduced models agree tightly with the detailed models along the entire curves including the turning points, which are the nominal extinction states of the flames, with the worst-case relative error being approximately 15%.

B. A universal reduced HyChem model

Because the oxidation cores for the three target fuels are largely identical, a universal skeletal model is developed by combining the oxidation cores of three target fuels and using programmable fuel properties and fuel cracking reactions. Procedurally, the three skeletal models are first merged to obtain a universal skeletal oxidation core with 47 species and 263 reactions after removing 37 reactions that are unimportant for all the three fuels. The three target fuels and their fuel-specific cracking reactions are replaced with 1 nominal fuel species and 7 nominal fuel cracking reactions, of which the rates and stoichiometric coefficients are evaluated using a special subroutine. Among the 48 species (including the nominal fuel) in the universal skeletal model, 13 species are identified to be global QSS species, and a 35-species universal reduced model is finally obtained.

Fig. 4 shows selected validations of the 35-species universal reduced model with Cat A2, C1, and C5 as the fuel respectively against the detailed models for ignition delay and laminar flame speed. It is seen that the universal reduced models agree slightly better with the detailed models than the fuel-specific reduced models.

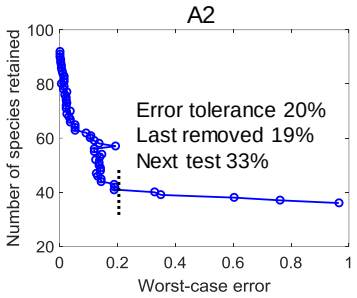

Fig.1 Accumulative worst-case error in the target parameters in sensitivity analysis as function of the number of retained species in the skeletal model for Cat A2.

TABLE I. Sizes of the detailed, skeletal and reduced HyChem models

	Cat A2		Cat C1		Cat C5	
	Species & Reactions		Species & Reactions		Species & Reactions	
Detailed	119	843	119	843	119	843
Skeletal	41	202	34	182	41	200
Reduced	31		26		31	

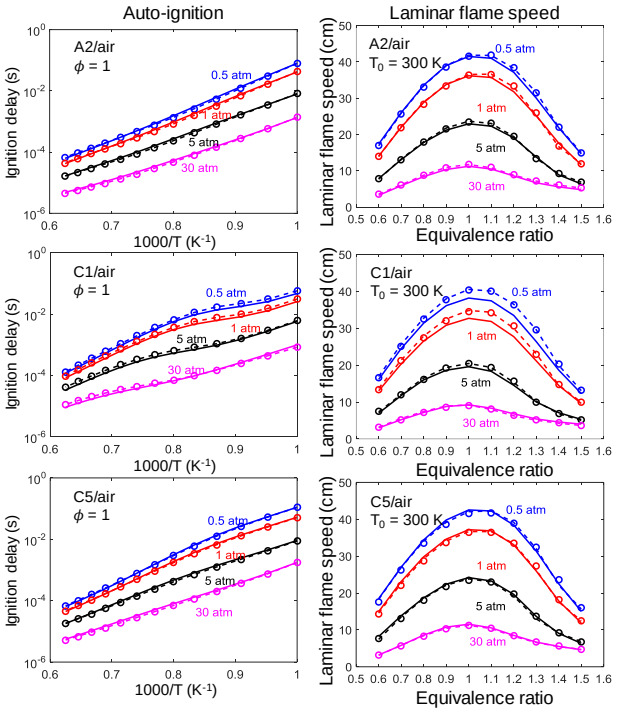

Fig. 2 Ignition delay (left) and laminar flame speed (right) at pressure of 0.5, 1, 5, and 30 atm for Cat A2, C1, and C5, calculated with the detailed (solid lines), skeletal (dashed lines) and reduced (symbols) models, respectively.

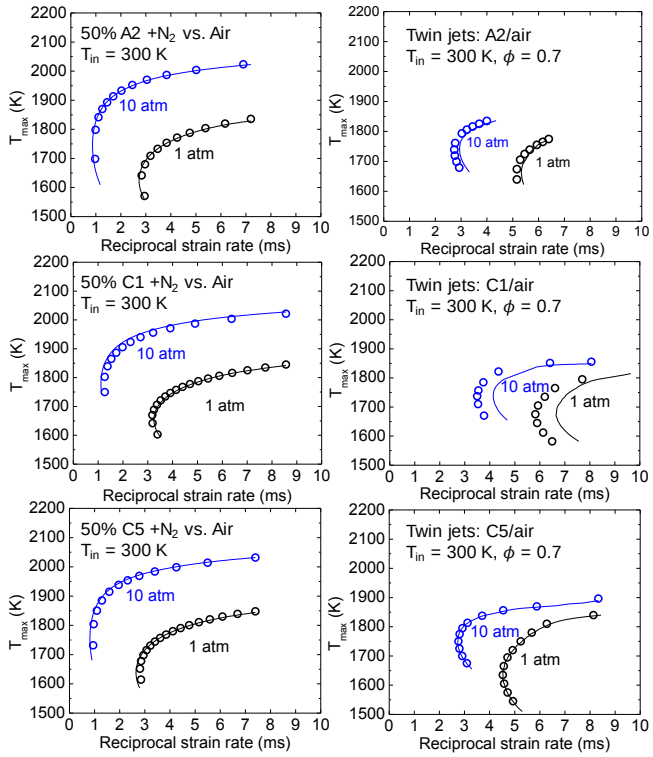

Fig. 3 Comparison of the maximum temperature, T_{max}, in counterflow non-premixed (left) and premixed (right) flames as function of the reciprocal strain rate for Cat A2, C1, and C5, calculated with the detailed (solid lines) and reduced (symbols) models, respectively.

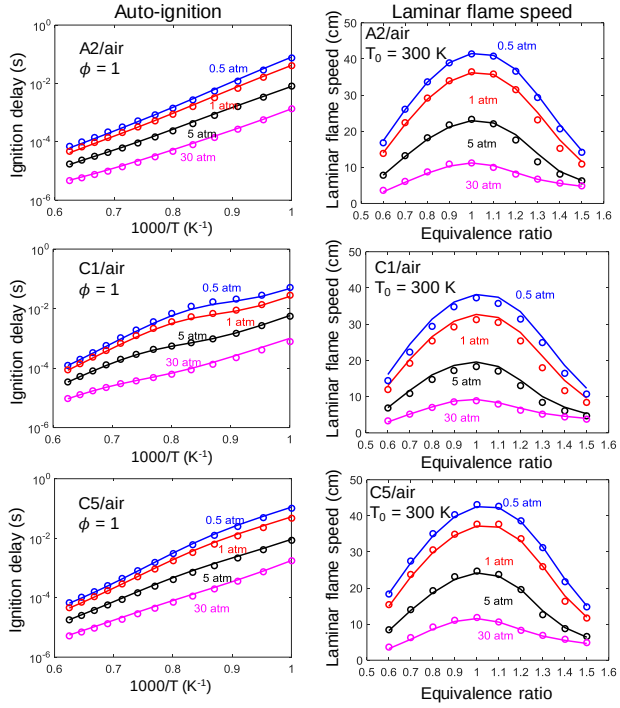

Fig. 4 Ignition delay (left) and laminar flame speed (right) at pressure of 0.5, 1, 5, and 30 atm for Cat A2, C1, and C5, calculated with the detailed (solid lines) and universal reduced (symbols) models, respectively.

III. Conclusions

The detailed HyChem models for real jet fuels, including Cat A2, C1, and C5, are systematically reduced for high-temperature applications using DRG, sensitivity analysis and LQSSA. Fuel-specific reduced models with 31, 26, and 31 species are obtained for Cat A2, C1, and C5, respectively. In addition, a 35-species universal reduced model is obtained using programmable fuel properties and fuel cracking reactions. The reduced models are validated against the detailed HyChem models for 0-D homogenous reactors, including auto-ignition and PSR, and 1-D diffusive systems, including laminar flame speed and extinction of premixed and non-premixed counterflow flames. The validation results show good agreements between the detailed and reduced models over a wide range of parameters. The compact reduced models are amenable for efficient CFD simulations with real fuel chemistry.

Acknowledgment

This work was supported by NASA NRA NNX15AU96A and NNX15AV05A under the technical monitoring of Dr. Jeff Moder, and by the US AFOSR under grant numbers FA9550-14-1-0235 and FA9550-16-1-0195 under technical monitoring of Dr. Chiping Li.

References

[1] R. Xu, H. Wang, R. K. Hanson, D. F. Davidson, C. T. Bowman, F. N. Egolfopoulos, Evidence supporting a simplified approach to modeling high-temperature combustion chemistry, in: *10th U.S. National Combustion Meeting*, Maryland, April 23-26, 2017.

[2] R. Xu, D. Chen, K. Wang, Y. Tao, J. K. Shao, T. Parise, Y. Zhu, S. Wang, R. Zhao, D. J. Lee, F. N. Egolfopoulos, D. F. Davidson, R. K. Hanson, C. T. Bowman, H. Wang, HyChem model: application to petroleum-derived jet fuels, in: *10th U.S. National Combustion Meeting*, Maryland, April 23-26, 2017.

[3] H. Wang, X. You, A. Joshi, S. Davis, A. Laskin, F. Egolfopoulos, C. Law USC Mech Version II. High-Temperature Combustion Reaction Model of H_2/CO/C_1-C_4 Compounds. http://ignis.usc.edu/USC_Mech_II.htm

[4] J. T. Edwards, Reference Jet Fuels for Combustion Testing, in: *55th AIAA Aerospace Sciences Meeting*, Grapevine, Texas, USA, 9-13 January, 2017.

[5] M. B. Colket, J. Heyne, M. Rumizen, J. T. Edwards, M. Gupta, W. M. Roquemore, J. P. Moder, J. M. Tishkoff, C. Li, An Overview of the National Jet Fuels Combustion Program, in: *54th AIAA Aerospace Sciences Meeting*, San Diego, California, USA, 4-8 January, 2016.

[6] T. Lu, C. K. Law, A directed relation graph method for mechanism reduction, *Proc. Combust. Inst.* 30 (2005) 1333-1341.

[7] X. Zheng, T. Lu, C. K. Law, Experimental counterflow ignition temperatures and reaction mechanisms of 1,3-butadiene, *Proc. Combust. Inst.* 31 (2007) 367-375.

[8] T. Lu, C. K. Law, Strategies for mechanism reduction for large hydrocarbons: n-heptane, *Combust. Flame* 154 (1-2) (2008) 153-163.

[9] T. Lu, C. K. Law, Systematic approach to obtain analytic solutions of quasi steady state species in reduced mechanisms, *J. Phys. Chem. A* 110 (49) (2006) 13202-13208.

Information

Contact:

Dr. Temistocle Grenga (co-host) Tel: 574-299-3428 Email: tgrenga@princeton.edu

Prof. Yiguang Ju (co-host) Email: yju@princeton.edu

Emergencies:

For emergencies, the University Department of Public Safety can be reached by dialing 911 from a campus phone or 609-258-3333 from a cell phone. In non-emergencies, the Department of Public Safety can be reached at 609-258-1000.

Princeton University maintains a website for any Emergency Alerts (https://www.princeton.edu/main/news/emergency).

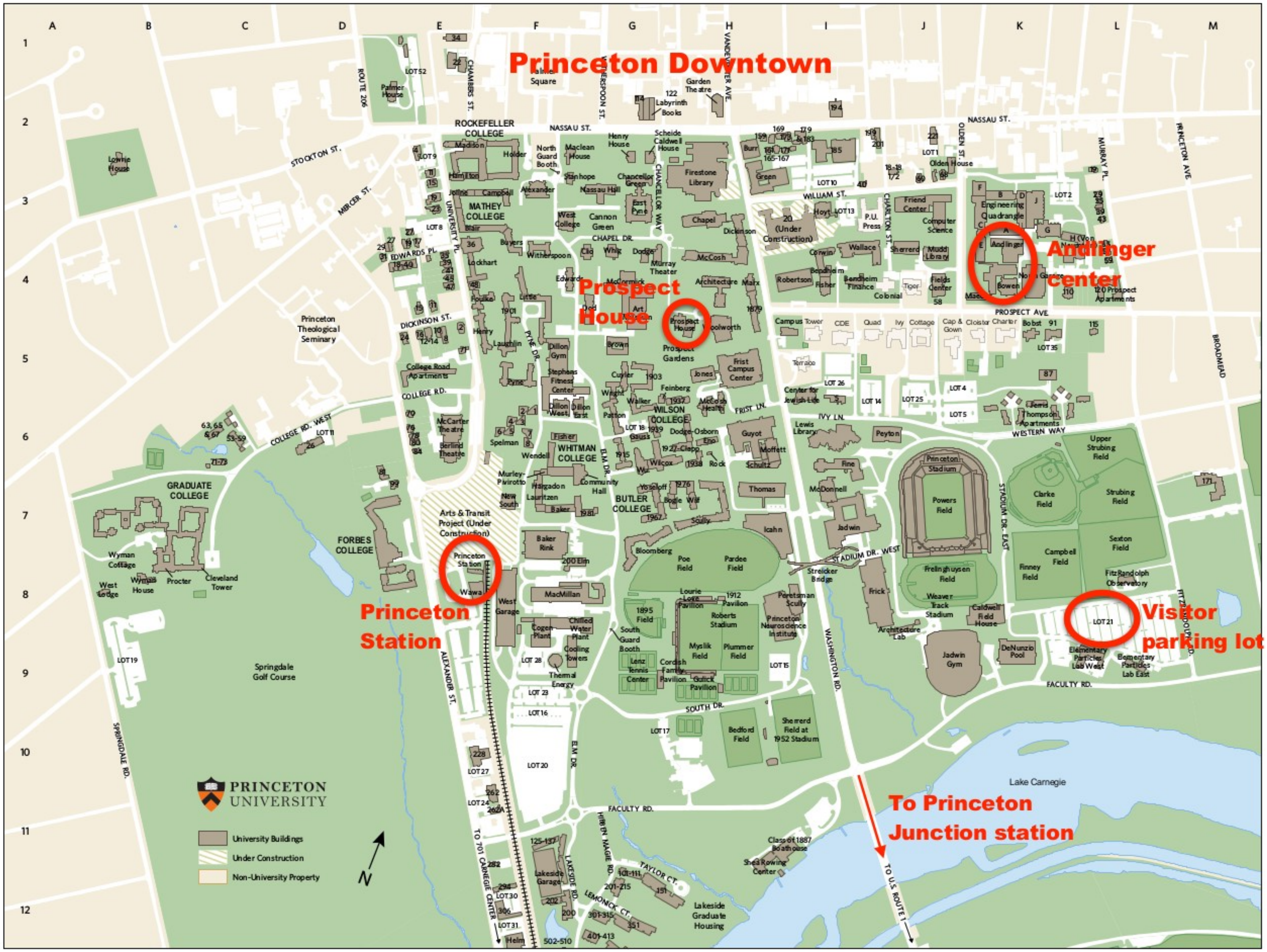
Princeton Downtown
Andlinger center
Prospect House
Princeton Station
Visitor parking lot
To Princeton Junction station
Lake Carnegie
PRINCETON UNIVERSITY
University Buildings
Under Construction
Non-University Property
NASSAU ST.
WASHINGTON RD.
ALEXANDER ST.
PROSPECT AVE
FACULTY RD.
GRADUATE COLLEGE
FORBES COLLEGE
ROCKEFELLER COLLEGE
MATHEY COLLEGE
WHITMAN COLLEGE
WILSON COLLEGE
BUTLER COLLEGE
Firestone Library
Princeton Stadium
Jadwin Gym
Springdale Golf Course
Princeton Theological Seminary
Engineering Quadrangle
Frist Campus Center
TO U.S. ROUTE 1
TO 701 CARNEGIE CENTER